Alma Mater Studiorum – Università di Bologna

DOTTORATO DI RICERCA IN

INGEGNERIA ENERGETICA, NUCLEARE E DEL CONTROLLO AMBIENTALE

Ciclo XXII

Settore scientifico-disciplinare di afferenza: FISICA TECNICA INDUSTRIALE ING-IND10

TITOLO TESI

Stability, viscous dissipation and local thermal non-equilibrium in fluid saturated porous media

Presentata da: **CELLI MICHELE**

Coordinatore Dottorato **Relatore**

Prof. Antonio Barletta **Prof. Antonio Barletta**

Esame finale anno 2010

Foreword

This thesis contains a part of the research work done at the University of Bologna. In the three years PhD curriculum, several subjects have been tackled and, in particular, MHD effects in electrically conducting fluids, stability analyses of parallel flows with viscous dissipation in fluid saturated porous media, local non-equilibrium phenomena in porous media and mixed convection flows in a vertical channel filled with a porous medium. Both for reasons of space and of homogeneity, I have decided to devote this thesis to just two of these subjects: the effect of viscous dissipation for the onset of instability in fluid saturated porous media, the presence of local thermal non-equilibrium in fluid saturated porous media. The researches on both these subjects have been developed partly in Bologna and partly in the Department of Mechanical Engineering, University of Bath (UK), under the supervision of Dr. Andrew Rees. Recently, researches on the stability of parallel flows in porous media have been also developed in collaboration with Prof. Don Nield, Department of Engineering Science, University of Auckland (NZ).

I would like to thank my supervisor professor Antonio Barletta for the effort given in these three years to the development of my skills and the good fulfilment of this Thesis.

Michele Celli

To Mauro, Stefania and my dear friends Claudio, Luca and Silvia

Abstract

In this thesis, the field of study related to the stability analysis of fluid saturated porous media is investigated. In particular the contribution of the viscous heating to the onset of convective instability in the flow through ducts is analysed. In order to evaluate the contribution of the viscous dissipation, different geometries, different models describing the balance equations and different boundary conditions are used. Moreover, the local thermal non-equilibrium model is used to study the evolution of the temperature differences between the fluid and the solid matrix in a thermal boundary layer problem.

On studying the onset of instability, different techniques for eigenvalue problems has been used. Analytical solutions, asymptotic analyses and numerical solutions by means of original and commercial codes are carried out.

Contents

List of Figures

List of Tables

Nomenclature

0.1 Roman letters

a	nondimensional wavenumber, Eq. (3.34)
A_n	nth series coefficient, Eq. (3.45)
Bi	Biot number, Eq. (2.39)
Br	Brinkman number, Eq. (2.29)
$B(y)$	nondimensional function, Eq. (4.25)
c	specific heat of the fluid, $[J/(kg \cdot K)]$
C_f	Forchheimer parameter
c_p	specific heat at constant pressure, $[J/(kg \cdot K)]$
c_v	specific heat at constant volume, $[J/(kg \cdot K)]$
c_{wave}	nondimensional phase velocity, Eq. (3.41)
C_1, C_2	constants
Da	Darcy number, Eq. (2.29)
D_p	particles diameter, $[m]$
D_{ij}	dimensional strain tensor, Eq. (2.5)
$D_n(\bar{x})$	Dirichlet boundary condition function, Eq. (1.16)
$\vec{e}_y$	unit vector of the y-axis
E_φ, E_h	residuals, Eqs. (5.55)-(5.56)
$f(y), h(y)$	eigenfunctions, Eqs. (5.31)-(5.33)
$\mathbf{F}_d$	force drag term
F_b	buoyancy force
g	modulus of the gravitational acceleration, $[m/s^2]$
$\vec{g}$	gravitational acceleration, $[m/s^2]$
G	nondimensional parameter, Eq. (3.51)

Ge	Gebhart number, Eq. (3.16)
h	heat transfer coefficient, $[W/(m^2 \cdot K)]$
h_{sf}	interphase heat transfer coefficient, $[W/(m^3 \cdot K)]$
H	scaled value of h
i	$\sqrt{-1}$
$\Im$	imaginary part
k	thermal conductivity of the fluid phase, $[W/(m \cdot K)]$
$\tilde{k}$	effective thermal conductivity, $[W/(m \cdot K)]$
K	permeability, $[m^2]$
l	REV length scale, $[m]$
L	natural length scale, $[m]$
$\mathcal{L}_n$	differential operator, Eqs. (3.66), (3.67)
M	2×2 matrix, Eq. (5.59)
n	integer number
N	nondimensional number, Eq. (2.28)
$N_n(\bar{x})$	Neumann boundary condition function, Eq. (1.17)
p	pressure, $[Pa]$,
$\mathcal{P}$	pressure disturbance contribution
$P(y)$	pressure eigenfunction, Eq. (4.28)
Pe	P*é*clet number, Eq. (3.19)
$P_+(y)$	nondimensional function, Eq. (4.43)
q_g	internal heat generation per unit volume, $[W/m^3]$
q_h	horizontal heat flux, $[W/m^2]$
R	nondimensional parameter, Eq. (3.38)
Ra	Darcy-Rayleigh number, Eq. (2.17)
Ra_h	Darcy-Rayleigh horizontal number, Eq. (5.2.1)
Re_K	Darcy-Reynolds number, Eq. (1.10)
$R_n(\bar{x})$	Robin boundary condition function, Eq. (1.18)
$\Re$	real part
t	time, $[s]$
T_w	upper boundary temperature or external temperature, $[K]$
T_0	reference temperature, $[K]$
$\mathbf{u}$	velocity vector (u, v, w), $[m/s]$

$\bar{u}_I$	intrinsic velocity, $[m/s]$
U_∞	dimensional undisturbed velocity, $[m/s]$
$\bar{\mathbf{u}}_\mathbf{L}$	local velocity vector, $[m/s]$
$\mathbf{U}$	velocity disturbances vector, (U, V, W)
$\mathcal{V}$	volume, $[m^3]$
$\mathbf{x}$	Cartesian coordinates vector (x, y, z), $[m]$

0.2 Greek letters

α	thermal diffusivity of the fluid phase, $[m^2/s]$
$\tilde{\alpha}$	effective thermal diffusivity, $[m^2/s]$
β	isobaric thermal expansion coefficient, $[K^{-1}]$
γ	reduced exponential coefficient, Eq. (3.35)
δy	step-size of the Runge-Kutta method
ΔT_B	nondimensional temperature difference, Eq. (5.19)
ϵ	nondimensional parameter, Eq. (3.58)
ε	perturbation parameter, Eq. (4.19)
γ	nondimensional parameter, Eq. (6.12)
σ	heat capacity ratio, Eq. (2.10)
η	vertical boundary layer variable, Eq. (6.20)
η_f	nondimensional Forchheimer parameter, Eq. (4.16)
η_+	nondimensional modified Forchheimer parameter, Eqs. (4.42)
θ	nondimensional fluid temperature disturbance, Eq. (2.23)
Θ	nondimensional fluid temperature boundary layer variable, Eq. (2.23)
$\Theta(y)$	nondimensional function, Eq. (5.27)
ι	parameter of separation of the porous medium scales, Eq. (1.14)
λ	exponential coefficient, Eq. (5.27)
λ_1, λ_2	real and imaginary parts of λ
Λ	threshold nondimensional parameter, Eq. (6.60)
μ	dynamic viscosity, $[Pa \cdot s]$
$\tilde{\mu}$	effective dynamic viscosity, $[Pa \cdot s]$
ν	kinematic viscosity, $[m^2/s]$

ξ	streamwise boundary layer variable, Eq. (6.20)
Ξ	complex parameter, $f(0)$, Eq. (5.38)
ρ	mass density of the fluid phase, $[kg/m^3]$
ρ_0	reference mass density at temperature T_0, $[kg/m^3]$
ϕ	nondimensional solid temperature, Eq. (6.9)
Φ	nondimensional solid temperature disturbance, Eq. (6.9)
$\boldsymbol{\Phi}$	nondimensional solid modified temperature boundary layer variable, Eq. (6.9)
Φ_{NS}, Φ_D	viscous dissipation terms, Eqs. (2.18) and (2.20); $[W/m^3]$
Φ_F, Φ_B	viscous dissipation terms, Eqs. (2.22) and (2.25); $[W/m^3]$
φ	porosity
$\varphi(y), h(y)$	eigenfunctions, Eqs. (5.50)-(5.53)
φ_n, h_n	nondimensional coefficients, Eq. (5.54)
χ	angle between basic flow direction and x-axis
ψ	streamfunction, Eq. (3.30)
ω	real exponential coefficient, $\Im(\lambda)$, Eq. (5.30)

0.3 Superscripts, subscripts

B	basic flow
cr	critical value
f	fluid phase
s	solid phase
$\bar{}$	dimensional quantity
∞	environment conditions
$\tilde{}$	nondimensional quantity

0.4 Acronyms

DB	Darcy, B enard
DBP	Darcy, B enard, Prats
HRL	Horton, Rogers and Lapwood

ODE	Ordinary Differential Equation
LTE	Local Thermal Equilibrium
$LTNE$	Local Thermal Non-Equilibrium
REV	Representative Elementary Volume

1

Introduction

The study of heat transfer and fluid dynamic in saturated porous media involves several different fields of interest, from engineering to geophysics and medicine. The modeling of cooling/heating devices, fluid intrusions in volcano magma chambers, CO_2 sequestration, transfer of gases to blood within the lung and drugs delivery to the brain are few examples of the widespread fields involved. This first chapter is focused on presenting an introduction to porous media and to the momentum balance modelling. The chapter ends with a discussion on the hydrodynamic boundary conditions.

1.1 Porous Medium

A porous medium (or a porous material) is a solid medium which is characterised by the presence of void spaces within its own volume. The medium can thus be modeled as a solid matrix permeated by a network of channel, or pores, where a fluid (liquid or gas) can move. Usually both the solid matrix and the fluid are assumed to be continuous. A good example of a porous medium can be a sponge, see Figure 1.1. Many natural substances such as rocks, soils, biological tissues (e.g. bones), and man made materials such as cements, foams and ceramics can be considered as porous media. A porous medium is defined by its porosity, permeability as well as by the properties of its constituents (solid matrix and fluid). The solid matrix is usually considered as a rigid non-deformable medium. Moreover the porous medium is assumed to be isotropic, non soluble in the fluid and chemically inert. In the following, a single phase fluid saturating the porous material is analysed.

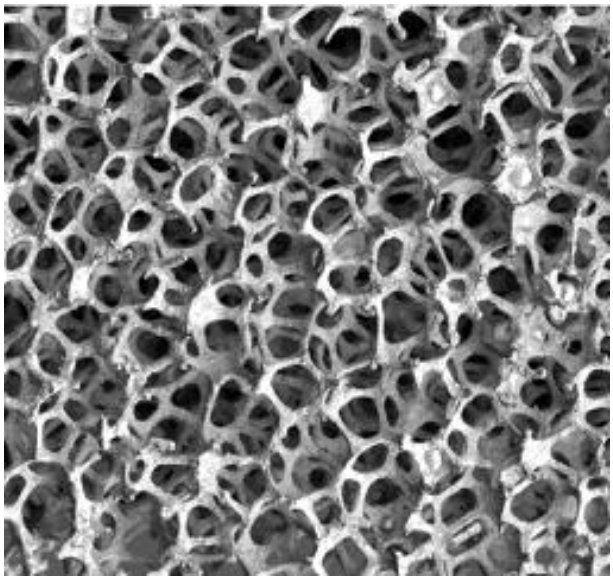

Figure 1.1: An example of porous medium.

1.2 Porosity

The governing macroscopic equations for the fluid flow and heat transfer in a porous medium are obtained by averaging the local variables over a "sufficiently large" representative elementary volume (R.E.V.). "Sufficiently large" means that the length scale of the REV is much larger than the pore scale, but much smaller than the length scale of the flow domain under consideration.

A basic characteristic of the porous medium is its porosity φ defined as the fraction of the volume of the system that is occupied by the void space, i.e. the volume occupied by the saturating fluid,

$$\varphi = \frac{\mathcal{V}_f}{\mathcal{V}}. \tag{1.1}$$

Natural media have porosity usually less than 0.6: the sandstone lies in the range $0.08 - 0.38$, the soil between $0.43 - 0.54$ and the leather between $0.56 - 0.59$. Artificial materials like fiberglass, mineral wool may have a porosity slightly less than the value 1 that corresponds to the limit of a clear fluid.

Let us define $\bar{\mathbf{u}} = (\bar{u}, \bar{v}, \bar{w})$ as the average velocity of the fluid with respect to a volume

element of the medium incorporating both the solid phase and the fluid phase, namely

$$\bar{\mathbf{u}} = \frac{1}{\mathcal{V}} \int_{\mathcal{V}} \bar{\mathbf{u}}_{\mathbf{L}}\, d\mathcal{V}, \tag{1.2}$$

where $\bar{\mathbf{u}}_{\mathbf{L}}$ is the local dimensional velocity vector. On the other hand, let us define $\bar{\mathbf{u}}_I = (\bar{u}_I, \bar{v}_I, \bar{w}_I)$ the intrinsic average velocity of the fluid taken with respect to the volume element consisting of the space occupied by the fluid only as

$$\bar{\mathbf{u}}_I = \frac{1}{\mathcal{V}_f} \int_{\mathcal{V}_f} \bar{\mathbf{u}}_{\mathbf{L}}\, d\mathcal{V}. \tag{1.3}$$

The average velocity $\bar{\mathbf{u}}$ and the intrinsic velocity $\bar{\mathbf{u}}_I$ are related by means of the Dupuit-Forchheimer relationship

$$\bar{\mathbf{u}} = \varphi\, \bar{\mathbf{u}}_{\mathbf{I}}. \tag{1.4}$$

The velocity $\bar{\mathbf{u}}$ is called in many ways: seepage velocity, filtration velocity, Darcy's velocity. According to Nield and Bejan (48) here $\bar{\mathbf{u}}$ is called Darcy's velocity.
By the definition of Darcy's velocity $\bar{\mathbf{u}}$ and porosity φ the mass balance equation or continuity equation can be written as

$$\varphi \frac{\partial \bar{\rho}}{\partial \bar{t}} + \bar{\nabla} \cdot (\bar{\rho}\, \bar{\mathbf{u}}) = 0, \tag{1.5}$$

where ρ is the fluid density and the porosity φ is considered as independent of the time. If the density is considered as a constant, the fluid is taken to be incompressible and Eq.(1.5) reduces to

$$\bar{\nabla} \cdot \bar{\mathbf{u}} = 0. \tag{1.6}$$

Eq.(1.6) is the form of the continuity equation used in this thesis.

1.3 The momentum balance equation

In clear fluids, the momentum balance equation commonly used is the well known Navier-Stokes equation. On modelling flows in porous media the Navier-Stokes equation does not provide a satisfactory description of the system. In fact, different approaches to the formulation of the momentum balance equation for fluid flowing in saturated porous

media have been proposed. First, the Darcy model is presented. This is the oldest and the most widely employed model. The Darcy model is very simple and, nonetheless, it allows one to investigate a wide range of flow cases. However, in order to enlarge the domain of investigation, other models have been proposed. In the following, after the Darcy model, the Forchherimer model and the Brinkman model will be discussed. These two models, adding new terms to the Darcy model, yield a more complex analysis of fluids flowing in saturated porous media. Finally, an extension of Darcy's model is discussed such that a time-dependent term is included.

1.3.1 Darcy's law

Henry P. G. Darcy was a French scientist and engineer. He worked for the design of the water distribution of the city of Dijon, France. Based on this work he published *The Public Fountains of the City of Dijon* (24). Inside this publication, there is an appendix entitled *Determination of the Laws of Water Flow Through Sand*. In this pioneering work Darcy formulated what is today the well known Darcy's law. He based his law on the results of experiments on the flow of water through layers of sand. Darcy's law refers to the case of laminar flow in the porous medium and, moreover, it refers to a tight packed solid with a fluid flowing in very small pores. The latter condition describes a flow regime very far from the clear fluid flow. This low porosity regime allows one to obtain a momentum balance equation that is dramatically simpler than the Navier-Stokes equation. This momentum balance equation is called Darcy's law and it is an heuristic relationship. This law describes a proportionality relationship between Darcy's velocity and the pressure gradient, namely

$$\bar{\mathbf{u}} = -\frac{K}{\mu}\,\bar{\nabla}\bar{p}, \tag{1.7}$$

where μ the dynamic viscosity of the fluid, $\bar{p}$ is the pressure and K is the permeability of the porous medium. The permeability K is a measure of the ability of a porous material to let fluids flowing through itself and it depends only on the geometry of the medium and not on the properties of the fluid. The size of the pores and their shape are characteristics that influence the permeability value. The limiting case $K \to 0$ refers to a compact solid without void or pores. On the other hand the limiting case $K \to \infty$ refers to a clear fluid. In Eq.(1.7), due to the fact that the porous medium

is assumed to be isotropic, the permeability can be considered as a constant. The permeability range of values is from 10^{-7} for clean gravel to 10^{-20} for unweathered clay. Carman and Kozeny, (21; 38), found a relationship that relates permeability and porosity: the Carman-Kozeny equation. This relationship holds for a packed layer of uniform particles of diameter D_p and it states that

$$K = \frac{D_p^2 \, \varphi^3}{180 \, (1-\varphi)^2}, \tag{1.8}$$

where the constant 180 was obtained by seeking the best fit of experimental results. The validity of this equation decreases either in those cases in which the solid particles that build the porous matrix strongly deviate from the spherical shape or in those cases where there is a broad particle-size distribution. Nevertheless this relationship is widely used since it seems to be the best simple expression available.

In order to take into account the gravity field influence on the system the term $\rho \, \mathbf{g}$ is usually added to the momentum balance equations. From Eq.(1.8) and Darcy's law, Eq.(1.7), one obtains

$$\bar{\mathbf{u}} = \frac{K}{\mu} \, (-\bar{\nabla} \bar{p} + \rho_0 \, \bar{\mathbf{g}}), \tag{1.9}$$

where $\mathbf{g}$ is the gravitational acceleration.

Darcy's law has been verified by the results of many experiments. Many authors have used statistical concepts to find a theoretical support for Darcy's law. Whitaker, (94), has theoretically derived Darcy's law, for the case of an incompressible fluid. This theoretical development is not restricted to either homogeneous or spatially periodic porous media, but it assumes that there are no abrupt changes in the structure of the medium.

1.3.2 Forchheimer's model

Darcy's equation, Eq.(1.9), is linear in the Darcy velocity $\bar{\mathbf{u}}$. It is valid when $\bar{\mathbf{u}}$ is sufficiently small. Increasing the velocity $\bar{\mathbf{u}}$ of the fluid a flow transition to an hydraulic regime begins at the pores scale. In this regime the fluid head loss is proportional to the

square of the mass flow rate in the pores. If one defines a permeability-based Reynolds number as

$$Re_K = \frac{\bar{u}\,\rho_0\,\sqrt{K}}{\mu}, \tag{1.10}$$

on increasing Re_K from 0 to 100 a smooth transition to a nonlinear drag occurs. According to Joseph et al. (36) the appropriate modification to Darcy's equation is to replace Eq.(1.9) with a balance equation that has been associated with the names of Dupuit (27) and Forchheimer (30) and is usually called Forchheimer equation, namely

$$\bar{\mathbf{u}} + \frac{\rho_0\,C_f\,\sqrt{K}}{\mu}\,|\bar{\mathbf{u}}|\,\bar{\mathbf{u}} = -\frac{K}{\mu}\,(\bar{\nabla}\bar{p} + \rho_0\,\bar{\mathbf{g}}), \tag{1.11}$$

where C_f is a nondimensional quantity called form drag coefficient. In the early papers on this model, it was sustained that C_f is a universal constant and Ward, (91), found an approximate value equal to 0.55. More recently, it has been pointed out that the Forchheimer coefficient is sensitive to the geometry of the duct and to the solid material the porous medium is made of. Forchheimer's model also include Darcy's law as a special case and, like Darcy's law, it refers to a tight packed solid with a fluid flowing in very small pores. Taking the limit $Re_K \to 0$, Eq.(1.11) reduces to Darcy's equation, Eq.(1.9). When the value of Re_K approaches 100 Darcy's law is no longer reliable.

1.3.3 Brinkman's model

Darcy's law and Forchheimer's model are suitable for a relatively low porosity. Moreover they cannot allow the assignment of no-slip conditions on a boundary surface. The latter is a severe difference between the porous media models and the free flowing fluid momentum balance equation, the Navier-Stokes equation. On increasing the porosity of the medium, a continuous transition from a clear fluid momentum balance equation to a porous medium momentum balance equation is likely to occur. Brinkman in (19; 20) proposed a momentum balance equation adding, with respect to the Darcy equation, a Laplacian term analogous to the Laplacian term that appears in the Navier-Stokes equation, namely

$$\frac{\mu}{K}\,\bar{\mathbf{u}} = -\bar{\nabla}\bar{p} + \tilde{\mu}\,\bar{\nabla}^2\bar{\mathbf{u}}, \tag{1.12}$$

where $\tilde{\mu}$ is defined as the effective viscosity. Originally Brinkman assumed $\tilde{\mu}$ equal to μ but subsequently it has been shown that $\tilde{\mu}$ is a function of the dynamic viscosity and porosity of the particular porous medium. A frequently used correlation between the dynamic viscosity μ and the effective viscosity $\tilde{\mu}$ is the Einstein formula for dilute suspensions, namely

$$\tilde{\mu} = \mu[1 + 2.5\,(1 - \varphi)]. \tag{1.13}$$

When the porosity approaches the unit value the effective viscosity tends to the dynamic viscosity, $\tilde{\mu} \to \mu$ and the permeability tends to infinity, $K \to \infty$. In this limiting case the Brinkman equation Eq.(1.12) reduces to the Navier-Stokes equation without the inertial contribution. The Laplacian term in the right hand side of Brinkman's equation allows one to apply the no slip conditions at the rigid boundaries, while the Darcy equation or the Forchheimer equation do not. Lundgren (45) showed that the validity of Eq.(1.12) is restricted to those systems with a sufficiently high porosity, greater than 0.6. The range of values of porosity allowed by Lundgren is a severe limitation because most of the porous media have porosity less than 0.6. Another discussion on the domain of validity of the Brinkman model has been performed by Auriault (5). He defined the quantity ι as

$$\iota = \frac{l}{L}, \tag{1.14}$$

where l is the characteristic length of the REV and L the characteristic length scale of the macroscopic flow. For $\iota \ll 1$, a condition of low permeability, Auriault showed that the Brinkman term is negligible up to the third-order in ι. In case of a moderate separation of the two scales l and L, $\iota < 1$, the permeability is higher with respect to the last case and the Brinkman term is still a second order corrector in ι. From the latter considerations he concludes that the Brinkman model has a quite restricted range of validity.

Many authors have recently proposed a Brinkman-Forchheimer formulation of the momentum balance equation. The two models have, as said in the previous Sections, different ranges of validity for what concern the value of porosity. Therefore the validity of a Brinkman-Forchheimer equation is not completely clear. Lage, in a scale analysis (40), showed the different regimes in which the various terms in the Brinkman-Forchheimer

equation were important or not. Hsu and Cheng (33) proposed a formulation of the Brinkman-Forchheimer model, based on earlier works of Vafai and Tien (89; 90), that can be expressed as

$$\frac{\partial \bar{\mathbf{u}}}{\partial \bar{t}} + \bar{\nabla}\left(\frac{\bar{\mathbf{u}}\cdot\bar{\mathbf{u}}}{\varphi}\right) = -\frac{\varphi}{\rho_0}\,\bar{\nabla}\bar{p} - \frac{\varphi\,\nu}{K}\,\bar{\mathbf{u}} + \frac{\tilde{\mu}}{\rho_0}\,\bar{\nabla}^2\bar{\mathbf{u}} - \frac{\varphi\,C_f}{\sqrt{K}}\,|\bar{\mathbf{u}}|\,\bar{\mathbf{u}}. \tag{1.15}$$

1.4 Hydrodynamic boundary conditions

A detailed account of the boundary conditions is a matter of primary importance. These can be distinguished in hydrodynamic conditions and thermal conditions. In the following the hydrodynamic conditions are described. A discussion about the thermal boundary conditions can be found at the end of the next chapter.

A boundary condition can be distinguished in first type, or Dirichlet condition, second type, or Neumann condition and third type, or Robin condition. To simplify the discussion let us consider a horizontal two dimensional, $(\bar{x}, \bar{y})$, duct infinitely wide in the $\bar{x}$ direction and with boundary walls at $\bar{y} = 0$ and $\bar{y} = L$, with streamwise velocity component $\bar{u}$ and vertical component $\bar{v}$. In a general form, the Dirichlet condition can be expressed, for instance in the case of a given velocity $(\bar{u}, \bar{v})$ at a given boundary, as

$$\bar{u} = D_1(\bar{x}) \qquad \bar{v} = D_2(\bar{x}), \tag{1.16}$$

where $D_1(\bar{x})$ and $D_2(\bar{x})$ are functions defined on the boundary. On the other hand, at a given boundary, the Neumann conditions is expressed by

$$\frac{\partial \bar{u}}{\partial \bar{y}} = N_1(\bar{x}) \qquad \frac{\partial \bar{v}}{\partial \bar{y}} = N_2(\bar{x}), \tag{1.17}$$

where $N_1(\bar{x})$ and $N_2(\bar{x})$ are functions defined on the boundary. For the third type conditions, the Robin conditions, on a given boundary the velocity $(\bar{u}, \bar{v})$ is such that

$$C_1\,\bar{u} + C_2\,\frac{\partial \bar{u}}{\partial \bar{y}} = R_1(\bar{x}) \qquad C_3\,\bar{v} + C_4\,\frac{\partial \bar{v}}{\partial \bar{y}} = R_2(\bar{x}), \tag{1.18}$$

where $R_1(\bar{x})$ and $R_1(\bar{x})$ are functions defined on the boundary and C_1, C_2, C_3, C_4 are constants.

On modelling the hydrodynamical behaviour of the fluid at the boundaries, different configurations can be used: permeable or impermeable walls, slipping or no-slipping

walls, moving walls, free boundaries and interface conditions between a clear fluid and a porous medium are taken into account. The impermeability condition is a Dirichlet condition that, on the two boundaries of the two dimensional duct, can be expressed as

$$\bar{y} = 0 \quad \longmapsto \quad \bar{v} = 0 \qquad \text{and} \qquad \bar{y} = L \quad \longmapsto \quad \bar{v} = 0. \tag{1.19}$$

If the impermeability condition is applied together with the Darcy model one has that, since the Darcy equation is of the first order, it is the only one condition that can be applied for a given boundary. In this case one assumed that the fluid slips on the boundaries with velocity $\bar{u}$.
If the Brinkman model is used, the momentum balance equation becomes of second order and the no-slip conditions, again Dirichlet conditions, at the two boundaries can be applied, namely

$$\bar{y} = 0 \quad \longmapsto \quad \bar{u} = 0 \qquad \text{and} \qquad \bar{y} = L \quad \longmapsto \quad \bar{u} = 0. \tag{1.20}$$

If, instead of being impermeable, a boundary is free (as in the case of a liquid saturated porous medium exposed to the atmosphere), then the appropriate condition is that the pressure is constant along the boundary

$$\bar{y} = \text{free boundary} \quad \longmapsto \quad \bar{p} = cost. \tag{1.21}$$

From Eq.(1.21) $\partial\bar{p}/\partial\bar{x} = 0$, hence, from Darcy's law, $\bar{u} = 0$ on the free boundary. From the latter conclusion one obtains that also the derivative of the horizontal velocity vanishes, thus, from the continuity equation Eq.(1.6), the free surface boundary condition can be expressed as

$$\bar{y} = \text{free boundary} \quad \longmapsto \quad \frac{\partial \bar{v}}{\partial \bar{y}} = 0, \tag{1.22}$$

that it is a Neumann condition on the velocity. Assuming that, for instance, the top wall is moving in the $\bar{x}$ direction with a velocity $\bar{u}_B$, Couette like boundary conditions are taken into account by imposing the following relationship

$$\bar{y} = L \quad \longmapsto \quad \bar{u} = \bar{u}_B, \tag{1.23}$$

that is again a Dirichlet condition and it can be applied only in the case that the no-slip condition is allowed on the moving wall. This implies that Couette like boundary conditions make sense only when the Brinkman model is used.

In that case of an interface between a clear fluid and a porous medium, one needs special boundary conditions. Beaver and Joseph (13) state that, if there is a flow in the horizontal direction, $\bar{x}$ for example, the appropriate boundary condition is the empirical relationship

$$\frac{\partial \bar{u}_I}{\partial \bar{y}} = \frac{\alpha_{BJ}}{K^{1/2}} (\bar{u}_I - \bar{u}) \tag{1.24}$$

where α_{BJ} is a nondimensional quantity and is independent of the viscosity of the fluid, but it depends on the material characteristics of the porous medium. Sahraoui and Kaviany (78) have shown that the value of α_{BJ} depends on the flow direction at the interface, the clear fluid Reynolds number and nonuniformities in the porous medium interface.

Finally let us consider the case of a boundary layer. When a boundary layer is investigated it is usually imposed a undisturbed basic flow outside the layer itself. The value of the basic flow velocity is here taken to be U_∞ and the value of temperature is taken to be T_∞.

All the boundary walls considered in this thesis are assumed to be impermeable. Moreover only the Darcy model and Forchheimer model are used, thus the no-slip conditions and the Couette boundary conditions will not be taken into account.

2

Instability

This chapter is focused on the analysis of the convection in porous media and the related stability analysis modelling. First an historical introduction on buoyancy effects is presented, then the thermal energy balance equation modelling is discussed and finally the concept of stability and the basic methods for analysing convective instability are introduced. Particular attention is given to the role of the viscous dissipation contribution to the onset of convection. The chapter ends with a discussion of the thermal boundary conditions.

2.1 Buoyancy effects

Spontaneous or natural convection belongs to those physical phenomena that have fascinated people since the time of Archimedes (213 B.C.). Convection usually arises when some strong inhomogeneity exists in a medium and/or some interplay occurs between the density or concentration distributions and external forces, gravitational, electric, or magnetic. Convective phenomena are very common in Nature and they hold a key role in many scientific fields, from physics to engineering, from astrophysics to meteorology. The term convection (from the Latin word *convectio, convectionis*, transport) seems to have been coined by Prout (66) to denote a mode of propagation of heat (by fluid motion). This kind of propagation of heat by fluid motion is described by Rumford (77) forty years earlier to account for the heat transport in a hot apple pie. This concept nowadays covers a broader spectrum of interest and involves all those physical properties other than heat that may be involved in a transport process. The term

convection is now associated with the terms natural, forced and mixed to identify three different regimes. Natural convection is a term that refers to heat transport by fluid flow generated by a thermal or solute concentration gradient. On the other hand, the term forced convection refers to convection phenomena generated by imposed pressure gradients. If both natural and forced convection occurs the term mixed convection is used.

Natural convection in atmospheric sciences has been first investigated by Hadley with his well known study on the generation of trade winds. He considered a model of atmosphere with uniform temperature rotating with the Earth. He assumed a heating of the lower atmosphere in the equatorial areas that forces the air present in those areas to rise, creating a high pressure zone. This high pressure area located at equatorial latitudes, due to the low pressure zone close to the poles, generates a north-south pressure gradient. This pressure gradient forces the high levels air masses to move toward the poles, to sink over these areas and, eventually, to return to the equator at low levels. In Earth sciences the natural convection is used to explain the plate tectonics theory. This theory describes the large scale motion of the lithosphere and it is based on a previous theory called continental drift and developed by Wegener (93). The lithosphere is the upper part of the the solid earth including the crust and the upper mantle. By the plate tectonics theory, the lithosphere is broken in a number of plates that move drive by the convective displacements of the mantle under the crust.

From a smaller scale point of view the convection can involve many kinds of phenomena: Faraday (28), for instance, studied the convective motion in liquids under the action of electric currents. Weber (92) observed a tesselated structure and motions in a layer of alcohol and water on the slide of a microscope, but attributed the circulation observed to electric forces and thus gave a wrong interpretation of his observation. Lehmann (44) pointed out the purely thermal origin of the phenomenon and gave the correct interpretation. One remarkable subsequent study was performed by J. Thomson (the older brother of W. Thomson, better known as Lord Kelvin) (84; 85) who gave a theoretical explanation of the phenomena happening in a glass of wine: he studied the cellular convection due to evaporative phenomena driven by unbalanced surface tension stresses.

The first controlled experiments on cellular convection were carried out by Bénard. He carefully reported (15; 16) experiments of convective motions in thin horizontal liquid

layers heated from below. In his experiments he managed to work in the approximation of the infinitely wide horizontal plate reducing as much as possible the influence of the lateral walls. Moreover, he tried to provide a uniform temperature at the bottom boundary of the system in order to work in the simplest and most uniform case possible. Bénard observed a phenomenon in which instability due to the temperature dependence of the surface tension coefficient played an important role. In fact he observed the production of a cellular pattern in the instability. These cells are, in surface tension driven convection, usually of polygonal shape and he found them to be mostly hexagonal. Although in his experiments the driving mechanism is the surface tension traction and Bénard attributed the convective motion to the buoyancy effects, a number of important observations were made by Bénard. For instance he correctly attributed the surface deflection to the surface tension tractions: "*...La tension superficielle à elle seule, provoqu déjà une depression au centre des cellules et un excès de pression sur les lignes de faite qui séparent les cuvettes concaves les unes des autres...*" (16). Also Lord Rayleigh (J. W. Strutt) disregarded the role of surface tension and Block, (17), published a pioneering experimental study that identified the surface tension as the cause of the Bénard cells. On the other hand, the first that proposed a theoretical description of surface tension driven convection phenomena was Pearson, (62).

2.1.1 Oberbeck-Boussinesq approximation

Oberbeck and Boussinesq published, between the end of the nineteenth century and the beginning of the twentieth century, the pioneering works (18; 59) where they introduced an extremely useful hypothesis that allows a dramatic simplification in the approach to the convection studies. Although recognizing that the dependence of the fluid physical properties on the temperature is a key point in the study of fluid dynamics and heat transfer, Oberbeck and Boussinesq assumed that all the physical properties of the fluid are temperature independent, except for the density in the gravitational body force term of the momentum balance equation. Here the density is considered as a linear function of the temperature, basically a Taylor series expansion around the reference value $\bar{\rho}_0$ truncated to the first order, namely

$$\bar{\rho} = \bar{\rho}_0 \left[1 - \beta \left(\bar{T} - \bar{T}_0\right)\right], \tag{2.1}$$

where β is the isobaric thermal expansion coefficient defined as

$$\beta = -\frac{1}{\bar{\rho}} \left(\frac{\partial \bar{\rho}}{\partial \bar{T}} \right)_p , \tag{2.2}$$

and $\bar{T}_0$ is the reference temperature. The choice of this reference temperature is a nontrivial task because of the sensitivity of the results to the value of $\bar{T}_0$. For clear fluids a reference study has been done by Barletta and Zanchini (12).
Now one can rewrite Darcy's law Eq.(1.9) with the approximation just introduced in Eq.(2.1)

$$\bar{\mathbf{u}} = -\frac{K}{\mu} \left[\bar{\nabla} \bar{p} + \bar{\rho}_0 \, \beta \, \bar{\mathbf{g}} \, (\bar{T} - \bar{T}_0) \right], \tag{2.3}$$

where $\bar{p} = \bar{p} - \bar{\rho}_0 \, \mathbf{g} \cdot \bar{\mathbf{x}}$ is the piezometric head. The buoyancy term in Eq.(2.3) couples the momentum balance equation to the thermal energy equation (described in the following subsection) giving rise to a feedback effect of the temperature field on the velocity field. Given the definition of density in Eq.(2.1) the continuity equation simplifies to Eq.(1.6).
From the assumption that the only term in which the density is variable is the buoyancy term, the Oberbeck-Boussinesq approximation leads to a fluid that is mechanically incompressible. On the other hand, the linear dependence of the density on the temperature in the buoyancy term, returns a weakly thermally compressible fluid. Throughout all this thesis the Oberbeck-Boussinesq approximation is assumed to be valid.

2.1.2 Thermal energy balance

In the analysis of convective flows, a thermal energy balance is necessary to define the temperature field and the heat transport. In the Oberbeck-Boussinesq approximation the energy equation has been written in different ways. Chandrasekhar and White, (23; 95), propose, for the clear fluids, the formulation

$$\bar{\rho}_0 \, c_v \, \frac{D\bar{T}}{D\bar{t}} = k \, \bar{\nabla}^2 \bar{T} + 2 \, \mu \, D_{ij} \;\; D_{ij}, \tag{2.4}$$

where $2 \, \mu \, D_{ij} \, D_{ij}$ is the heat generated by the viscous dissipation and the summation over repeated indexes is assumed. The term D_{ij} is the dimensional strain tensor defined

by

$$D_{ij} = \frac{1}{2}\left(\frac{\partial \bar{u}_j}{\partial \bar{x}_i} + \frac{\partial \bar{u}_i}{\partial \bar{x}_j}\right). \tag{2.5}$$

On the other hand, Martynenko (46) and Turcotte (86), propose an enthalpy formulation, again for the clear fluids, expressed by

$$\bar{\rho}_0\, c_p\, \frac{D\bar{T}}{D\bar{t}} = k\, \bar{\nabla}^2 \bar{T} + 2\,\mu\, D_{ij}\;\; D_{ij} + \beta\, \bar{T}\, \frac{D\bar{p}}{D\bar{T}}, \tag{2.6}$$

where the last term refers to the contribution of the pressure work. Another formulation of the thermal energy equation for clear fluids can be found in Landau-Lifshitz (14; 41) and Kundu-Cohen (39), namely

$$\bar{\rho}_0\, c_p\, \frac{D\bar{T}}{D\bar{t}} = k\, \nabla^2 \bar{T} + 2\,\mu\, D_{ij}\;\; D_{ij}. \tag{2.7}$$

Barletta, in (7), proposed a formulation for a clear fluid given by

$$\bar{\rho}_0\, c\, \frac{D\bar{T}}{D\bar{t}} = k\, \nabla^2 \bar{T} + 2\,\mu\, D_{ij}\, D_{ij}. \tag{2.8}$$

Barletta, in (7), also proposed a formulation for porous media. The latter is the thermal energy balance equation used in this thesis. In this formulation, valid for a (isotropic) solid matrix in thermal equilibrium with the saturating fluid, the local volume-averaged energy balance can be written as

$$\bar{\rho}_0\, c\, \left(\sigma\, \frac{\partial \bar{T}}{\partial \bar{t}} + \bar{\mathbf{u}} \cdot \bar{\nabla} \bar{T}\right) = \tilde{k}\, \nabla^2 \bar{T} + \Phi, \tag{2.9}$$

where Φ is the viscous dissipation contribution. A more precise discussion on this term can be found in section 2.2. Barletta (7) proved that, in a duct filled with a porous medium displaying an impressed basic flow, no pressure work term of the type $\beta\, \bar{T}\, \partial\bar{p}/\partial\bar{t}$ must be introduced. The letter σ refers to the heat capacity ratio defined as

$$\sigma = \frac{\varphi\, \bar{\rho}_0\, c + (1-\varphi)\, \bar{\rho}_s\, c_s}{\bar{\rho}_0\, c}, \tag{2.10}$$

and $\tilde{k}$ is the effective thermal conductivity of the system fluid plus porous medium and it is defined as

$$\tilde{k} = \varphi\, k + (1-\varphi)\, k_s, \tag{2.11}$$

while c is the heat capacity per unit mass defined as

$$c = c_p - \frac{\bar{p}\,\beta}{\bar{\rho}_0}. \tag{2.12}$$

The thermal diffusivity is then defined as $\alpha = k/(\bar{\rho}\,c)$ and the effective thermal diffusivity as $\tilde{\alpha} = \tilde{k}/[\varphi\,\bar{\rho}_0\,c + (1-\varphi)\,\bar{\rho}_s\,c_s]$. In Eqs.(2.10) and (2.11) the properties $\bar{\rho}_0$, c and k refer to the fluid phase, while $\bar{\rho}_s$, c_s and k_s refer to the solid matrix. From Barletta (7) the thermodynamic coefficient c coincides with the specific heat at constant volume, c_v, for a perfect gas while, for a liquid, c is definitely well approximated by the specific heat at constant pressure, c_p.

Equation (2.9) is the well known thermal energy balance equation for saturated porous media, except for the choice of the specific heat.

2.1.3 Rayleigh-Bénard problem

Lord Rayleigh (67; 68) studied the dynamic origins of convective cells and, also thanks to the Bénard studies, proposed his theory on the buoyancy driven convection. He approached the analysis as a stability problem, searching for unstable modes and their growth rates. He used Euler's equation, the thermal energy balance and he worked within the Oberbeck-Boussinesq approximation. Moreover, he performed a linear stability analysis, neglecting all the non linear terms, a hypothesis that allowed him to solve analytically the problem. He considered the same setup as in the Bénard experiments except for the top and bottom boundary conditions: he assumed the boundaries to be stress-free. This choice led him away from the original Bénard setup because he disregarded the surface tension effects. His analysis thus led to the basic result that a top-heavy fluid layer was stable under the joint influence of viscosity and heat diffusion until the vertical temperature drop was large enough to overcome these two dissipative and stabilising mechanisms. More precisely the kinematic viscosity ν inhibits the onset of convection from the mechanical point of view damping the motion, whereas heat diffusivity $\tilde{\alpha}$ inhibits the onset of convection from the thermal point of view reducing the strength of the temperature gradient. Lord Rayleigh found that the only parameter governing the stability was the temperature difference, made nondimensional by

a combination of parameters that corresponds to what is now known as the Rayleigh number

$$Ra = \frac{\beta\, g\, \Delta T\, L^3}{\alpha\, \nu}, \tag{2.13}$$

where ΔT is the temperature difference between the two boundaries and L is the natural length scale of the system. The Rayleigh number is a nondimensional number that arises from the buoyancy term on the momentum balance equation the Oberbeck-Boussinesq approximation. This nondimendional Rayleigh number describes the ratio of energy released by the buoyancy forces compared to the energy dissipated by heat conduction and viscous drag.

In the following an heuristic approach to the Rayleigh convection is presented. The aim of this approach is to better understand, from the physical point of view, the nature of the mechanisms that prevent the onset of convection. Let us consider an horizontal fluid layer heated from below in the presence of gravity. According to Lord Rayleigh, above a critical vertical temperature difference the system may become unstable. A small perturbation of this potentially unstable condition can easily produce a bubble of relatively hot fluid (relative to the surrounding fluid) that moves upward due to the Archimedean buoyancy force. Thus let us consider a system composed by a bubble of a given radius $\bar{R}$ moving upward with a constant velocity $\bar{V}$ in a constant vertical temperature gradient $\partial\bar{T}/\partial\bar{z}$. To let the bubble move, the stabilising viscous drag must be necessarily overcome by the buoyancy forces. The $\mu\,\bar{\nabla}^2\bar{V}$ term of the Navier-Stokes momentum equation can give an approximation of the viscous force acting on the bubble: for a volume of order R^3 it gives an order of magnitude of $-\mu\,\bar{R}\,\bar{V}$. On the other hand, the buoyancy forces arise from the instantaneous difference between the fluid density and temperature in the bubble and their local environment. Now, due to the heat diffusivity, the relaxation time required by the bubble to adapt itself to the external temperature is of the order of $\tau \approx \bar{R}^2/k$. Recalling that the bubble is moving vertically with velocity $\bar{V}$, at a given instant time $\bar{t}$ the temperature inside the bubble is approximately the external temperature of the layer where the bubble was at the time $\bar{t} - \tau$. Thus at the time $\bar{t}$ the temperature difference between the bubble and the surrounding fluid is

$$\Delta\bar{T} = \tau\,\bar{V}\,\frac{\partial\bar{T}}{\partial\bar{z}} \approx \frac{\bar{R}^2\bar{V}}{k}\,\frac{\partial\bar{T}}{\partial\bar{z}}. \tag{2.14}$$

This temperature difference yields an Archimedean buoyancy force acting on a bubble of radius $\bar{R}$

$$\bar{F}_b = \rho_0\, g\, \beta\, \Delta\bar{T}\, \bar{R}^3 \approx \frac{\rho_0\, g\, \beta\, \bar{R}^5 \bar{V}}{k}\, \frac{\partial \bar{T}}{\partial \bar{z}}. \tag{2.15}$$

Thus the rest state reaches an unstable state when the buoyancy forces overcome the viscous drag, namely

$$\bar{F}_b \geq \mu\, \bar{R}\, \bar{V} \qquad \longrightarrow \qquad \frac{g\, \beta\, \bar{R}^4}{\nu\, k}\, \frac{\partial \bar{T}}{\partial \bar{z}} \geq O(1), \tag{2.16}$$

in the latter inequality the Rayleigh number can be recognised. Eq.(2.16) leads to a rough estimate for the Rayleigh number of the unstable state, $Ra \geq O(1)$.

2.1.4 Buoyancy effects in porous media: Horton, Rogers and Lapwood problem

Beside the studies on the onset of convection in clear fluids, the stability analysis of a basic rest state has been also applied to fluid saturated porous media in order to assess the threshold conditions for the onset of buoyant flows. In particular Horton Rogers and Lapwood (HRL) (32; 42) contribute with two cornerstone works on the convection in porous media. They investigated the onset of convection in porous layers heated from below, the well known Darcy-Bénard problem. The latter problem consists in a uniform-thickness infinitely wide horizontal porous layer with uniform temperature and impermeable lower and upper boundaries. This configuration is basically a Rayleigh-Bénard problem in a layer filled by a porous medium. The presence of a porous medium naturally modifies the definition of the Rayleigh number. To take into account this contribution in the further analyses, the so called Darcy-Rayleigh number defined as

$$Ra = \frac{\beta\, g\, \Delta T\, K\, L}{\alpha\, \nu}, \tag{2.17}$$

will be used. Horton, Rogers and Lapwood found the critical Rayleigh number to be $4\,\pi^2$ for the onset of convection. This configuration has been studied in great detail both with the weakly non linear studies of Palm et al. (61) and with the detailed numerical stability analysis of Straus (81). The main reason of the subsequent studies on this subject is the possibility of many extensions to the governing Darcy-Boussinesq equations. For instance, boundary effects, inertial effects, local thermal non equilibrium

effects have been investigated. Nield (49) was the first to consider the variety of possible boundary conditions for the top and bottom of an infinitely wide horizontal porous layer of uniform thickness. He determined the criteria for the onset of convection for all different combinations of open, closed, conducting and insulating boundaries, see also Nield and Bejan (48), but no such investigation exists of the possible combinations of lateral boundary conditions for finite porous boxes. A number of papers have been written which take into account heat conduction in the lateral walls of a porous box. Nilsen and Storesletten (58) found an exact analytical solution for a two-dimensional box with conducting lateral walls.

An important problem closely related to the HRL problem is the Prats problem (65). This problem is the linear stability analysis, according to Darcy's model, of the HRL configuration in the presence of a uniform horizontal flow. By using a comoving reference frame, Prats proved that this uniform basic flow does not alter the condition for the onset of instability. In Prats' treatment, the critical value of the Rayleigh number is the same as in the DB problem, $4\,\pi^2$. Moreover the full non linear equations, when written in the comoving frame, reduce to those which apply when there is no basic flow. Therefore the full nonlinear behaviour of the DB problem is recovered in an infinitely wide layer. Another consequence is that there is no preferred direction for the roll orientation at the onset of instability, a feature not shared with the Bénard-Poiseuille convection.

2.2 The effect of viscous dissipation

In Eq.(2.9) the term Φ is defined as the viscous dissipation contribution. In many theoretical studies on convection the contributions of viscous dissipation to the thermal energy equation have been neglected. Viscous dissipation is an ubiquitous phenomenon and it is encountered in both the viscous flow of clear fluids and the fluid flow within porous media. However, in recent years it has been noted that in some circumstances these contributions are important for buoyant flows in porous media; see, for example, Nield (53; 55) and Nield and Barletta (56; 57). In fact, classical studies of the viscous heating effect in the instability of shear flows in clear fluids exist (35; 82). These studies show that the viscous heating leads to a destabilisation of the flow. In this respect, the modelling of the buoyant flow with viscous dissipation plays an important role.

When compared with other thermal influences on the fluid motion (i.e., by means of buoyancy forces induced by heated or cooled walls, and by localized heat sources or sinks) the effect of the heat released by viscous dissipation covers a wide range of magnitudes from being negligible to being significant. Gebhart (31) discussed this range and stated that "*...a significant viscous dissipation may occur in natural convection in various devices which are subject to large decelerations or which operate at high rotational speeds. In addition, important viscous dissipation effects may also be present in stronger gravitational fields and in processes where the scale of the process is very large, e.g., on larger planets, in large masses of gas in space, and in geological processes in fluids internal to various bodies...* ".

In contrast to such situations, many free convection processes are not sufficiently vigorous to result in a significant quantitative effect, although viscous dissipation sometimes acts to alter the qualitative nature of the flow. Although viscous dissipation is generally regarded as a weak effect, a property it shares with relativistic and quantum mechanical effects in everyday life, it too has played a seminal role in the history of physics. It was precisely this weak physical effect that allowed Joule (37) to determine the mechanical equivalent of heat using his paddlewheel experiments, and thereby to place one of the milestones toward the formulation of the first principle of thermodynamics. From a mathematical point of view the effect of viscous dissipation arises as an additional term in the energy equation. It expresses the rate of the conversion of mechanical energy into thermal energy by internal friction in the presence of a fluid flow. The dissipation function Φ depends on the momentum balance equation adopted. For incompressible clear fluids Φ is uniquely defined by the Navier-Stokes equations, namely

$$\Phi_{NS} = 2\,\mu\, D_{ij}\;\; D_{ij}, \tag{2.18}$$

For fluid saturated porous media the volumetric heat generation Φ depends on the model taken into account. Nield (52) stated that the form of Φ can easily be obtained by using the relationship

$$\Phi = \bar{\mathbf{F}}_d \cdot \bar{\mathbf{u}}, \tag{2.19}$$

where $\bar{\mathbf{F}}_d$ is the drag force expression that depends on the model. The drag force expression in the Darcy model for an isotropic porous medium is defined as in Eq.(1.7),

namely

$$\bar{\mathbf{F}}_d = \frac{\mu}{K}\,\bar{\mathbf{u}}, \tag{2.20}$$

so that the viscous dissipation function can be written as

$$\Phi_{Da} = \bar{\mathbf{F}}_d \cdot \bar{\mathbf{u}} = \frac{\mu}{K}\,\bar{\mathbf{u}} \cdot \bar{\mathbf{u}}. \tag{2.21}$$

For the Forchheimer extension to the Darcy model, the drag force is defined as in Eq.(1.11), namely

$$\bar{\mathbf{F}}_d = \frac{\mu}{K}\,\bar{\mathbf{u}} \left(1 + \frac{C_f\sqrt{K}}{\mu}\,|\bar{\mathbf{u}}|\right), \tag{2.22}$$

so that the viscous dissipation function is

$$\Phi_{Fo} = \bar{\mathbf{F}}_d \cdot \bar{\mathbf{u}} = \frac{\mu}{K}\,\bar{\mathbf{u}} \cdot \bar{\mathbf{u}} \left(1 + \frac{C_f\sqrt{K}}{\mu}\,|\bar{\mathbf{u}}|\right), \tag{2.23}$$

Equation (2.23) shows that the additional dissipation contribution provided by the Forchheimer drag force is independent of the viscosity. The paradox of the lack of dependence on viscosity of the Forchheimer dissipation term was resolved by Nield (51). The explanation is based on the recognition that the quadratic term models essentially a form drag effect. Nield stated that the pore scale convective inertial effects contributing to the quadratic drag term lead to a substantial modification of the velocity field, and in particular, to an enlargement of the macroscopic region in which the pore scale velocity gradients are large. This leads to an increase in the total viscous dissipation. Hence, due to the fundamental equality between the viscous dissipation and the power of the drag force, this feedback process shows the (implicit) dependence of the additional Forchheimer dissipation term on the viscosity of the fluid.

In the case of Brinkman's model the drag force expression is defined by Eq.(1.12), namely

$$\bar{\mathbf{F}}_d = \frac{\mu}{K}\,\bar{\mathbf{u}} - \tilde{\mu}\,\nabla^2\bar{\mathbf{u}}, \tag{2.24}$$

thus, according to the Nield rule in Eq.(2.19), the viscous dissipation function is

$$\Phi_{Br} = \bar{\mathbf{F}}_d \cdot \bar{\mathbf{u}} = \frac{\mu}{K}\,\bar{\mathbf{u}} \cdot \bar{\mathbf{u}} - \tilde{\mu}\,\bar{\mathbf{u}} \cdot \nabla^2\bar{\mathbf{u}}. \tag{2.25}$$

The Nield relationship Eq.(2.19) is a subject of debate about the viscous dissipation and Brinkman's model. In fact, for $K \to \infty$, one expects to find $\Phi_{Br} \to \Phi_{NS}$ but, in the limit of clear fluids, according to Einstein's relationship Eq.(1.13), one has

$$\Phi_{Br} \to -\mu\, \bar{\mathbf{u}} \cdot \nabla^2 \bar{\mathbf{u}}. \tag{2.26}$$

The differences between Φ_{Br} and Φ_{NS} in the clear fluid limit are evident: there is a different order of derivatives, first order for clear fluids and second order for Brinkman's model. Moreover $\Phi_{NS} \geq 0$ while Φ_{Br} may be negative.
Recently, Al-Hadharami *et al.* (1) proposed a different expression of Φ_{Br}, namely

$$\Phi_{Br} = \frac{\mu}{K}\, \bar{\mathbf{u}} \cdot \bar{\mathbf{u}} + 2\, \tilde{\mu}\, D_{ij}\ D_{ij}. \tag{2.27}$$

The expression in Eq.(2.27) cannot be negative and satisfies the two limits for K: $K \to 0$, the Darcy's law limit, and $K \to \infty$, the clear fluids limit, are both correctly modelled. It has been noted, Nield (54), that the model proposed by Al-Hadharami *et al.* is built as a sum of two dissipation terms that are valid in two different ranges of permeability: one is valid for small values of permeability, the Darcy term, and the other is valid for large values of permeability, the Navier-Stokes term. Thus the debate on this topic is still open, (54).
Eventually one can also estimate the magnitude of the viscous dissipation term with reference to the other contributions in the thermal energy equation. The viscous dissipation term is of the order of magnitude $\mu\, \bar{u}^2/K$. On the other hand, the thermal conduction term that appears in the same equation is of the order of magnitude of $k\, \Delta T/L^2$. Let us define the ratio between the two terms as

$$N = \frac{\mu\, \bar{u}^2\, L^2}{K\, k\, \Delta T} = \frac{Br}{Da}, \tag{2.28}$$

where Da is the Darcy number and Br is the Brinkman number. They are given by

$$Da = \frac{K}{L^2} \qquad Br = \frac{\mu\, \bar{u}^2}{k\, \Delta T}. \tag{2.29}$$

The Darcy number measures the width of the pores with respect to the overall width of the system. On the other hand, the Brinkman number measures the ratio, hence the relative magnitude, between the viscous heat input in the fluid and the heat transported by conduction. The viscous dissipation term turns out to be not negligible in the case

$N \gg 1$: when there is a high basic flow velocity, when the typical length scale of the system is significantly larger than the square root of the permeability, when the thermal conductivity is small and the viscosity of the fluid is large.

2.3 Local thermal non-equilibrium model

In most cases studied in the literature it has been assumed that the porous matrix and the fluid flowing through it are in local thermal equilibrium, LTE. At the microscopic level, the temperature and the rate of heat flux at the interface between solid and fluid phases must be identical, but the average value over a REV should not yield locally equal temperatures for the two phases. In this case the two phases are in local thermal non-equilibrium (LTNE). Rees and Pop (76) showed that LTNE is not necessarily an unsteady phenomenon, but it can also arise in steady flows. A recent review by Rees and Pop (76) summarises much of the present knowledge, including the various models used for LTNE and their application to free, mixed and forced convective flows and to stability analyses. Following Nield and Bejan (48) and Barletta (7) the simplest way to model the LTNE in an isotropic porous medium is to use two thermal balance equations, one for the fluid phase and one for the solid matrix, namely

$$\rho_0 \, c \left(\varphi \, \frac{\partial \bar{T}_f}{\partial \bar{t}} + \bar{\mathbf{u}} \cdot \bar{\nabla} \bar{T}_f \right) = \varphi \, k \, \bar{\nabla}^2 \bar{T}_f + \mu \, \Phi + h \, (\bar{T}_s - \bar{T}_f), \tag{2.30}$$

$$(1 - \varphi) \, (\rho \, c_v)_s \, \frac{\partial \bar{T}_s}{\partial \bar{t}} = (1 - \varphi) \, k_s \, \bar{\nabla}^2 \bar{T}_s + h \, (\bar{T}_f - \bar{T}_s), \tag{2.31}$$

where $\bar{T}_f$ refers to the fluid temperature, $\bar{T}_s$ refers to the solid temperature and h is the interphase heat transfer coefficient. Most papers which deals with convective flows in porous media assume that LTE holds. However, important cases where LTE cannot be invoked may exist. First introduced by Anzelius (4) and Schumann (79), Eqs.(2.30) and (2.31) use simple linear source/sink terms to model the local (i.e. microscopic) heat transfer between the phases at the pore level.

Nield (50), using Eqs.(2.30) and (2.31), considered the steady conduction case in a porous medium subject to a prescribed temperature on the boundary of the domain. Under the hypothesis of uniform phase conductivities, he showed that $\bar{T}_f = \bar{T}_s$ in this case by deriving a Helmoltz equation for $\bar{T}_f - \bar{T}_s$ which is subject to $\bar{T}_f - \bar{T}_s = 0$ on the boundary. Thus LTE always occurs in steady conduction problems where the boundary

temperature is imposed. Then one may infer that any departure from this special state will give rise to LTNE in general, although cases where LTE holds may always be derived as special cases. The study of Minkowycz et al. (47) confirms that, in various situations, the commonly used assumption of LTE is satisfactory. However, studies like Vafai and Sozen (87; 88), Amiri and Vafai (2; 3), and Lee and Vafai (43), show that the assumption of LTE fails in a substantial number of applications. Minkowycz et al. (47) establish one such area of failure corresponding to the presence of a rapidly changing surface heat flux.

2.4 Linear stability

A phenomenon that may satisfy all conservation laws of nature exactly, may still be unobservable. For the phenomenon, such as a smooth laminar flow, to occur in Nature, it has to satisfy one more condition, namely, it must be stable to small disturbances. In other words, infinitesimal disturbances, which are invariably present in any real system, must not amplify spontaneously. In fluid flows, smooth laminar flows are stable to small disturbances only when certain conditions are satisfied. For example, in flows of homogeneous viscous fluids in a channel, the Reynolds number must be less than some critical value and in a channel heated from below, the Rayleigh number must be lower than a critical value. When these conditions are not satisfied, infinitesimal disturbances grow spontaneously. Sometimes the disturbances can grow to a finite amplitude and reach equilibrium, resulting in a new steady state. The new state may then become unstable to other types of disturbances, and may grow to another steady state, and so on. Finally, the flow becomes a superposition of various large disturbances of random phases, and reaches a chaotic condition that is commonly described as turbulent. One shall introduce perturbations on a particular flow, and determine whether the equations of motion imply that the perturbations should grow or decay with time. In this analysis the problem is linearised by neglecting terms quadratic in the perturbation variables and their derivatives. This linear method of analysis, therefore, only examines the initial behaviour of the disturbances. The loss of stability does not in itself constitute a transition to turbulence, and the linear theory can at best describe only the very beginning of the process of transition to turbulence. Moreover, a real flow may be stable to infinitesimal disturbances (linearly stable), but still can be unstable

to sufficiently large disturbances (nonlinearly unstable). Nevertheless, the successes of the linear stability theory have been considerable. For instance, there is almost an exact agreement between experiments and theoretical prediction of the onset of thermal convection in a layer of fluid, and of the onset of the Tollmien-Schlichting waves in a viscous boundary layer. Taylor's (83) experimental verification of his own theoretical prediction of the onset of secondary flow in a rotating Couette flow is so striking that it has led people to suggest that Taylor's work is the first rigorous confirmation of the Navier-Stokes equations, on which the calculations are based.

For what concerns the definition of stable systems, the Lyapunov's stability concept is taken into account. It is ascribed to Lyapunov though the original mathematical development was made by Lagrange and Dirichlet. Lagrange stated a theorem proved by Dirichlet that assures that an equilibrium position of a conservative system is stable if the potential energy has a minimum there. Lyapunov proved under restrictions that the same position is unstable if the potential energy has no minimum there, or if it is a maximum. Now if the system has an initial deviation from its equilibrium position, it starts moving. The equilibrium position is called *stable* if the system does not go far from this position for arbitrary initial deviations. If due to this initial deviation the system, in some macroscopic relaxation time, gets back to its original state this configuration is called *asymptotically stable*. If this asymptotic stability holds only for a small neighborhood around the initial equilibrium state and not for every kind of initial deviation amplitude it is called *local* asymptotic stability. The equilibrium position is called unstable if the system, for arbitrary initial deviations, moves from his original position with no chances to come back to the equilibrium position. Figure 2.1 shows clearly the possible stability states where one can find a basic mechanical system. The last case of Figure 2.1 refers to those systems that are stable for linear disturbances but in case of nonlinear effects the system could overtake the well walls.

In the following the attention will be focused on the stability analysis of fluid flows in saturated porous media. A very common and useful method, widely employed also in this thesis, for the investigation of the onset of convective motion is the linear stability analysis by means of the normal modes. This analysis allows one to describe the fate of a small perturbation of a given thermodynamic state. It attempts, moreover, to investigate the conditions under which a system spontaneously undergoes transitions between

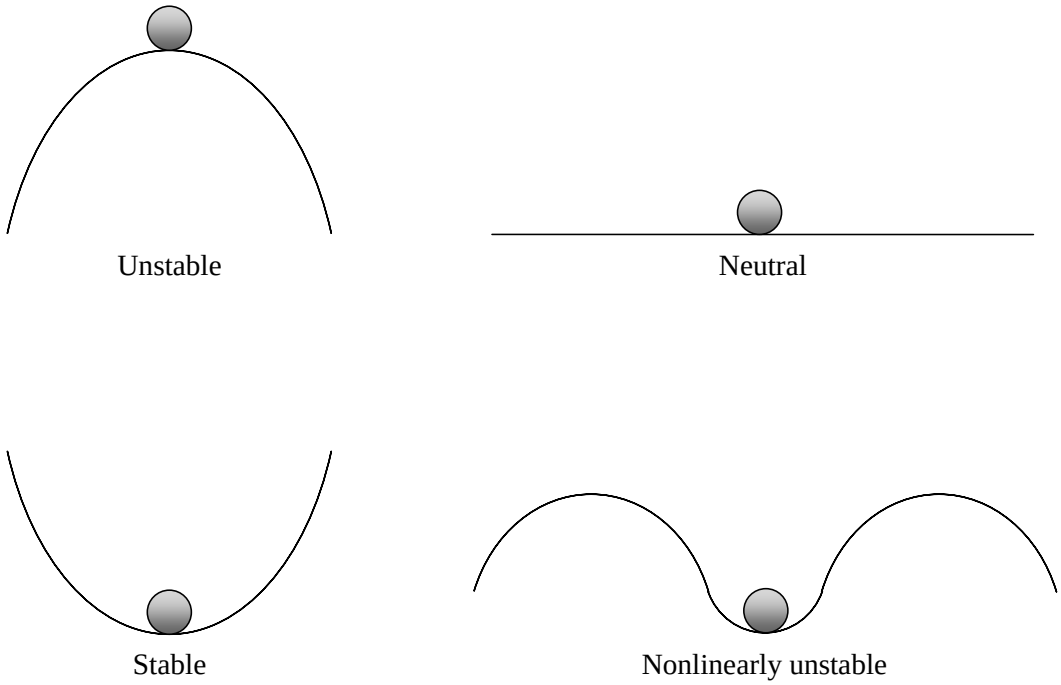

Figure 2.1: Stable and unstable systems from the mechanical point of view.

different states that may not be stationary. Is is assumed that the field variables undergo infinitesimal perturbations that consists in sinusoidal disturbances applied to a nondimensional basic state (also called background or initial state), which is the flow whose stability is being investigated, namely

$$\mathbf{u} = \mathbf{u}_B + \varepsilon\,\mathbf{U} \qquad p = p_B + \varepsilon\,P \qquad T_f = T_{fB} + \varepsilon\,\theta \qquad T_s = T_{sB} + \varepsilon\,\phi, \quad (2.32)$$

where ε is an asymptotically small perturbation parameter. The hypothesis that the disturbances are infinitesimal allows one to investigate the linear stability of the system. It is called linear stability analysis because all the terms that are of $O(\varepsilon^2)$ or higher can be neglected. In the following only two dimensional stability problems are treated. This allows one to choose between a pressure-temperature and a streamfunction-temperature formulation of the eigenvalue problem. The streamfunction ψ is defined such that,

$$U = \frac{\partial \psi}{\partial y}, \quad V = -\frac{\partial \psi}{\partial x}. \qquad (2.33)$$

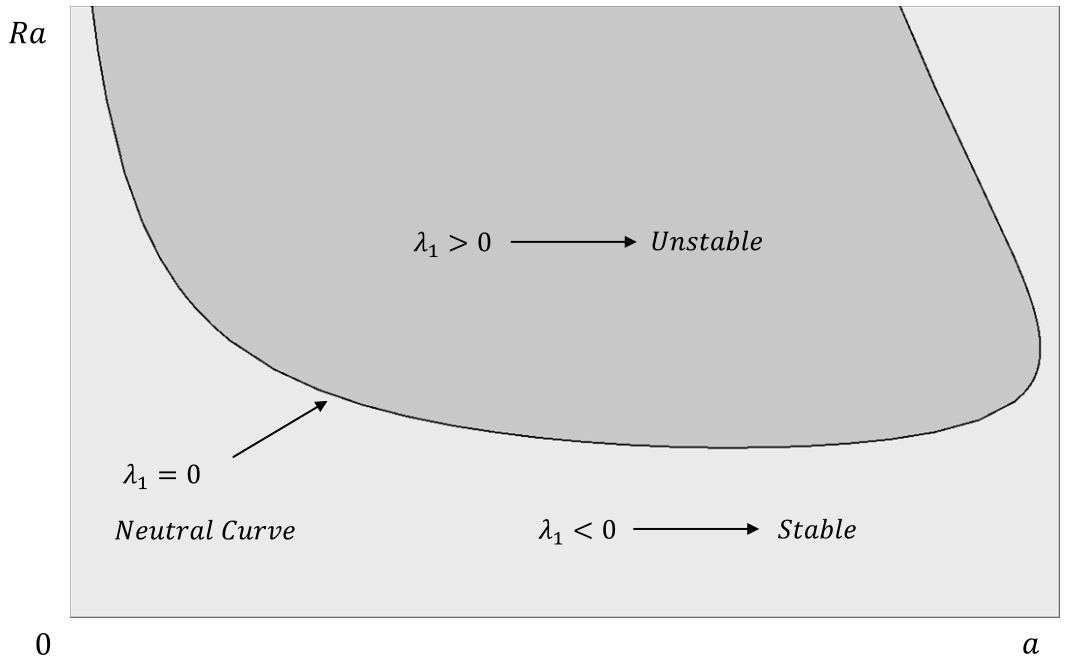

Figure 2.2: Stable and unstable regions in the plane (a, Ra).

The form of the disturbances superposed to the basic flow are chosen to be plane waves. Considering both the possible formulations and considering an infinitely wide horizontal porous layer with y as the vertical coordinate, the disturbances can be written in the form

$$\psi(\mathbf{x},t) = \Re\left\{\Psi(y)\, e^{\lambda t}\, e^{i\,(a_x\, x + a_z\, z)}\right\}, \qquad P(\mathbf{x},t) = \Re\left\{\mathcal{P}(y)\, e^{\lambda t}\, e^{i\,(a_x\, x + a_z\, z)}\right\}, \quad (2.34)$$
$$\theta(\mathbf{x},t) = \Re\left\{\Theta(y)\, e^{\lambda t}\, e^{i\,(a_x\, x + a_z\, z)}\right\},$$

where $\Re$ defines the real part of a given function and $\Psi(y)$, $\mathcal{P}(y)$, $\Theta(y)$, $\Phi(y)$ are complex amplitudes; it is understood that the real part of the right-hand side is taken in order to obtain the physical quantities. The complex notation is motivated by an easier formulation. The flow field is assumed to be unbounded in the x and z directions, hence the wavenumber components a_x and a_z can only be real so that the dependent variables remain bounded as $x, z \to \infty$; $\lambda = \lambda_1 + i\,\lambda_2$ where λ_1 is a real number and λ_2 is a complex number. If λ_1 is positive for any value of the wavenumber, the system is unstable to disturbances of this wavenumber vector (a_x, a_z), while if $\lambda_1 < 0$ the system

is stable. One can say that

$\lambda_1 < 0$: stable,

$\lambda_1 > 0$: unstable,

$\lambda_1 = 0$: neutrally or marginally stable.

This scheme is shown in Figure 2.2 where a typical example of thermoconvective instability governed by the Rayleigh number Ra is considered, and the plane (a, Ra) is divided in two regions both identified by different values of λ_1 and separated by the neutral or marginal stability curve.
The normal modes method, as it is clear from Eq.(2.34), involves decomposition of an arbitrary disturbance into a complete set of Fourier components. In this method the stability of each of the modes is examined separately, as the linearity of the problem implies that the various modes do not interact. The method leads to an eigenvalue problem. When $\lambda = \lambda_1 + i\,\lambda_2$ is set to zero, the marginal stability condition defines a region where a steady convective regime is to be expected. The minimum value of Ra on the neutral or marginal stability curve defines the critical point. Below the neutral stability curve all infinitesimal perturbations are damped. Here the principle of exchange of stabilities is assumed to hold. This principle establishes that all non-decaying disturbances are non oscillatory in time, Davis (25). In particular, it implies that when $\lambda_1 \geq 0$ then $\lambda_2 = 0$. Moreover, one can say that, if the principle of exchange of stabilities holds, travelling disturbances are forbidden. The term principle of exchange of stabilities was introduced by Jeffreys (34) in analogy with the stability theory of steady states of holonomic conservative systems. If $\lambda_2 \neq 0$ and $\lambda_1 \geq 0$ then the instability sets in as travelling waves of steady or growing amplitude. This kind of solutions is called over-stable.

2.4.1 Viscous dissipation and stability

Viscous dissipation can play an important role in the stability analysis of a basic throughflow in porous media. In this kind of problems, as for instance the Prats problem, a sufficiently intense temperature gradient is needed for the onset of convective instability. In the absence of a thermal forcing induced by the boundary conditions, the viscous dissipation effect may be the only possible cause of instability. For instance,

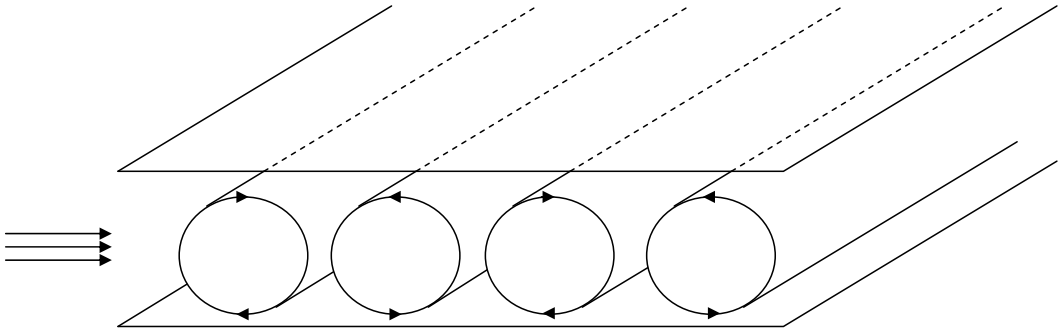

Figure 2.3: Sketch of transverse rolls, $\chi = 0$.

in a horizontal porous layer with a top isothermal boundary and a bottom adiabatic boundary, a possibly unstable stratification may be induced by the frictional heating associated with a basic horizontal throughflow. In the classical Darcy-Bénard problem the basic temperature gradient is forced by the boundary conditions and the viscous dissipation provides a non linear contribution or, more precisely, a second order term in the perturbations. The latter term, in a linear stability analysis, is neglected. On the other hand, if a basic throughflow is imposed, the viscous dissipation provides also a linear term in the perturbations and, thus, it may influence the onset conditions of the instability. From a Darcy-Bénard problem we are thus moving to a Prats-like problem. On studying the stability of a system with a given throughflow it is interesting to investigate the interaction between the orientation of the basic flow and the orientation of the disturbances. In the pressure-temperature formulation of the eigenvalue problem, for instance, one can assume disturbances of the form

$$P(\mathbf{x}, t) = \Re \left\{ \mathcal{P}(y)\, e^{\lambda t} e^{ia(x\, \cos\chi + z \sin\chi)} \right\}, \tag{2.35}$$

where χ is the angle between the basic flow direction and the perturbations direction. Now the limits $\chi = 0$, transverse rolls, and $\chi = \pi/2$, longitudinal rolls, correspond to the two cases shown in Figures 2.3 and 2.4

Each orientation of the disturbances is characterised by different values of the critical parameters for the onset of instability.

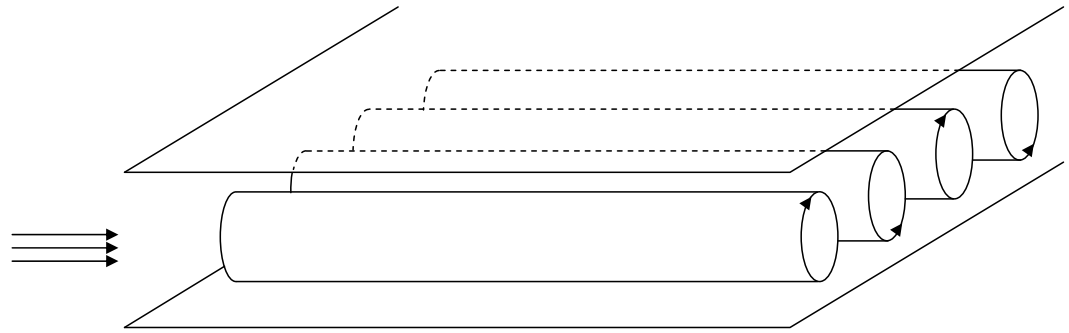

Figure 2.4: Sketch of longitudinal rolls, $\chi = \pi/2$.

2.5 Thermal boundary conditions

After the introduction, in the previous chapter, of the hydrodynamic boundary conditions and after the introduction of the thermal energy balance equations, the thermal boundary conditions are here discussed.

To simplify the discussion let us consider a horizontal two dimensional plane $(\bar{x}, \bar{y})$ layer with boundary walls at $\bar{y} = 0$ and $\bar{y} = L$. The boundaries $\bar{y} = 0$ and $\bar{y} = L$ could be adiabatic, with a prescribed nonvanishing heat flux, isothermal or imperfectly isothermal. If, for instance, the bottom wall is isothermal, the boundary condition is of the Dirichlet type and a prescribed temperature can be imposed, namely

$$\bar{y} = 0 \quad \longmapsto \quad \bar{T} = \bar{T}_w(\bar{x}). \tag{2.36}$$

If, on the other hand, there is an impressed heat flux on the bottom wall, a Neumann condition has to be used. Moreover, the prescribed heat flux condition a particular limit that can be expressed as

$$\bar{y} = 0 \quad \longmapsto \quad \frac{\partial \bar{T}}{\partial \bar{y}} = N(\bar{x}). \tag{2.37}$$

When the function $N(\bar{x}) \to 0$ one obtains the adiabatic condition, or zero heat flux condition. The imperfectly isothermal condition is a third type condition, Robin condition, and it is defined by

$$\bar{y} = 0 \quad \longmapsto \quad -k \frac{\partial \bar{T}}{\partial \bar{y}} = h\,[\bar{T} - \bar{T}_w(\bar{x})], \tag{2.38}$$

where h is the external heat transfer coefficient or the conductance of the boundary wall. Equation (2.38) implies, in its nondimensional form, the introduction of a parameter that describes the behaviour of the wall in the heat transfer to the external environment. In nondimensional coordinates this parameter is called Biot number and it is defined as

$$Bi = \frac{h\,L}{\tilde{k}}. \tag{2.39}$$

In this thesis all these types of thermal boundary conditions are used.

3

Viscous dissipation instabilities and Darcy's law

3.1 Introduction

The topic analysed in this chapter is the effect of viscous dissipation on a parallel Darcy flow. The system is composed by an horizontal porous layer with an adiabatic lower boundary and an isothermal upper boundary.

Many authors have developed variants of the HRL stability problem either by employing porous models that are more complicated than Darcy's law, or by altering the external conditions, such as imperfectly conducting boundaries or the presence of internal heating, rotation or vertical throughflow. With regard to what we shall call the Darcy-Bénard-Prats (DBP) problem, there exist some recent papers which have extended the work of Prats (65). Rees (69) considered the effect of quadratic form drag in the momentum equation. He showed that the critical Darcy-Rayleigh number depends on both the form drag coefficient and on the basic flow velocity. Moreover, the critical Darcy-Rayleigh number is also dependent on the roll orientation, with longitudinal rolls forming the preferred pattern. The additional effects of lateral confinement were considered by Delache, Ouarzazi and Néel (26); these authors found discontinuous transitions between preferred roll states. Postelnicu (64) extended the work of Rees (69) by combining it with the work of Banu and Rees (6), who employed the LTNE model for the local energy balance. A comprehensive set of results is presented by Postelnicu (64) showing the detailed effect on the critical Darcy-Rayleigh number and

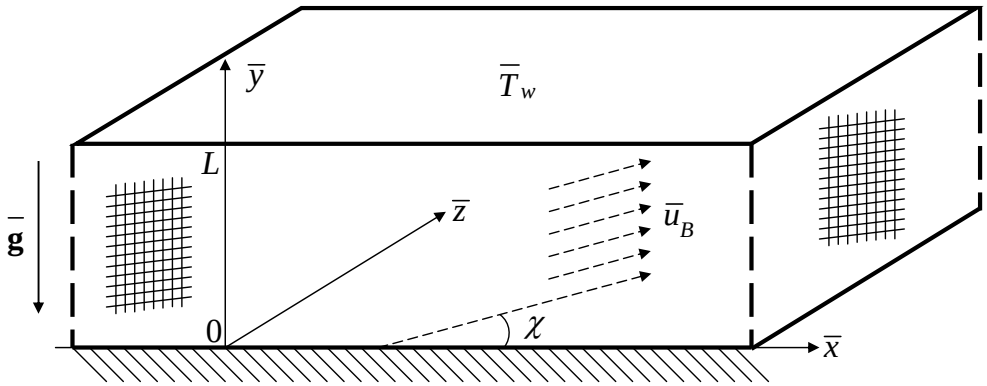

Figure 3.1: Sketch of the horizontal porous channel

wavenumber of the inertia parameter, the flow rate and the three parameters that are associated with local thermal non-equilibrium.

The aim of this chapter is to consider a variant of the DBP problem. In the above-cited works the thermoconvective instability was driven by an unstable temperature gradient that is imposed externally. In the present paper we shall assume that there is no imposed temperature gradient across the layer, but rather that heat is generated internally by the action of viscous dissipation. In particular the upper surface will be taken to be isothermal (infinite Biot number), while the lower surface is thermally insulated. The former boundary condition is relaxed later in the paper by using a finite-Biot-number condition to represent external heat transfer to the ambient temperature. A linear stability analysis of oblique rolls which are orientated arbitrarily with respect to the uniform basic flow direction is performed. The disturbance equations are solved both analytically by a series method and numerically by a fourth order Runge Kutta method. We present information on how the critical Darcy-Rayleigh number and wavenumber vary with the Gebhart and Péclet numbers. Asymptotic expressions for the critical quantities versus the Péclet number are obtained.

The contents of this chapter are based on the paper (10) by Barletta, Celli and Rees.

3.2 Mathematical model

We shall consider laminar buoyant flow in a horizontal parallel channel with height L. A sketch of the channel is shown in Figure 3.1.

Both the Darcy model and the Oberbeck-Boussinesq approximation are invoked. It is assumed that local thermal equilibrium holds. Heat generation due to the viscous dissipation contribution is taken into account. The components of the Darcy velocity along the $\bar{x}$-, $\bar{y}$- and $\bar{z}$-directions are denoted by $\bar{u}$, $\bar{v}$ and $\bar{w}$, respectively. The lower boundary wall $\bar{y} = 0$ is assumed to be adiabatic, while the upper boundary wall $\bar{y} = L$ is supposed to be isothermal with temperature $\bar{T}_w$. Both boundary walls are impermeable. Later in the paper we relax the assumption of having a perfectly conducting upper boundary.

In the Oberbeck-Boussinesq approximation the mass balance equation reduces to Eq.(1.6), namely

$$\bar{\nabla} \cdot \bar{\mathbf{u}} = 0. \tag{3.1}$$

The momentum balance equations are composed by the Darcy equations Eq.(1.9) with the buoyancy term simplified by the Oberbeck-Boussinesq approximation

$$\bar{\mathbf{u}} = \frac{K}{\mu} \left[-\bar{\nabla}\bar{p} + \rho_0 \, \bar{\mathbf{g}} \, \beta \, (\bar{T} - T_w) \right], \tag{3.2}$$

where $\bar{T}_0$ is here considered as equal to the boundary temperature $\bar{T}_w$. Equation (3.2) shows a dependence on $\bar{\mathbf{u}}$, $\bar{p}$ and $\bar{T}$. In the following we will apply a procedure that allows one to remove the explicit pressure contribution from our set of equations. In fact, if one applies the curl operator to both sides of Eq.(3.2), the pressure field disappears from the balance equation.

The thermal balance equation here used is Eq.(2.9), with the Darcy viscous dissipation term defined in Eq.(2.21), namely

$$\sigma \, \frac{\partial \bar{T}}{\partial \bar{t}} + \bar{\mathbf{u}} \cdot \bar{\nabla} \bar{T} = \tilde{\alpha} \, \bar{\nabla}^2 \bar{T} + \frac{\nu}{K \, c} \, \bar{\mathbf{u}} \cdot \bar{\mathbf{u}}, \tag{3.3}$$

where σ is defined by Eq.(2.10). The governing mass, momentum and energy balance equations can thus be expressed as

$$\frac{\partial \bar{u}}{\partial \bar{x}} + \frac{\partial \bar{v}}{\partial \bar{y}} + \frac{\partial \bar{w}}{\partial \bar{z}} = 0, \tag{3.4}$$

$$\frac{\partial \bar{v}}{\partial \bar{x}} - \frac{\partial \bar{u}}{\partial \bar{y}} = \frac{g \, \beta \, K}{\nu} \, \frac{\partial \bar{T}}{\partial \bar{x}}, \tag{3.5}$$

$$\frac{\partial \bar{v}}{\partial \bar{z}} - \frac{\partial \bar{w}}{\partial \bar{y}} = \frac{g\,\beta\,K}{\nu}\,\frac{\partial \bar{T}}{\partial \bar{z}}, \tag{3.6}$$

$$\frac{\partial \bar{u}}{\partial \bar{z}} - \frac{\partial \bar{w}}{\partial \bar{x}} = 0, \tag{3.7}$$

$$\sigma\,\frac{\partial \bar{T}}{\partial \bar{t}} + \bar{u}\,\frac{\partial \bar{T}}{\partial \bar{x}} + \bar{v}\,\frac{\partial \bar{T}}{\partial \bar{y}} + \bar{w}\,\frac{\partial \bar{T}}{\partial \bar{z}} = \tilde{\alpha}\left(\frac{\partial^2 \bar{T}}{\partial \bar{x}^2} + \frac{\partial^2 \bar{T}}{\partial \bar{y}^2} + \frac{\partial^2 \bar{T}}{\partial \bar{z}^2}\right) + \frac{\nu}{K\,c}\left(\bar{u}^2 + \bar{v}^2 + \bar{w}^2\right). \tag{3.8}$$

The velocity and temperature boundary conditions are expressed as

$$\bar{y} = 0: \quad \bar{v} = 0 = \frac{\partial \bar{T}}{\partial \bar{y}}, \qquad\qquad \bar{y} = L: \quad \bar{v} = 0, \quad \bar{T} = \bar{T}_w. \tag{3.9}$$

In this paper a horizontal pressure gradient is applied that produces a uniform flow of magnitude $\bar{u}_B$ having an inclination angle χ with respect to the x-direction; this is defined more precisely below.

3.2.1 Nondimensional formulation

Reducing the equations to a nondimensional form is a well established method that allows one to simplify the formulation of the set of equations describing the system studied. In particular, this procedure allows one to rewrite the equations in terms of nondimensional group numbers. To nondimensionalise an equation means rescaling each variable by its characteristic unit of measure. Here the characteristic length is chosen to be the height of the channel L, the characteristic time is defined by the ratio $\sigma\,L^2/\tilde{\alpha}$, the characteristic velocity is defined by $\tilde{\alpha}/L$ and the characteristic temperature is taken to be $\nu\,\tilde{\alpha}/K\,c$. Let us introduce nondimensional variables such that

$$\begin{aligned} (\bar{x}, \bar{y}, \bar{z}) &= (x, y, z)\,L, \qquad \bar{t} = t\,\frac{\sigma\,L^2}{\tilde{\alpha}}, \\ (\bar{u}, \bar{v}, \bar{w}) &= (u, v, w)\,\frac{\tilde{\alpha}}{L}, \qquad \bar{T} = \bar{T}_w + T\,\frac{\nu\,\tilde{\alpha}}{K\,c}. \end{aligned} \tag{3.10}$$

Then, Eqs. (3.4)–(3.8) can be rewritten as

$$\frac{\partial u}{\partial x} + \frac{\partial v}{\partial y} + \frac{\partial w}{\partial z} = 0, \tag{3.11}$$

$$\frac{\partial v}{\partial x} - \frac{\partial u}{\partial y} = Ge\,\frac{\partial T}{\partial x}, \tag{3.12}$$

$$\frac{\partial v}{\partial z} - \frac{\partial w}{\partial y} = Ge\,\frac{\partial T}{\partial z}, \tag{3.13}$$

$$\frac{\partial u}{\partial z} - \frac{\partial w}{\partial x} = 0, \tag{3.14}$$

$$\frac{\partial T}{\partial t} + u\,\frac{\partial T}{\partial x} + v\,\frac{\partial T}{\partial y} + w\,\frac{\partial T}{\partial z} = \frac{\partial^2 T}{\partial x^2} + \frac{\partial^2 T}{\partial y^2} + \frac{\partial^2 T}{\partial z^2} + u^2 + v^2 + w^2, \tag{3.15}$$

where the Gebhart number is given by,

$$Ge = \frac{g\,\beta\,L}{c}. \tag{3.16}$$

The Gebhart number introduced in Eq.(2.2) and it is a nondimensional parameter associated with the viscous dissipation. It measures the extent to which compression work and viscous dissipation influence the energy balance in the fluid flow. The boundary conditions (3.9) may be expressed in a nondimensional form as

$$y = 0: \qquad v = \frac{\partial T}{\partial y} = 0, \qquad\qquad y = 1: \qquad v = T = 0. \tag{3.17}$$

3.2.2 Fully developed basic flow

A horizontal steady parallel flow in the direction of the unit vector $\mathbf{s} = (\cos\chi, 0, \sin\chi)$ lying in the $x - z$–plane is here assumed. Moreover, a purely vertical heat flux exists due to the effect of the viscous dissipation.

The basic state, which we will analyse for stability, is thus given by,

$$u_B = Pe\,\cos\chi, \quad v_B = 0, \quad w_B = Pe\,\sin\chi, \quad T_B = \frac{Pe^2}{2}(1 - y^2), \tag{3.18}$$

where

$$Pe = \frac{\bar{\mathbf{u}}_B \cdot \mathbf{s}\,L}{\tilde{\alpha}}, \tag{3.19}$$

defines the Péclet number based on the uniform basic flow velocity $\bar{\mathbf{u}}_B \cdot \mathbf{s}$. This nondimensional number measures the ratio between the strength of the basic fluid flow and the strength of molecular diffusion. Obviously, it is not restrictive to assume that $\bar{\mathbf{u}}_B \cdot \mathbf{s} > 0$, i.e. $Pe > 0$. We choose to incline the basic flow and not to incline the disturbances in order to simplify the formulation of the eigenvalue problem algebra.

3.2.3 Linear disturbances

A stability analysis is performed in the following sections and the approach used here to investigate stability is the normal modes method described in Chapter 2. The normal modes method requires the introduction of the disturbances. These disturbances are meant to perturb the basic state defined by Eq. (3.18) and are taken to be of the form of Eq. (2.32), namely

$$u = u_B + \varepsilon\, U, \quad v = v_B + \varepsilon\, V, \quad w = w_B + \varepsilon\, W, \quad T = T_B + \varepsilon\, \theta. \tag{3.20}$$

where ε is an asymptotically small perturbation parameter. The stability analysis that follows has been chosen to be linear, this implies that all those terms that are, after the substitution of Eq. (3.20) in Eqs. (3.11)-(3.15), of order greater than ε are neglected. Thus, on substituting Eq. (3.20) in Eqs. (3.11)-(3.15) and neglecting nonlinear terms in the perturbations, i.e. terms of $O(\varepsilon^2)$, we obtain the linearized stability equations,

$$\frac{\partial U}{\partial x} + \frac{\partial V}{\partial y} + \frac{\partial W}{\partial z} = 0, \tag{3.21}$$

$$\frac{\partial V}{\partial x} - \frac{\partial U}{\partial y} = Ge\, \frac{\partial \theta}{\partial x}, \tag{3.22}$$

$$\frac{\partial V}{\partial z} - \frac{\partial W}{\partial y} = Ge\, \frac{\partial \theta}{\partial z}, \tag{3.23}$$

$$\frac{\partial U}{\partial z} - \frac{\partial W}{\partial x} = 0, \tag{3.24}$$

$$\begin{aligned} &\frac{\partial \theta}{\partial t} + Pe\, \cos\chi\, \frac{\partial \theta}{\partial x} + Pe\, \sin\chi\, \frac{\partial \theta}{\partial z} - Pe^2 V y \\ &\qquad = \frac{\partial^2 \theta}{\partial x^2} + \frac{\partial^2 \theta}{\partial y^2} + \frac{\partial^2 \theta}{\partial z^2} + 2\, Pe\, \cos\chi\, U + 2\, Pe\, \sin\chi\, W, \end{aligned} \tag{3.25}$$

where use has been made of Eq. (3.18). The linearity of Eqs. (3.21)–(3.25) implies that, due to the superposition property, one may treat rolls of different orientations separately with regard to instability. An advantage is that each of these cases can be dealt with using a purely 2D analysis.

3.3 Instability with respect to oblique rolls

We will introduce disturbances in the form of periodic roll solutions. Given that χ is an arbitrary direction it is not restrictive to consider rolls with axis along the z-direction by setting,

$$U = U(x, y, t), \quad V = V(x, y, t), \quad W = 0, \quad \theta = \theta(x, y, t). \tag{3.26}$$

Substituting Eqs. (3.26) in Eqs. (3.21)–(3.25) the system of equations thus becomes

$$\frac{\partial U}{\partial x} + \frac{\partial V}{\partial y} = 0, \tag{3.27}$$

$$\frac{\partial V}{\partial x} - \frac{\partial U}{\partial y} = Ge\, \frac{\partial \theta}{\partial x}, \tag{3.28}$$

$$\frac{\partial \theta}{\partial t} + Pe\, \cos\chi\, \frac{\partial \theta}{\partial x} - Pe^2 V y = \frac{\partial^2 \theta}{\partial x^2} + \frac{\partial^2 \theta}{\partial y^2} + 2\, Pe\, \cos\chi\, U. \tag{3.29}$$

One can introduce a streamfunction, ψ, such that

$$U = Pe^{-2}\, \frac{\partial \psi}{\partial y}, \quad V = -\, Pe^{-2}\, \frac{\partial \psi}{\partial x}. \tag{3.30}$$

Applying Eqs. (3.30) to the set of Eqs. (3.27)-(3.29) then one can note that Eq. (3.24) is satisfied identically. We choose to divide both components by Pe^2 to rearrange the nondimensional numbers in a convenient form. Eqs. (3.27)-(3.29) may now be rewritten in the form

$$\frac{\partial^2 \psi}{\partial x^2} + \frac{\partial^2 \psi}{\partial y^2} + GePe^2\, \frac{\partial \theta}{\partial x} = 0, \tag{3.31}$$

$$\frac{\partial \theta}{\partial t} + Pe \cos\chi\, \frac{\partial \theta}{\partial x} + y \frac{\partial \psi}{\partial x} = \frac{\partial^2 \theta}{\partial x^2} + \frac{\partial^2 \theta}{\partial y^2} + 2\, Pe^{-1} \cos\chi\, \frac{\partial \psi}{\partial y}. \tag{3.32}$$

The boundary conditions fulfilled by ψ and θ are easily inferred from Eqs. (3.17), (3.18), (3.20) and (3.30), namely

$$y = 0: \quad \psi = \frac{\partial \theta}{\partial y} = 0, \qquad\qquad y = 1: \quad \psi = \theta = 0. \tag{3.33}$$

Solutions of Eqs. (3.31)-(3.33) are sought in the form of plane waves. These waves can be expressed as in Eq. (2.34), namely

$$\psi(x, y, t) = \Re\Big\{ \Psi(y)\, e^{\lambda t} e^{iax} \Big\}, \quad \theta(x, y, t) = \Re\Big\{ \Theta(y)\, e^{\lambda t} e^{iax} \Big\}, \tag{3.34}$$

where the positive real constant a is the prescribed wavenumber, while $\lambda = \lambda_1 + i\lambda_2$ is a complex exponential growth rate to be determined. We shall set $\lambda_1 = 0$ in order to investigate neutral stability. Moreover, for numerical convenience we shall also set,

$$\gamma = \lambda_2 + aPe\cos\chi. \tag{3.35}$$

By substituting Eq. (3.34) in Eqs. (3.31) and (3.32), we obtain

$$\Psi'' - a^2\,\Psi + ia\,R\,\Theta = 0, \tag{3.36}$$

$$\Theta'' - (i\gamma + a^2)\,\Theta + 2\,P^{-1}\Psi' - ia\,y\,\Psi = 0, \tag{3.37}$$

where the primes denote differentiation with respect to y, and where we have introduced the nondimensional parameters,

$$R = GePe^2, \qquad P = Pe/\cos\chi. \tag{3.38}$$

In Eq. (3.38) R plays the role of a Darcy-Rayleigh number as it multiplies the buoyancy term, while P is a modified Péclet number. Elimination of Θ between Eqs. (3.36) and (3.37) yields a fourth order ordinary differential equation for $\Psi(y)$, namely

$$\Psi'''' - (2a^2 + i\gamma)\Psi'' - 2iaRP^{-1}\Psi' + a^2(a^2 - Ry + i\gamma)\Psi = 0. \tag{3.39}$$

The boundary conditions fulfilled by $\Psi(y)$ are easily deduced from Eqs. (3.33)-(3.34),

$$y = 0: \quad \Psi = \Psi''' - a^2\,\Psi' = 0, \qquad\qquad y = 1: \quad \Psi = \Psi'' = 0. \tag{3.40}$$

Equations (3.34) and (3.35) imply that the perturbation wave travels in the x-direction with a nondimensional phase velocity

$$c_{wave} = Pe\cos\chi - \frac{\gamma}{a}\ . \tag{3.41}$$

If $c_{wave} > 0$, the wave travels in the same direction as the basic flow. On the other hand, if $c_{wave} < 0$, the wave travels in the direction opposite to the basic flow.

3.3.1 The eigenvalue problem

The homogeneity of Eqs. (3.39) and (3.40) implies that $\Psi(y)$ is defined only up to an arbitrary overall scale factor, which means that we may set $\Psi'(0) = 1$ as a normalisation condition.

These equations form an ordinary differential eigenvalue problem for R and γ for any chosen wavenumber, a, and modified Péclet number, P. Given the definition of R in Eq. (3.38), this means that the critical Gebhart number may be found in terms of the Péclet number. It is more satisfactory from a physical point of view to obtain a critical Péclet number as a function of the Gebhart number, but although one may plot the variation of the critical Gebhart number with the Péclet number, it turns out that R remains of $O(1)$ through the physically acceptable range of values of Ge.

3.3.2 Longitudinal rolls

Let us first analyse the longitudinal rolls. A basic flow inclined of $\chi = \pi/2$ is considered. With $\chi = \pi/2$ the parameter P tends to ∞. Applying the latter condition to Eq.(3.39) one obtains

$$\Psi'''' - (2a^2 + i\gamma)\Psi'' + a^2(a^2 - Ry + i\gamma)\Psi = 0, \tag{3.42}$$

Equation (3.42), together with its boundary conditions Eqs.(3.40), can be solved for a real valued function $\Psi(y)$ by setting $\gamma = 0$. This means that the eigenvalue problem is self-adjoint in this case.

3.3.3 Transverse rolls

Transverse rolls refer to those basic flows parallel to the x–direction, i.e. $\chi = 0$. With $\chi = 0$ the parameter P reduces to Pe. Applying the latter condition to Eq.(3.39) one obtains

$$\Psi'''' - (2a^2 + i\gamma)\Psi'' - 2iaRPe^{-1}\Psi' + a^2(a^2 - Ry + i\gamma)\Psi = 0. \tag{3.43}$$

The flow under exam has a source of possible instability that is connected to the combined effects of viscous heating and buoyancy. The viscous heating inside the fluid is both caused by the basic flow and by the small perturbation of this flow. In other words,

the nonuniform temperature distribution in the channel responsible of the buoyancy force is partly generated by the basic flow dissipation, u_B^2, and partly by the linearized perturbation flow dissipation, $2\,u_B\,U$. However, the former contribution is expected to be far more intense than the latter. Hence, when analyzing the propagation of the perturbation wave, one can neglect the last term on the right hand side of Eq.(3.32), $2\,Pe^{-1}\,\partial\psi/\partial y$. This simplification implies that Eq.(3.43) loses the term proportional to Ψ' and thus reads

$$\Psi'''' - (2a^2 + i\gamma)\Psi'' + a^2(a^2 - Ry + i\gamma)\Psi = 0. \tag{3.44}$$

that is the same result as shown by the Eq.(3.42).

There is an alternative view of the approximation introduced. In Equation (3.39), the linearized perturbation flow dissipation, Ψ' results into a term proportional to R/Pe, while the vertical convective term Ψ results into a term proportional to R. One can easily verify that, for most convection problems involving liquids, Ge can hardly be greater than 10^{-6}, unless $L \approx 1\,m$ or higher. Therefore, R/Pe is expected to be normally much smaller than 1. Moreover, flows such that viscous dissipation yields an important viscous heating and possibly produces a buoyancy induced instability of the uniform basic flow are expected to yield values of Pe significantly greater than one. Thus, it is reasonable to assume that the term proportional to R/Pe is negligible with respect to the other terms in Eq.(3.39) and, in particular, to that proportional to R. In these circumstances, therefore, the onset criterion is independent of χ, as in the DBP problem (65).

3.4 Series solution

Equations (3.39) subject to (3.40) may be solved by a power series method using

$$\Psi(y) = \sum_{n=0}^{\infty} \frac{A_n}{n!}\, y^n. \tag{3.45}$$

The three known initial conditions on the eigenfunction $\Psi(y)$ allow one to obtain the coefficients A_0, A_1 and A_3, namely

$$A_0 = 0, \quad A_1 = 1, \quad A_3 = a^2, \tag{3.46}$$

while A_2 will need to be obtained by prescribing the boundary conditions at $y = 1$, Eq. (3.40). Higher order coefficients A_n may be determined by substituting Eq. (3.45) into Eq. (3.39) and collecting like powers of y. One thus obtains

$$A_4 = \left(2\,a^2 + i\,\gamma\right) A_2 + 2\,i\,aRP^{-1}, \tag{3.47}$$

and the recursion relationship

$$\begin{aligned} A_{n+4} &= \left(2\,a^2 + i\,\gamma\right) A_{n+2} + 2\,i\,aRP^{-1}\,A_{n+1} - a^2\left(a^2 + i\,\gamma\right) A_n \\ &+ n\,a^2\,R\,A_{n-1}\ , \quad \forall\, n \geq 1. \end{aligned} \tag{3.48}$$

The series solution given by Eq. (3.45) has a very rapid convergence. The real values of R and γ and the complex value of A_2 are obtained by ensuring that the two complex boundary conditions at $y = 1$ are satisfied. In all the following cases six digits of accuracy may be achieved by truncating the sum to the first 40 terms. Neutral curves may be traced out by varying the value of a. The value of a which minimises R is termed the critical wavenumber, and denoted by a_{cr}.
We also used a 4th order Runge Kutta code together with the shooting method as an alternative numerical procedure. In the following, all the numerical results are obtained by both methods in order to ensure their cross-validation.

3.5 Stability analysis

When considering longitudinal rolls, Eq. (3.42), a complex 4th order system has to be solved. The neutral stability curve for this case is given in Figure 3.2, which shows that it has the classical shape for Bénard-like problems. In this case we find that

$$R_{cr} = 61.8666 \qquad \text{and} \qquad a_{cr} = 2.44827. \tag{3.49}$$

Therefore we may state that

$$Pe_{cr} = 7.8655 Ge^{-1/2}, \tag{3.50}$$

where all decimal places quoted are exact. Given the order of magnitude of the values just obtained, the approximation introduced in Section 3.3.3 can be considered as valid.

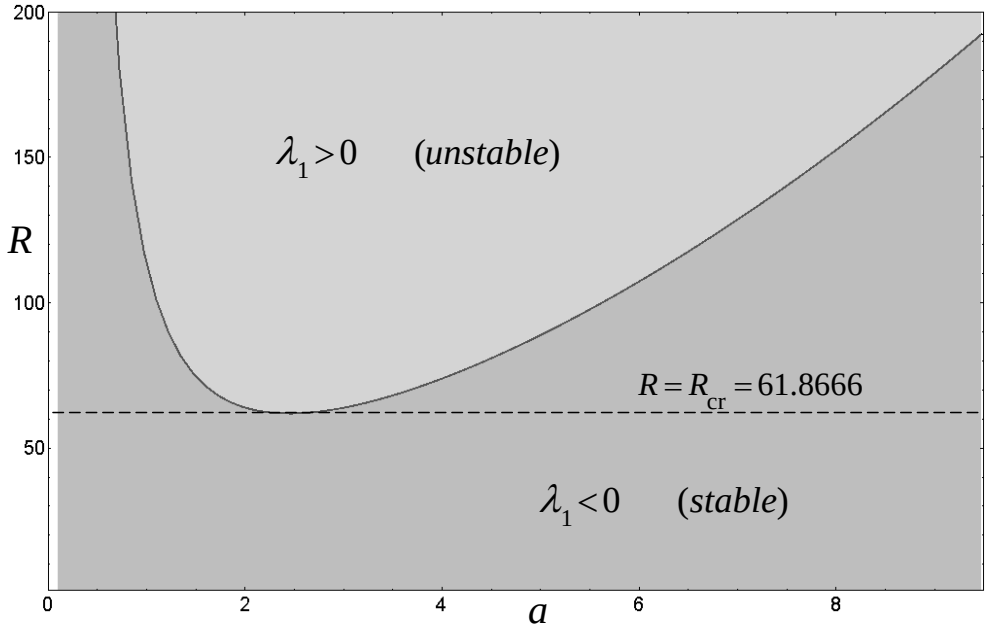

Figure 3.2: Stability diagram in the plane (a, R) in the case of perfectly isothermal upper wall ($Bi \to \infty$) for longitudinal rolls, $\chi = \pi/2$.

In Figs. 3.3 and 3.4 we show the respective variation of R_{cr} with P and G, where G is defined as

$$G = Ge\,(\cos\chi)^2. \tag{3.51}$$

From Eq. (3.38), the latter parameter is such that $R = G\,P^2$. Also shown are the three-term large-P asymptotic solutions given by Eq. (3.90). These figures show that there is only a fairly weak variation in the critical values with both these parameters. In fact, the three-term asymptotic expansion of R_{cr} yields extremely accurate solutions over a range of G which is much bigger than is physically achievable for a porous medium. A detailed comparison between the asymptotic and the numerical results shows that the error in R_{cr} exceeds 1% once $Ge > 0.45$ or, equivalently, $Pe < 0.64$.

The physical meaning of the governing parameter R is the following. Let us consider the basic temperature difference between the lower and upper wall; from Eqs. (3.10), (3.18) and (3.19) it is

$$\Delta T = \bar{T}_B(0) - \bar{T}_B(L) = \frac{\nu\,\alpha}{K\,c}\frac{Pe^2}{2} = \frac{\nu\,L^2\,\bar{u}_B^2}{2\,K\,\alpha\,c}. \tag{3.52}$$

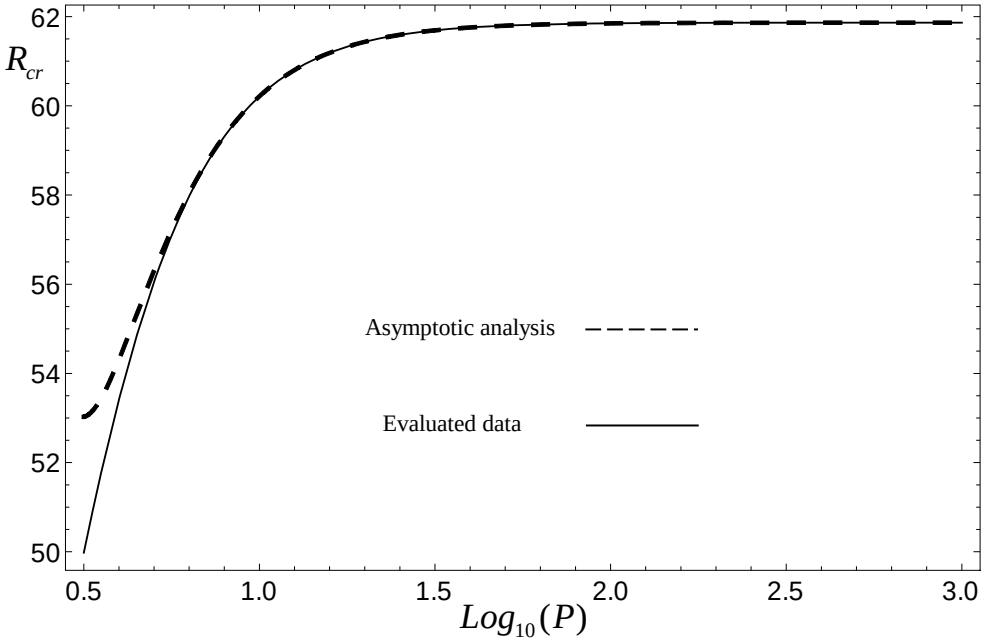

Figure 3.3: Perfectly isothermal upper wall ($Bi \to \infty$). R_{cr} vs P diagram: comparison between the evaluated data and the asymptotic expansions.

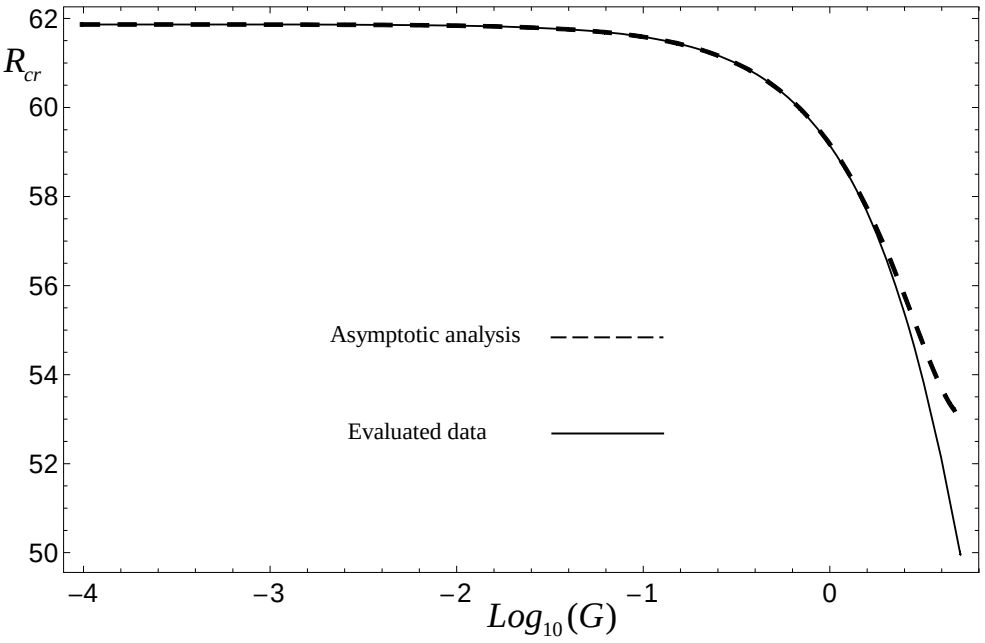

Figure 3.4: Perfectly isothermal upper wall ($Bi \to \infty$). R_{cr} vs G diagram: comparison between the evaluated data and the asymptotic expansions.

Then, on account of Eqs. (3.16), (3.19), (3.38) and (3.52), R can be rewritten as

$$R = 2\,\frac{g\,\beta\,\Delta T\,K\,L}{\nu\,\alpha} = 2\,Ra. \tag{3.53}$$

In fact, the ratio appearing in Eq. (3.53) is the Darcy-Rayleigh number, Ra, based on the wall temperature difference ΔT given by Eq. (3.52). This observation allows us to establish a possible comparison between the results of the present stability analysis with that of the classical HRL problem or, more precisely, of the Prats problem. In fact, Prats considered a horizontal porous layer subject to a uniform parallel flow and such that the lower boundary plane is isothermal at a temperature higher than that of the upper isothermal boundary plane. This author did not consider the effect of viscous dissipation and proved that, as in the HRL problem, the critical value of Ra for the onset of free convection rolls is

$$Ra_{cr} = 4\,\pi^2 \approx 39.4784, \tag{3.54}$$

where the Darcy-Rayleigh number is evaluated by taking ΔT as the prescribed temperature difference between the lower and the upper boundary planes. Obviously, Prats problem is substantially different from the problem examined in the present paper. However, a comparison between the value of Ra_{cr} predicted by Prats, Eq. (3.54), and that obtainable from Eqs. (3.49) and (3.53),

$$Ra_{cr} = 30.9333, \tag{3.55}$$

can be interesting. A physical explanation of the reason why Ra_{cr} for the present problem is smaller than that of the Prats problem is possible. For a given value of ΔT, the basic flow of the Prats problem corresponds to a linear decrease of temperature from the bottom boundary to the upper boundary. On the other hand, the basic flow of the present problem corresponds to a parabolic decrease of temperature from the bottom boundary to the upper boundary. More precisely, for a given temperature T_w of the upper boundary and a given temperature difference ΔT, the basic flow of the Prats problem corresponds to an average fluid temperature smaller than that of the present problem. Then, for a given value of Ra, the effect of buoyancy is higher for the present problem than for the Prats problem. This reasoning justifies why the onset of

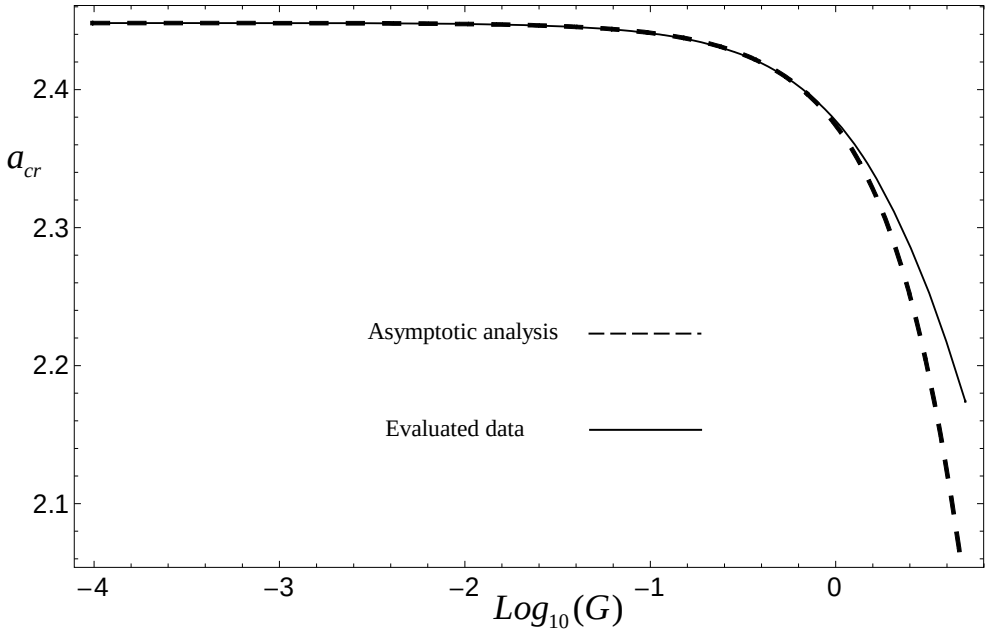

Figure 3.5: Perfectly isothermal upper wall ($Bi \to \infty$). a_{cr} vs G diagram: comparison between the evaluated data and the asymptotic expansions.

convective instability occurs for a smaller Ra_{cr} in the problem examined in the present paper.

The use of the parameter R in order to discuss the onset of instability in the present problem suggests a further reflection. In most stability analyses, where the buoyancy effect is driven by the prescribed thermal boundary conditions, the governing parameter is the Darcy-Rayleigh Ra number based on a temperature difference ΔT depending on the thermal boundary conditions. As a consequence, the existence of a critical value for Ra suggests that a basic flow or state can be stable or not depending on the permeability K of the porous layer. On the other hand, the analysis performed in present paper predicts that the instability may take place when $R > R_{cr}$, where R is independent of the permeability K as it is shown by Eqs. (3.16), (3.19) and (3.38). Therefore, one may conclude that, as long as the assumptions made in the present analysis hold, the permeability has no influence on the occurrence of the instability for the parallel viscous heating flow in a horizontal porous layer. The reason why, in the problem examined here, the use of R instead of Ra come forth naturally is that one does not impose directly a temperature difference ΔT to the fluid. On the contrary, a non-uniform

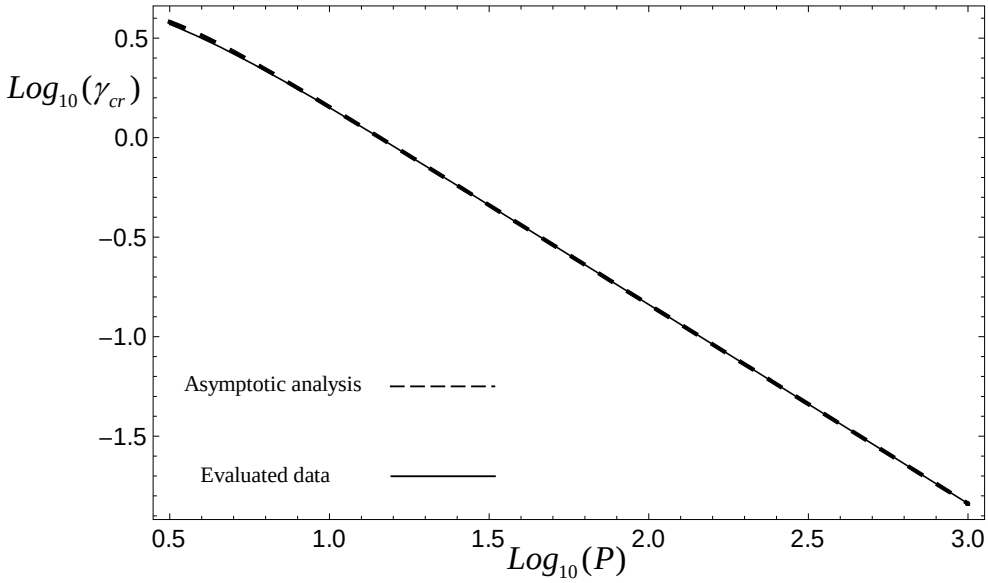

Figure 3.6: Perfectly isothermal upper wall ($Bi \to \infty$). γ_{cr} vs P diagram: comparison between the evaluated data and the asymptotic expansions.

temperature distribution naturally arises as a consequence of viscous dissipation, as it is expressed in Eq. (3.18).

Figure 3.5 shows how the critical wavenumber varies with G. At large values of P (or, equivalently, small values of G), the critical wavenumber is approximately constant, reducing strongly as P and G tend toward $O(1)$ magnitudes. Figure 3.6 shows the reduced wavespeed, γ. The variation of γ is roughly linear with P^{-1}, as shown in the next Section. In both cases, the asymptotic expansions given in the next Section yield extremely accurate representations of the numerical results. Finally, we note that, since $Ge \ll 1$ implies that $Pe_{cr} \gg 1$, it is possible that inertia drag effects will be significant; it will be reported on this aspect in the next chapter.

3.5.1 Asymptotic analysis of rolls for large P

Eqs. (3.36) and (3.37) are

$$\Psi'' - a^2\,\Psi + ia\,R\,\Theta = 0, \tag{3.56}$$

$$\Theta'' - (i\gamma + a^2)\,\Theta + 2\,P^{-1}\Psi' - ia\,y\,\Psi = 0, \tag{3.57}$$

The aim of this Appendix is to provide an asymptotic analysis of the solutions of the above equations which are valid in the limit of small Ge, or, equivalently, large P. We shall employ the following substitutions,

$$\Psi \longrightarrow i\,\Psi, \qquad \varepsilon = P^{-1}, \tag{3.58}$$

to transform Eqs. (3.56) and (3.57) into a form which is more convenient for the asymptotic analysis. We obtain the system,

$$\Psi'' - a^2\Psi + a\,R\,\Theta = 0, \tag{3.59}$$

$$\Theta'' - (\gamma + a^2)\,\Theta + (2i\Psi')\varepsilon + ay\Psi = 0. \tag{3.60}$$

According to the numerical results presented earlier, R remains of $O(1)$ throughout the whole physically admissible range of values of Ge. Moreover, the small parameter ε, multiplies just one term. In what follows various streamfunction and temperature terms will be defined as part of the asymptotic analysis, and they will all satisfy the boundary conditions given in Eq. (3.33).

Guided by the numerical results and by the form of the Eqs. (3.59) and (3.60), we shall introduce the small-ε expansions,

$$\Psi = \Psi_0 + \varepsilon\Psi_1 + \varepsilon^2\Psi_2 + \varepsilon^3\Psi_3 + \varepsilon^4\Psi_4 + \cdots, \tag{3.61}$$

$$\Theta = \Theta_0 + \varepsilon\Theta_1 + \varepsilon^2\Theta_2 + \varepsilon^3\Theta_3 + \varepsilon^4\Theta_4 + \cdots, \tag{3.62}$$

$$R = R_0 + \varepsilon^2 R_2 + \varepsilon^4 R_4 + \cdots, \tag{3.63}$$

$$\gamma = \varepsilon\gamma_1 + \varepsilon^3\gamma_3 + \cdots, \tag{3.64}$$

and

$$a = a_0 + \varepsilon^2 a_2 + \varepsilon^4 a_4 + \cdots. \tag{3.65}$$

At each stage we equate coefficients of like powers of ε to obtain equations for the various Ψ_n and Θ_n terms.

At $O(1)$ we obtain the system,

$$\mathcal{L}_1(\Psi_0, \Theta_0) \equiv \Psi_0'' - a_0^2\Psi_0 + a_0 R_0 \Theta_0 = 0, \tag{3.66}$$

$$\mathcal{L}_2(\Psi_0, \Theta_0) \equiv \Theta_0'' - a_0^2\Theta_0 + a_0 y \Psi_0 = 0. \tag{3.67}$$

Here we have introduced the notation $\mathcal{L}_n$ for later convenience. This homogeneous system may be solved by setting a normalisation condition such as $\Theta_0(0) = 1$, and then R_0 is found as an eigenvalue. Further terms in (3.62) will be taken to satisfy the boundary condition $\Theta_n(0) = 0$.

Equations (3.66) and (3.67) are such that R_0 is a function of the wavenumber, a, and it is necessary to minimise R_0 with respect to a. If we define Ψ_m and Θ_m to be the respective a-derivatives of Ψ_0 and Θ_0, then the a-derivative of Eqs. (3.66) and (3.67) yield the system,

$$\mathcal{L}_1(\Psi_m, \Theta_m) = 2a_0\Psi_0 - R_0\Theta_0, \tag{3.68}$$

$$\mathcal{L}_2(\Psi_m, \Theta_m) = 2a_0\Theta_0 - y\Psi_0, \tag{3.69}$$

where we have set $dR_0/da = 0$. The solution of this additional system yields the value of a_0 which minimises R_0.

At $O(\varepsilon)$ we obtain,

$$\mathcal{L}_1(\Psi_1, \Theta_1) = 0, \tag{3.70}$$

$$\mathcal{L}_2(\Psi_1, \Theta_1) = i\gamma_1\Theta_0 - 2i\Psi_0'. \tag{3.71}$$

This is an eigenvalue problem for γ_1 and it may be solved using real arithmetic by means of the substitutions, $\Psi_1 = i\Psi_{1a}$, $\Theta_1 = i\Theta_{1a}$.

At $O(\varepsilon^2)$ the resulting system is,

$$\mathcal{L}_1(\Psi_2, \Theta_2) = a_2\Big[2a_0\Psi_0 - R_0\Theta_0\Big] + \Big[-a_0 R_2\Theta_0\Big], \tag{3.72}$$

$$\mathcal{L}_2(\Psi_2, \Theta_2) = a_2\Big[2a_0\Theta_0 - y\Psi_0\Big] + i\Big[\gamma_1\Theta_1 - 2\Psi_1'\Big]. \tag{3.73}$$

Given that the terms multiplying a_2 on the right hand sides of (3.72) and (3.73) are identical to those on the right hand sides of (3.68) and (3.69), it is possible to write the solution in the form,

$$\Psi_2 = a_2\Psi_m + \Psi_{2a}, \qquad \Theta_2 = a_2\Theta_m + \Theta_{2a}. \tag{3.74}$$

The functions Ψ_{2a} and Θ_{2a} satisfy the system,

$$\mathcal{L}_1(\Psi_{2a}, \Theta_{2a}) = \Big[-a_0 R_2 \Theta_0\Big], \tag{3.75}$$

$$\mathcal{L}_2(\Psi_{2a}, \Theta_{2a}) = i\Big[\gamma_1\Theta_1 - 2\Psi_1'\Big]. \tag{3.76}$$

We note that Eqs. (3.75) and (3.76) have real inhomogeneous terms, and that the system is an eigenvalue problem for R_2. On the other hand, the value of a_2 is not determined at this order, but (3.74) shows that one component of the overall second order solution is proportional to a_2, which will be determined at $O(\varepsilon^4)$.
At $O(\varepsilon^3)$ we have,

$$\mathcal{L}_1(\Psi_3, \Theta_3) = a_2\Big[2a_0\Psi_1 - R_0\Theta_1\Big] - a_0 R_2\Theta_1, \tag{3.77}$$

$$\mathcal{L}_2(\Psi_3, \Theta_3) = a_2\Big[2a_0\Theta_1 - y\Psi_1\Big] + i\Big[-2\Psi_2' + \gamma_1\Theta_2 + \gamma_3\Theta_0\Big]. \tag{3.78}$$

We note that the inhomogeneous terms are purely imaginary, and given that a_2 appears again as a coefficient, we may split the solution of (3.77) and (3.78) into two components:

$$\begin{pmatrix}\Psi_3\\ \Theta_3\\ \gamma_3\end{pmatrix} = ia_2\begin{pmatrix}\Psi_{3a}\\ \Theta_{3a}\\ \gamma_{3a}\end{pmatrix} + i\begin{pmatrix}\Psi_{3b}\\ \Theta_{3b}\\ \gamma_{3b}\end{pmatrix}. \tag{3.79}$$

Therefore we need to solve the two systems of equations,

$$\mathcal{L}_1(\Psi_{3a}, \Theta_{3a}) = 2a_0\Psi_{1a} - R_0\Theta_{1a} + \gamma_{3a}\Theta_0, \tag{3.80}$$

$$\mathcal{L}_2(\Psi_{3a}, \Theta_{3a}) = 2a_0\Theta_{1a} - y\Psi_{1a} - 2\Psi_m' + \gamma_1\Theta_m, \tag{3.81}$$

and

$$\mathcal{L}_1(\Psi_{3b}, \Theta_{3b}) = -a_0 R_2\Theta_{1a}, \tag{3.82}$$

$$\mathcal{L}_2(\Psi_{3b}, \Theta_{3b}) = -2\Psi'_{2a} + \gamma_1\Theta_{2a} + \gamma_{3b}\Theta_0. \tag{3.83}$$

These are, respectively, eigenvalue problems for γ_{3a} and γ_{3b}. Finally, at $O(\varepsilon^4)$, the equations are

$$\begin{aligned}\mathcal{L}_1(\Psi_4, \Theta_4) = a_4\Big[2a_0\Psi_0 - R_0\Theta_0\Big] + a_2\Big[-R_2\Theta_0 - R_0\Theta_{2a} + 2a_0\Psi_{2a} - a_0R_2\Theta_m\Big] \\ + a_2^2\Big[\Psi_0 + 2a_0\Psi_m - R_0\Theta_m\Big] - a_0R_2\Theta_{2a} - a_0R_4\Theta_0,\end{aligned} \tag{3.84}$$

$$\begin{aligned}\mathcal{L}_2(\Psi_4, \Theta_4) = a_4\Big[2a_0 - \Psi_0\Big] + a_2\Big[2a_0\Theta_{2a} - y\Psi_{2a} - \gamma_1\Theta_{3a} + 2\Psi'_{3a}\Big] \\ + a_2^2\Big[\Theta_0 + 2a_0\Theta_m - y\Psi_{2m}\Big] + 2\Psi'_{3b} - \gamma_1\Theta_{3b} + \gamma_3\Theta_{1a}.\end{aligned} \tag{3.85}$$

This more complicated system may be split into four separate systems for ease of computation:

$$\begin{pmatrix}\Psi_4 \\ \Theta_4 \\ R_4\end{pmatrix} = a_4\begin{pmatrix}\Psi_m \\ \Theta_m \\ 0\end{pmatrix} + a_2^2\begin{pmatrix}\Psi_{4a} \\ \Theta_{4a} \\ R_{4a}\end{pmatrix} + a_2\begin{pmatrix}\Psi_{4b} \\ \Theta_{4b} \\ R_{4b}\end{pmatrix} + \begin{pmatrix}\Psi_{4c} \\ \Theta_{4c} \\ R_{4c}\end{pmatrix}. \tag{3.86}$$

We have already taken account of the fact that the solution corresponding to a_4 is already known. It is now routine to write out the remaining three systems, but these are omitted for the sake of brevity. However, these three systems form eigenvalue problems for R_{4a}, R_{4b} and R_{4c} respectively.

This latest solution means that, while R_0 and R_2 are computed constants, the value of R_4 is not; we have

$$R_4 = R_{4a}a_2^2 + R_{4b}a_2 + R_{4c}, \tag{3.87}$$

which is a quadratic in a_2. Not surprisingly we find that R_{4a} is positive and therefore a value of a_2 may be found which will minimise R_4. It is,

$$a_2 = -\frac{R_{4b}}{2R_{4a}}. \tag{3.88}$$

In turn, this value for a_2 means that the solution at $O(\varepsilon^3)$ is now known. Having solved the full 45th order system (where all the eigenvalues are listed) we obtain the following asymptotic expansions,

$$a \sim 2.44826615 - 4.38433187P^{-2}, \tag{3.89}$$

$$R \sim 61.86656690 - 173.51040218P^{-2} + 851.18063938P^{-4}, \tag{3.90}$$

$$\gamma \sim 14.50695111P^{-1} - 24.42147430P^{-3}. \tag{3.91}$$

All the coefficients are correct to the stated number of decimal places; this required a uniform grid of 1600 equally spaced points using a 4th order Runge Kutta code.

3.5.2 The effect of an imperfectly isothermal top boundary

The practical possibility of having a perfectly isothermal boundary is limited by the finite, although very high, efficiency of the thermal contact between the surface and the external environment through a properly designed convection process. Thus, a more realistic thermal condition at the upper boundary $\bar{y} = L$ is given by a third kind or Robin boundary condition. In this case the $\bar{y} = L$ boundary condition in Eq. (3.9) is replaced by

$$\bar{y} = L: \quad \bar{v} = 0, \quad -k\,\frac{\partial \bar{T}}{\partial \bar{y}} = h\left(\bar{T} - \bar{T}_w\right), \tag{3.92}$$

where k is the thermal conductivity and h the external heat transfer coefficient.
Then, instead of Eq. (3.17b), one has

$$y = 1: \quad v = 0 = \frac{\partial T}{\partial y} + Bi\,T, \tag{3.93}$$

where Bi is the Biot number, which is defined in Eq.(2.39). The temperature distribution for the basic flow is such that

$$T_B = \frac{Pe^2}{2}\left(\frac{2}{Bi} + 1 - y^2\right). \tag{3.94}$$

Nothing changes in the formulation of the fourth order differential equation for Ψ, which is still given by Eq. (3.39). On the other hand, as a consequence of Eqs. (3.36) and (3.93), the $y = 1$ boundary condition Eq. (3.40) is replaced by

$$y = 1: \qquad \Psi = \Psi''' + Bi\,\Psi'' - a^2\,\Psi' = 0. \tag{3.95}$$

From a mathematical point of view, this means that the only practical change in the series solution algorithm is in the definition of the constraint equations at $y = 1$ to determine the coefficient A_2, the overall procedure being the same. In the small-G

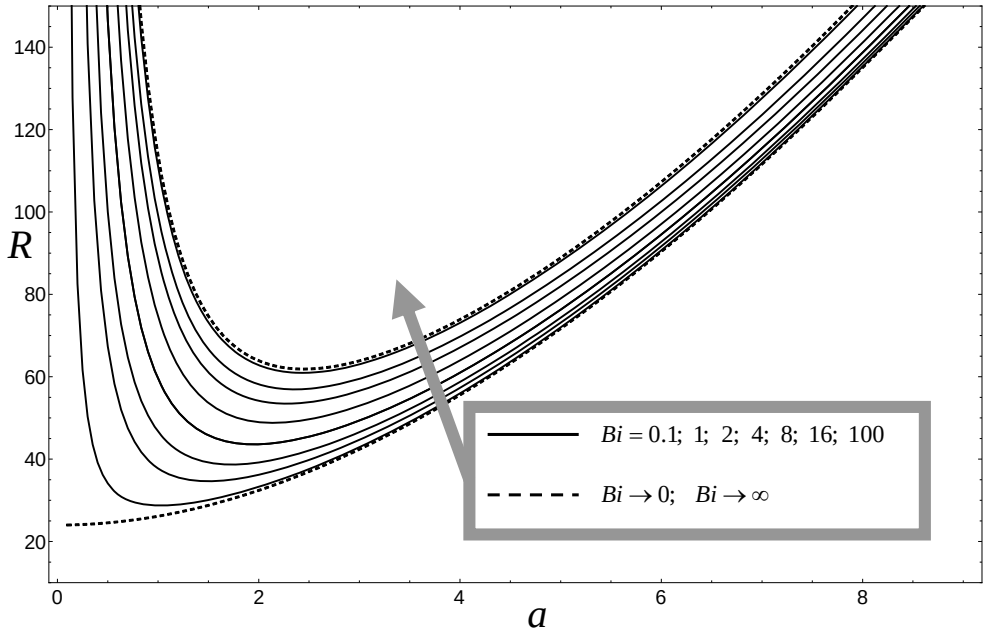

Figure 3.7: Neutral stability curves in the (a, R)-plane for different values of Bi.

limit, or, equivalently for longitudinal rolls, the effect of different values of Bi on the neutral curve is given in Figure 3.7. A perfectly conducting upper boundary corresponds to the limit $Bi \to \infty$, and we see that the critical values of both R and a reduce as Bi decreases. In the insulating limit, $Bi \to 0$, we obtain $a_{cr} = 0$, which is consistent with the similar case for the Darcy-Bénard problem (see pp 193 and 194 of Nield and Bejan (48)). Table 3.5.2 shows the behaviour of a_{cr} and R_{cr} as a function of the Bi number. When G takes nonzero values the variation of R_{cr}, a_{cr} and γ_{cr} may be seen in Figs. 3.8 to 3.10, respectively. The variation of R_{cr} with G is given in Figure 3.8 where substantial changes in the $G \ll 1$ values occur only as $G \to 1$, an unphysically large value. We see also that R_{cr} reduces as Bi decreases. The corresponding wavenumber variation is shown in Figure 3.9. When G takes physically significant values the reduction in the critical wavenumber is monotonic as Bi decreases. A similar behaviour arises for the reduced wavespeed, γ, shown in Figure 3.10.

The last three Figs 3.11 to 3.13 show the behaviour of the disturbances at neutral stability. Isotherms and streamlines are drawn for different values of Bi number. The first refers to the almost adiabatic top boundary and the isotherms show clearly the two constraints of insulation. The second and the third refer to cases in which the

Bi	a_{cr}	R_{cr}
0	0.0000	24.0000
0.1	1.0223	28.7426
0.5	1.4944	34.6331
1	1.7278	38.6913
2	1.9538	43.6007
4	2.1436	48.8102
8	2.2778	53.4693
16	2.3588	56.9462
100	2.4336	60.9438
∞	2.4483	61.8666

Table 3.1: Asymptotic values of a_{cr} and R_{cr} for different Biot numbers.

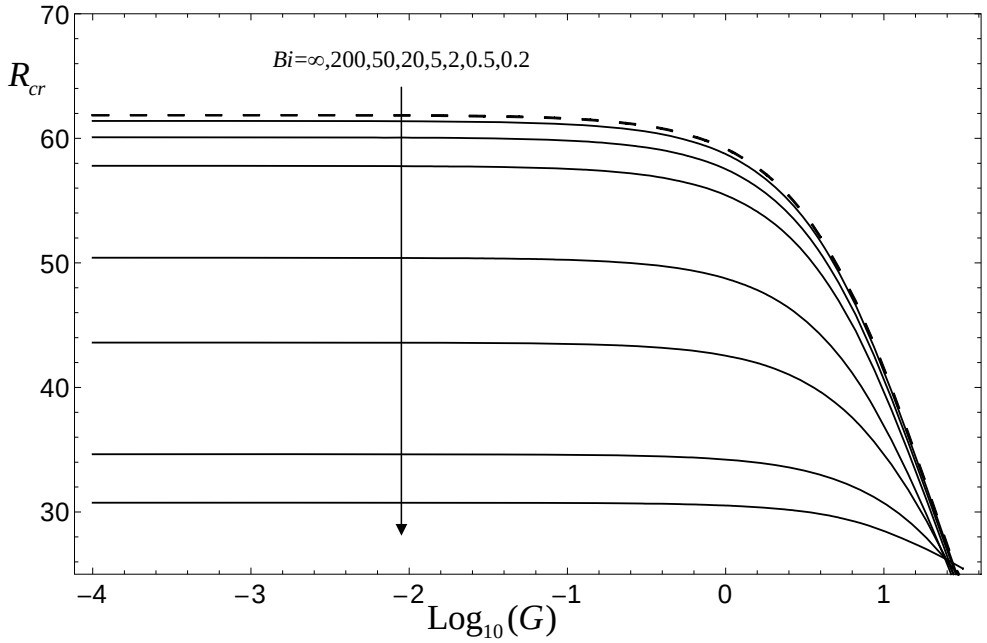

Figure 3.8: R_{cr} vs G diagram: plots corresponding to different Bi, the dashed line corresponds to $Bi \to \infty$.

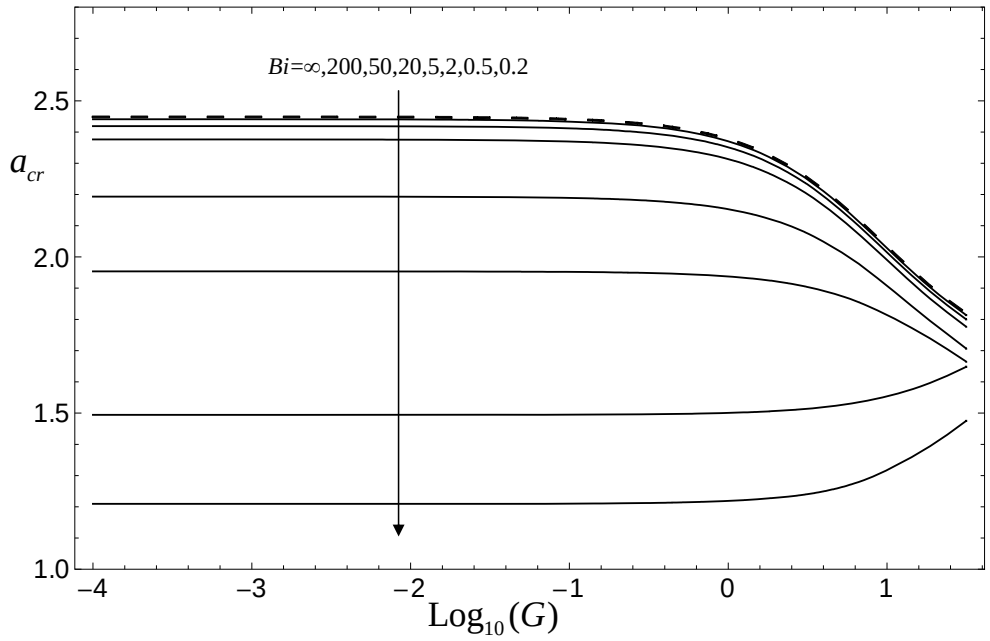

Figure 3.9: a_{cr} vs G diagram: plots corresponding to different Bi, the dashed line corresponds to $Bi \to \infty$.

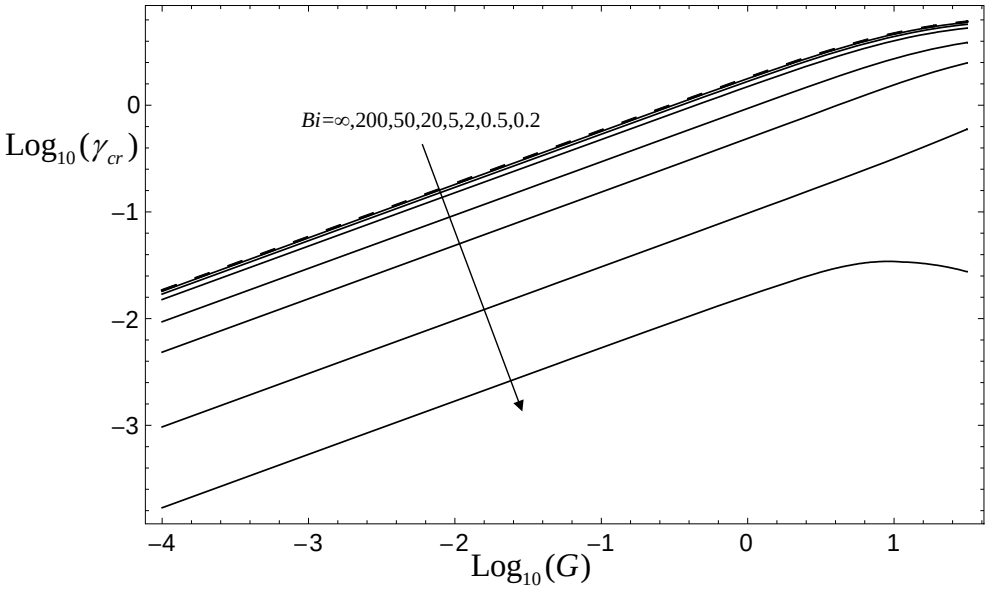

Figure 3.10: γ_{cr} vs G diagram: plots corresponding to different Bi, the dashed line corresponds to $Bi \to \infty$.

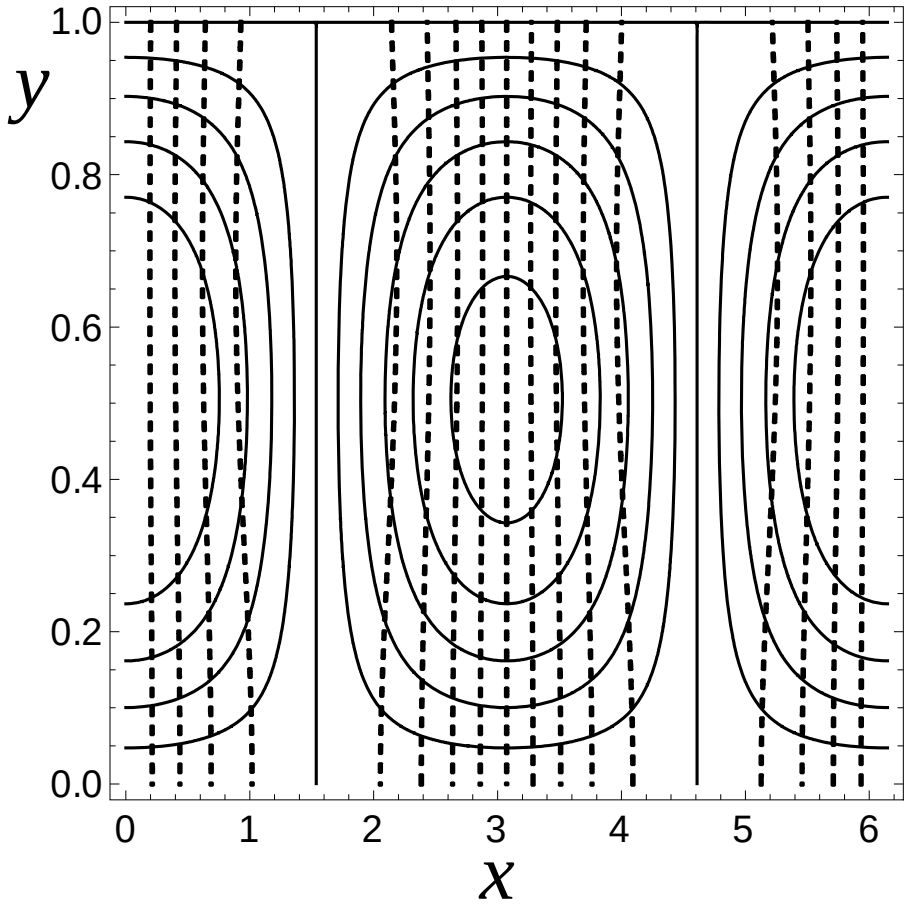

Figure 3.11: Plots of the streamlines (solid lines) of the velocity disturbances, **U**, and the isotherms (dashed lines) of the temperature disturbances, Θ, under critical conditions, $a = a_{cr}$ and $R = R_{cr}$, for $\chi = 0$ and for $Bi = 0.1$.

thermal insulation condition on the top boundary is relaxed and one can note the onset of circular isotherms when the Biot number value increases. For what concerns the velocity rolls, their behaviour is relatively the same on varying the value of Bi.

3.6 Conclusions

In this chapter we have considered horizontal flow in a porous layer where viscous dissipation serves to create a vertical temperature gradient across the moving fluid. The Darcy model, together with the Oberbeck-Boussinesq approximation, has been adopted. The basic temperature profile is nonlinear due to the effect of viscous dissipation.

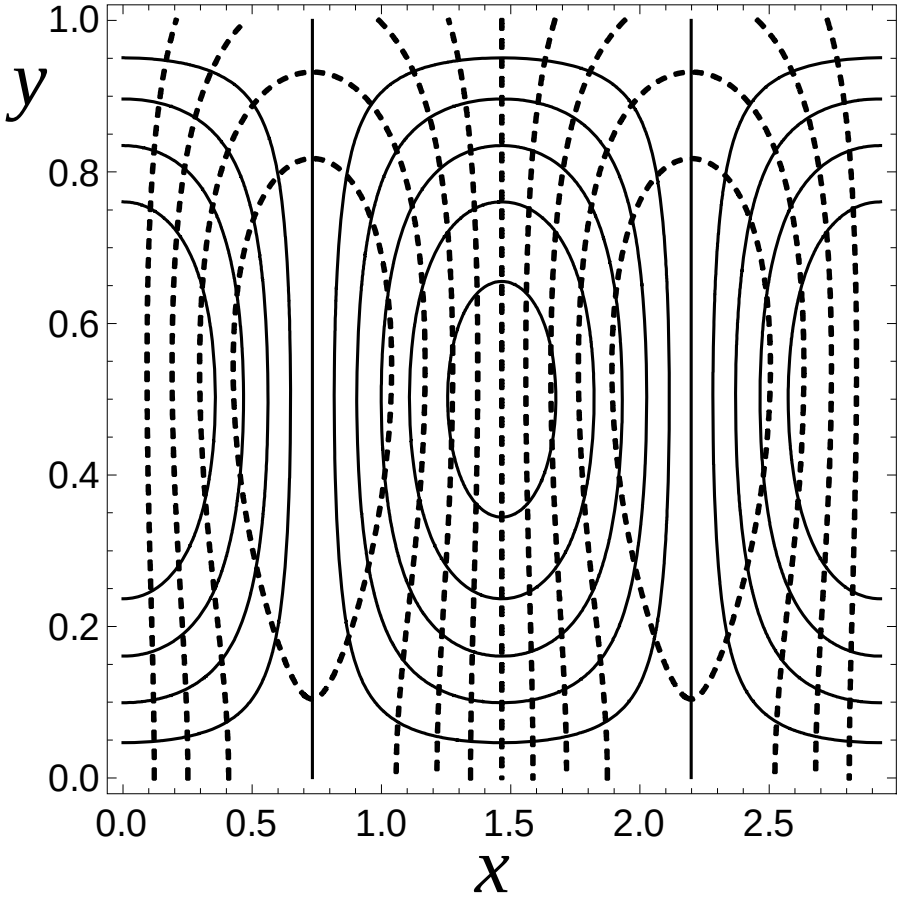

Figure 3.12: Plots of the streamlines (solid lines) of the velocity disturbances, **U**, and the isotherms (dashed lines) of the temperature disturbances, Θ, under critical conditions, $a = a_{cr}$ and $R = R_{cr}$, for $\chi = 0$ and for $Bi = 4$.

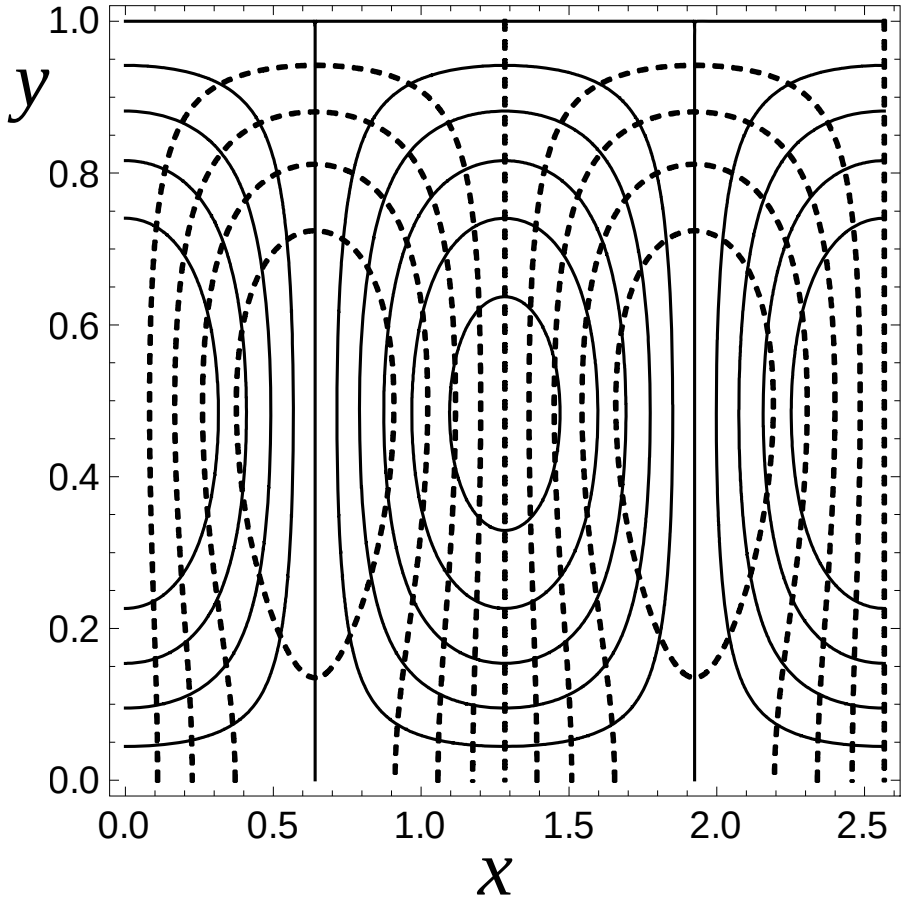

Figure 3.13: Plots of the streamlines (solid lines) of the velocity disturbances, **U**, and the isotherms (dashed lines) of the temperature disturbances, Θ, under critical conditions, $a = a_{cr}$ and $R = R_{cr}$, for $\chi = 0$ and for $Bi = \infty$.

Since the basic temperature decreases from the bottom adiabatic boundary to the top isothermal boundary, the basic flow is possibly unstable to convective rolls. Our aim has been to determine the criteria for the onset of convection.
We have found that:

- the parameter R, which plays the role of a Rayleigh number, remains of $O(1)$ over all physically realistic values of the Gebhart number;
- the critical Péclet number has been determined, as well as the associated wavenumber and phase speed, as a function of the Gebhart number;
- for a given Gebhart number , the transverse rolls require a smaller Péclet number before they are destabilised than any other roll orientation;
- other orientations may have physical significance when the layer is confined laterally, and our results may also be applied to these cases;
- a large Péclet number asymptotic analysis has been obtained. This analysis gives extremely accurate correlations for all physically realistic values of the Gebhart number.

4

Viscous dissipation instabilities and Forchheimer's law

4.1 Introduction

In this chapter a parallel Forchheimer flow in a horizontal porous layer with an isothermal top boundary and a bottom boundary which is subject to a third kind boundary condition is discussed. The effect of viscous dissipation is taken into account. The onset of linear instability in a horizontal porous layer induced by the viscous heating effect is investigated. This is a topic on which very few papers have been published; see (11; 74; 80). The system studied in the following is characterised by a isothermal top boundary surface and a bottom boundary subjected to a thermal boundary condition of the third kind for which a Biot number, Bi is defined. A linear stability analysis of oblique rolls, which are inclined arbitrarily with respect to the uniform basic flow direction, is performed. The disturbance equations are solved numerically by a fourth order Runge-Kutta method. The governing parameter for the onset of convective instability is a combination of Gebhart number and Péclet number, $R = Ge\,Pe^2$, as in Chapter 3.

The contents of this chapter are based on the paper (9) by Barletta, Celli and Rees.

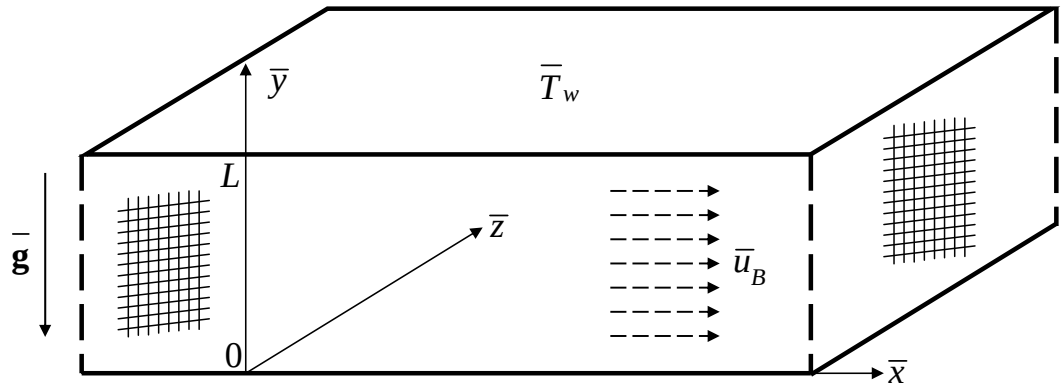

Figure 4.1: Sketch of the horizontal porous channel.

4.2 Mathematical model

A laminar buoyant flow in a horizontal parallel channel with height L is considered. A sketch of the channel is shown in Figure 4.1. Both the Forchheimer model and the Oberbeck-Boussinesq approximation are invoked. It is assumed that local thermal equilibrium holds. Heat generation due to the viscous dissipation contribution is taken into account. The horizontal boundary walls ($\bar{y} = 0, L$) exchange heat with an external environment at temperature T_w: the top surface is taken to be perfectly isothermal at temperature T_w (infinite Biot number), while the bottom surface is taken to be imperfectly isothermal (finite Biot number).
The mass balance equation is thus the same used in Chapter 3, namely

$$\bar{\nabla} \cdot \bar{\mathbf{u}} = 0. \tag{4.1}$$

The momentum balance equation includes the form drag contribution. The buoyancy term is simplified by the Oberbeck-Boussinesq approximation. The momentum balance equation can thus be expressed as

$$\frac{\nu}{K}\left(1 + \frac{C_f\sqrt{K}}{\nu}\sqrt{\bar{\mathbf{u}}\cdot\bar{\mathbf{u}}}\right)\bar{\mathbf{u}} = -\frac{1}{\rho_0}\bar{\nabla}\bar{p} + \mathbf{g}\,\beta\,(\bar{T} - \bar{T}_w), \tag{4.2}$$

The thermal energy balance equation here used is the same as in Chapter 3 except for the viscous dissipation term that takes into account the form drag contribution of the Forchheimer model, Eq.(2.23), namely

$$\sigma\,\frac{\partial \bar{T}}{\partial \bar{t}} + \bar{\mathbf{u}}\cdot\bar{\nabla}\bar{T} = \tilde{\alpha}\,\bar{\nabla}^2\bar{T} + \frac{\nu}{K\,c}\left(1+\frac{C_f\sqrt{K}}{\nu}\sqrt{\bar{\mathbf{u}}\cdot\bar{\mathbf{u}}}\right)\bar{\mathbf{u}}\cdot\bar{\mathbf{u}}, \tag{4.3}$$

The set of governing balance equations may now be expressed as

$$\bar{\nabla}\cdot\bar{\mathbf{u}} = 0, \tag{4.4}$$

$$\frac{\nu}{K}\left(1+\frac{C_f\sqrt{K}}{\nu}\sqrt{\bar{\mathbf{u}}\cdot\bar{\mathbf{u}}}\right)\bar{u} = -\frac{1}{\rho_0}\frac{\partial \bar{p}}{\partial \bar{x}}, \tag{4.5}$$

$$\frac{\nu}{K}\left(1+\frac{C_f\sqrt{K}}{\nu}\sqrt{\bar{\mathbf{u}}\cdot\bar{\mathbf{u}}}\right)\bar{v} = -\frac{1}{\rho_0}\frac{\partial \bar{p}}{\partial \bar{y}} + \beta\,g\,(\bar{T}-\bar{T}_w), \tag{4.6}$$

$$\frac{\nu}{K}\left(1+\frac{C_f\sqrt{K}}{\nu}\sqrt{\bar{\mathbf{u}}\cdot\bar{\mathbf{u}}}\right)\bar{w} = -\frac{1}{\rho_0}\frac{\partial \bar{p}}{\partial \bar{z}}, \tag{4.7}$$

$$\sigma\,\frac{\partial \bar{T}}{\partial \bar{t}} + \bar{\mathbf{u}}\cdot\bar{\nabla}\bar{T} = \tilde{\alpha}\,\bar{\nabla}^2\bar{T} + \frac{\nu}{K\,c}\left(1+\frac{C_f\sqrt{K}}{\nu}\sqrt{\bar{\mathbf{u}}\cdot\bar{\mathbf{u}}}\right)\bar{\mathbf{u}}\cdot\bar{\mathbf{u}}, \tag{4.8}$$

where σ is defined by Eq.(2.10). The velocity and thermal boundary conditions are defined by

$$\begin{aligned} \bar{y}=0: &\quad \bar{v}=0=\frac{\partial \bar{T}}{\partial \bar{y}}-\frac{h}{\tilde{\tilde{k}}}\left(\bar{T}-\bar{T}_w\right), \\ \bar{y}=L: &\quad \bar{v}=0=\bar{T}-\bar{T}_w. \end{aligned} \tag{4.9}$$

4.2.1 Nondimensional formulation

The characteristic scales used here to nondimensionalise the set of equations are the same as in Chapter 3, except for the contribution of the pressure p. Here the characteristic pressure is taken to be $\mu\,\tilde{\alpha}/K$. Let us now introduce the nondimensional variables, namely

$$(\bar{x},\bar{y},\bar{z}) = (x,y,z)\,L, \quad \bar{t} = t\,\frac{\sigma\,L^2}{\tilde{\alpha}}, \quad (\bar{u},\bar{v},\bar{w}) = (u,v,w)\,\frac{\tilde{\alpha}}{L},$$
$$\bar{T} = \bar{T}_w + T\,\frac{\nu\,\tilde{\alpha}}{K\,c}, \quad \bar{p} = p\,\frac{\mu\,\tilde{\alpha}}{K}. \tag{4.10}$$

Then, Eqs. (4.4)–(4.8) may be rewritten in the form,

$$\frac{\partial u}{\partial x} + \frac{\partial v}{\partial y} + \frac{\partial w}{\partial z} = 0, \tag{4.11}$$

$$\left(1 + \eta_f\,\sqrt{\mathbf{u}\cdot\mathbf{u}}\right)\,u = -\frac{\partial p}{\partial x}, \tag{4.12}$$

$$\left(1 + \eta_f\,\sqrt{\mathbf{u}\cdot\mathbf{u}}\right)\,v = -\frac{\partial p}{\partial y} + Ge\,T, \tag{4.13}$$

$$\left(1 + \eta_f\,\sqrt{\mathbf{u}\cdot\mathbf{u}}\right)\,w = -\frac{\partial p}{\partial z}, \tag{4.14}$$

$$\frac{\partial T}{\partial t} + u\,\frac{\partial T}{\partial x} + v\,\frac{\partial T}{\partial y} + w\,\frac{\partial T}{\partial z} = \frac{\partial^2 T}{\partial x^2} + \frac{\partial^2 T}{\partial y^2} + \frac{\partial^2 T}{\partial z^2}$$
$$+ \left(u^2 + v^2 + w^2\right)\left(1 + \eta_f\,\sqrt{\mathbf{u}\cdot\mathbf{u}}\right). \tag{4.15}$$

In the latter equations Ge is the Gebhart number defined in Eq.(3.16) and η_f is a nondimensional Forchheimer coefficient, namely

$$\eta_f = \frac{C_f\sqrt{Da}}{Pr}, \qquad Ge = \frac{g\,\beta\,L}{c}. \tag{4.16}$$

The Gebhart number measures the extent to which the viscous dissipation influence the energy balance in the fluid flow.

The boundary conditions (4.9) may now be expressed in a nondimensional form:

$$y = 0: \quad v = 0 = \frac{\partial T}{\partial y} - Bi\,T,$$
$$y = 1: \quad v = 0 = T, \tag{4.17}$$

where Bi is the Biot number, which is defined in Eq.(2.39).

4.2.2 Fully developed basic flow

As for the previous Chapter, a fully developed basic flow is assumed in order to take into account the contribute of the viscous dissipation term in the thermal energy balance equation. We assume a horizontal steady parallel flow in the x-direction and a purely vertical heat flux. Then, the basic state which has to be analysed for stability is given by,

$$\begin{aligned} &u_B = Pe > 0, \qquad v_B = 0, \qquad w_B = 0, \\ &\frac{\partial p_B}{\partial x} = -Pe(1+\eta_f\, Pe), \qquad \frac{\partial p_B}{\partial y} = Ge\, T_B, \qquad \frac{\partial p_B}{\partial z} = 0, \\ &T_B = -Pe^2\,(Pe\,\eta_f + 1)\,\frac{y^2(Bi+1) - Bi\,y - 1}{2\,(Bi+1)}, \end{aligned} \tag{4.18}$$

4.2.3 Linear disturbances

In the following a normal mode stability analysis is performed. In order to analyse the system with this method the basic flow has to be perturbed. Here, as in Chapter 3, we introduce perturbations of the basic flow described by Eq. (4.18), namely

$$u = u_B + \varepsilon\, U, \quad v = v_B + \varepsilon\, V, \quad w = w_B + \varepsilon\, W, \quad T = T_B + \varepsilon\, \theta, \quad p = p_B + \varepsilon\, P. \tag{4.19}$$

where ε is an asymptotically small perturbation parameter. The stability analysis that follows has been chosen to be linear. Thus, on substituting Eq. (4.19) into Eqs. (4.11)-(4.15) and neglecting nonlinear terms in the perturbations, i.e. terms of $O(\varepsilon^2)$, one obtains the linearized stability equations, namely,

$$\frac{\partial U}{\partial x} + \frac{\partial V}{\partial y} + \frac{\partial W}{\partial z} = 0, \tag{4.20}$$

$$U\,(1 + 2\,\eta_f\, Pe) = -\frac{\partial P}{\partial x}, \tag{4.21}$$

$$V\,(1 + \eta_f\, Pe) = -\frac{\partial P}{\partial y} + Ge\,\theta, \tag{4.22}$$

$$W\,(1 + \eta_f\, Pe) = -\frac{\partial P}{\partial z}, \tag{4.23}$$

$$\frac{\partial\theta}{\partial t}+Pe\,\frac{\partial\theta}{\partial x}-Pe^2\,(1+Pe\,\eta_f)\,V\,B(y)=\frac{\partial^2\theta}{\partial x^2}+\frac{\partial^2\theta}{\partial y^2}+\frac{\partial^2\theta}{\partial z^2}+Pe\,U\,(2+3\,Pe\,\eta_f). \quad (4.24)$$

where B is a function of both Bi and y and is defined as,

$$B(y)=y-\frac{Bi}{2\,(Bi+1)}. \quad (4.25)$$

4.3 Instability with respect to oblique rolls

Now, one may differentiate Eqs. (4.21)-(4.23) and substitute the results into Eq. (4.20). Then one may also substitute the velocity components in Eqs. (4.21)-(4.22) into Eq. (4.24) in order to obtain the following pressure/temperature formulation,

$$\left(\frac{1+Pe\,\eta_f}{1+2\,Pe\,\eta_f}\right)\frac{\partial^2 P}{\partial x^2}+\frac{\partial^2 P}{\partial y^2}+\frac{\partial^2 P}{\partial z^2}=Ge\,\frac{\partial\theta}{\partial y}, \quad (4.26)$$

$$\begin{aligned}&\frac{\partial\theta}{\partial t}+Pe\,\frac{\partial\theta}{\partial x}+Pe^2\left(\frac{\partial P}{\partial y}-Ge\,\theta\right)B(y)=\frac{\partial^2\theta}{\partial x^2}+\frac{\partial^2\theta}{\partial y^2}+\frac{\partial^2\theta}{\partial z^2} \quad (4.27)\\ &-Pe\left(\frac{2+3\,Pe\,\eta_f}{1+2\,Pe\,\eta_f}\right)\frac{\partial P}{\partial x}.\end{aligned}$$

In the previous chapter, an inclined basic flow is assumed in order to obtain a stability analysis that considers all the possible oblique rolls. Here, to achieve the same aim, the direction of the perturbations is assumed to inclined of an angle χ with respect to the x axis. Let us assume that the disturbances are given by

$$\begin{aligned}P(x,y,z,t)&=\Re\left\{\mathcal{P}(y)\,e^{\lambda\,t}e^{ia(x\,\cos\chi+z\sin\chi)}\right\},\\ \theta(x,y,z,t)&=\Re\left\{\Theta(y)\,e^{\lambda\,t}e^{ia(x\,\cos\chi+z\sin\chi)}\right\},\end{aligned} \quad (4.28)$$

where $\lambda=\lambda_1+i\lambda_2$ is a complex coefficient and χ is the angle between the basic flow direction and the propagation direction of the disturbance. The system of equations (4.26)-(4.27) now reduces to,

$$\mathcal{P}''-a^2\left[\left(\frac{1+Pe\,\eta_f}{1+2\,Pe\,\eta_f}\right)\cos^2\chi+\sin^2\chi\right]\mathcal{P}-Ge\,\Theta'=0, \quad (4.29)$$

$$\Theta'' - \left[\lambda + a^2 + i\,a\,Pe\,\cos\chi - Ge\,Pe^2\,B(y)\right]\Theta - Pe^2\,B(y)\,\mathcal{P}' - i\,a\,Pe\,\cos\chi\left(\frac{2+3\,Pe\,\eta_f}{1+2\,Pe\,\eta_f}\right)\mathcal{P} = 0. \tag{4.30}$$

where the primes denote differentiation with respect to y. The boundary conditions (4.17) may be expressed in terms of pressure and temperature as

$$y=0: \quad \mathcal{P}' = Ge\,\Theta\,, \;\; \Theta' - Bi\,\Theta = 0\,; \qquad\qquad y=1: \quad \mathcal{P}' = 0 = \Theta. \tag{4.31}$$

We will set $\Re(\lambda) = \lambda_1 = 0$ in order to investigate the neutral stability. Moreover, for numerical convenience, we shall also set

$$\gamma = \lambda_2 + a\,Pe\,\cos\chi \;\;, \tag{4.32}$$

so that Eq. (4.30) may be rewritten as

$$\Theta'' - [a^2 + i\gamma - Ge\,Pe^2\,B(y)]\,\Theta - Pe^2\,B(y)\,\mathcal{P}' - i\,a\,Pe\,\cos\chi\left(\frac{2+3\,Pe\,\eta_f}{1+2\,Pe\,\eta_f}\right)\mathcal{P} = 0. \tag{4.33}$$

4.3.1 Longitudinal rolls

The condition $\chi = \pi/2$ identifies the longitudinal rolls case. Eqs. (4.29), (4.31) and (4.33) become

$$\mathcal{P}'' - a^2\,\mathcal{P} - Ge\,\Theta' = 0, \tag{4.34}$$

$$\Theta'' - [a^2 + i\,\gamma - Ge\,Pe^2\,B(y)]\,\Theta - Pe^2\,B(y)\,\mathcal{P}' = 0, \tag{4.35}$$

$$y=0: \quad \mathcal{P}' = Ge\,\Theta\,, \;\; \Theta' - Bi\,\Theta = 0\,; \;\; y=1: \quad \mathcal{P}' = 0 = \Theta. \tag{4.36}$$

It is important to note the absence of the parameter η_f in Eqs. (4.34)-(4.36). Thus, longitudinal rolls are not affected by the dependence on the Forchheimer term in the momentum equation. Moreover, the problem becomes self-adjoint as one may now set $\gamma = 0$ and determine the solution $\{\mathcal{P}, \Theta\}$ in terms of real-valued functions.

4.3.2 Transverse rolls

The condition $\chi = 0$ identifies the transverse rolls case. Equations (4.29), (4.31) and (4.33) become

$$\mathcal{P}'' - a^2 \left(\frac{1 + Pe\,\eta_f}{1 + 2\,Pe\,\eta_f} \right) \mathcal{P} - Ge\,\Theta' = 0, \tag{4.37}$$

$$\Theta'' - \left[a^2 + i\gamma - Ge\,Pe^2\,B(y) \right] \Theta - Pe^2\,B(y)\,\mathcal{P}' - i\,a\,Pe \left(\frac{2 + 3\,Pe\,\eta_f}{1 + 2\,Pe\,\eta_f} \right) \mathcal{P} = 0, \tag{4.38}$$

$$y = 0: \quad \mathcal{P}' = Ge\,\Theta\,, \;\; \Theta' - Bi\,\Theta = 0\,; \qquad\qquad y = 1: \quad \mathcal{P}' = 0 = \Theta. \tag{4.39}$$

4.4 Eigenvalue problem

Equations (4.29) and (4.33) are a pair of coupled homogeneous complex second-order ODEs, and are subject to the four homogeneous boundary conditions Eq. (4.31). The system always admits zero solutions, but it may also be interpreted as an eigenvalue problem for λ where values for λ depend on Ge, Pe, η_f, χ and a. Alternatively, incipient instability is given by $\lambda_1 = 0$, therefore the system may now be regarded as a double eigenvalue problem for Pe and γ, for example, as functions of the remaining parameters. The computation of these eigenvalues requires further normalization conditions to force the solutions for $\mathcal{P}$ and Θ to be nonzero; we choose the following,

$$Bi\,\Theta'(0) + \Theta(0) = Bi + 1. \tag{4.40}$$

Equation (4.40) comes from the linear combination of two possible normalization choices: $\Theta'(0) - 1 = 0$ and $\Theta(0) - 1 = 0$. The combination Eq. (4.40) is chosen because it remains valid as the top boundary condition varies between the limits of isothermal boundary, $Bi \to \infty$, and adiabatic boundary, $Bi \to 0$. It is also proved convenient to work with the parameter,

$$R = Ge\,Pe^2, \tag{4.41}$$

rather than Ge. The critical value of R, which is denoted by R_{cr}, is now determined by seeking the minimum of R as a function of a in the neutral stability curve. In practice

this is done by extending the system, Eqs. (4.29) and (4.33), by differentiating it with respect to a, and by setting $\partial R/\partial a = 0$.

4.4.1 Stability analysis

In order to solve Eqs. (4.29), (4.31), (4.33) and (4.40), a numerical solver based on the classical fourth order Runge-Kutta method coupled with the shooting method has been used. In all cases we used 100 intervals and this, coupled with the fourth order accuracy of the method, yields highly accurate results.
The change of R_{cr} as a function of three parameters has been studied. These parameter are the Biot parameter Bi, the angle χ and the parameter η_+ that is defined as

$$\eta_+ = \frac{\eta_f}{\sqrt{Ge}}, \tag{4.42}$$

and allows one to remove the explicit dependence on Ge in the physically reasonable range of very small Ge. Indeed, if one substitutes Eq. (4.42) and the relationship

$$\mathcal{P}_+(y) = \frac{\mathcal{P}(y)}{Ge}, \tag{4.43}$$

in Eqs. (4.29), (4.31), (4.33) and (4.40), one obtains

$$\mathcal{P}''_+ - a^2 \left[\left(\frac{1 + \sqrt{R}\,\eta_+}{1 + 2\sqrt{R}\,\eta_+} \right) \cos^2\chi + \sin^2\chi \right] \mathcal{P}_+ - \Theta' = 0, \tag{4.44}$$

$$\begin{aligned} \Theta'' - \left[a^2 + i\gamma - R\,B(y)\right]\Theta - R\,B(y)\,\mathcal{P}'_+ \\ - \; i\,a\sqrt{Ge\,R}\,\cos\chi \left(\frac{2 + 3\sqrt{R}\,\eta_+}{1 + 2\sqrt{R}\,\eta_+} \right) \mathcal{P}_+ = 0, \end{aligned} \tag{4.45}$$

$$\begin{aligned} &y = 0: \qquad \mathcal{P}'_+ = \Theta \qquad \Theta' - Bi\,\Theta = 0 \qquad Bi\,\Theta' + \Theta = Bi + 1; \\ &y = 1: \qquad \mathcal{P}'_+ = 0 = \Theta. \end{aligned} \tag{4.46}$$

It must be mentioned that, on account of Eq. (4.42), the limit $\eta_+ \to 0$ can be interpreted as the limit of negligible form-drag effect, i.e. the limit of validity of Darcy's law. On the other hand, the limit $\eta_+ \to \infty$ is the limit of a very small Gebhart number.
Under the physically realistic assumption of $Ge \ll 1$, if R is of $O(1)$, then the last term on the left hand side of Eq. (4.45) is of $O(Ge^{1/2})$. As a consequence, this term is

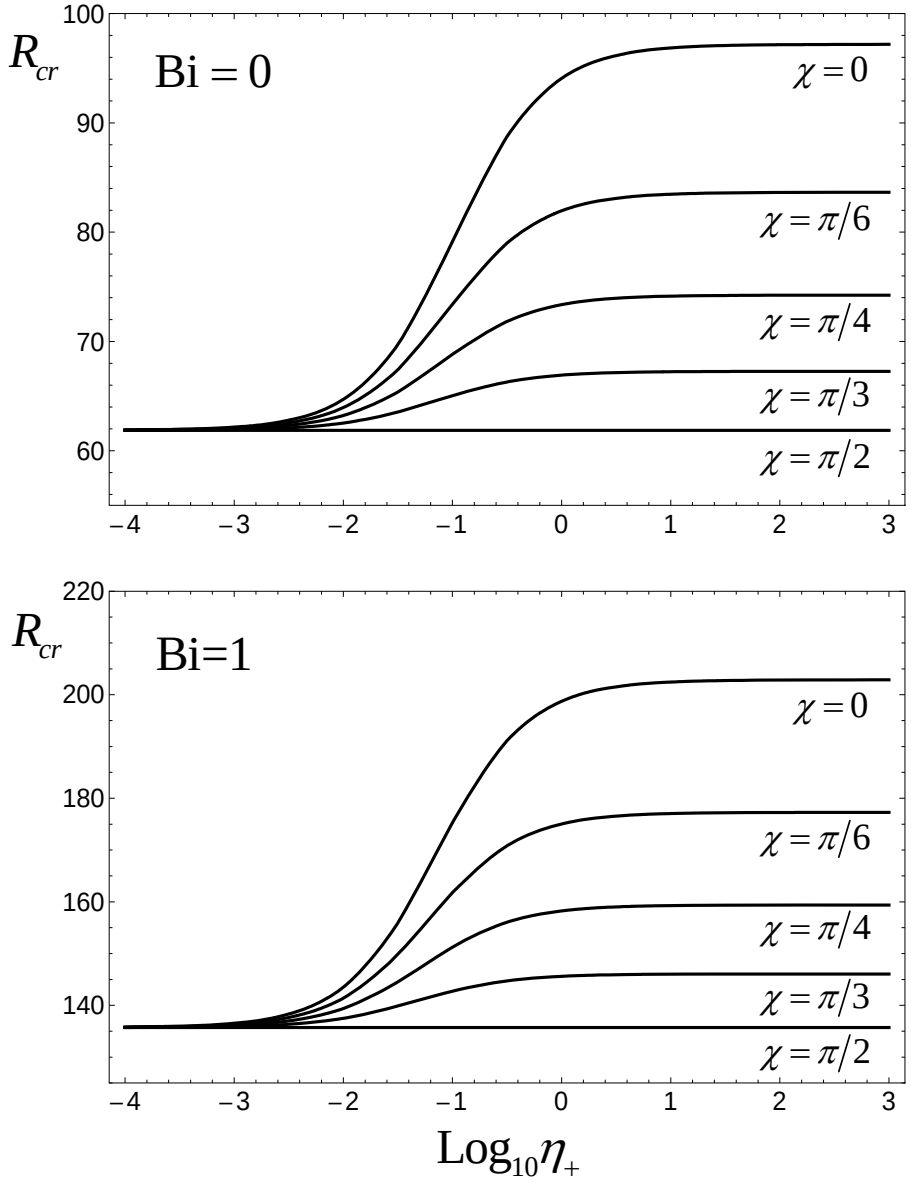

Figure 4.2: R_{cr} as a function of η_+ for different values of χ for $Bi = 0, 1$.

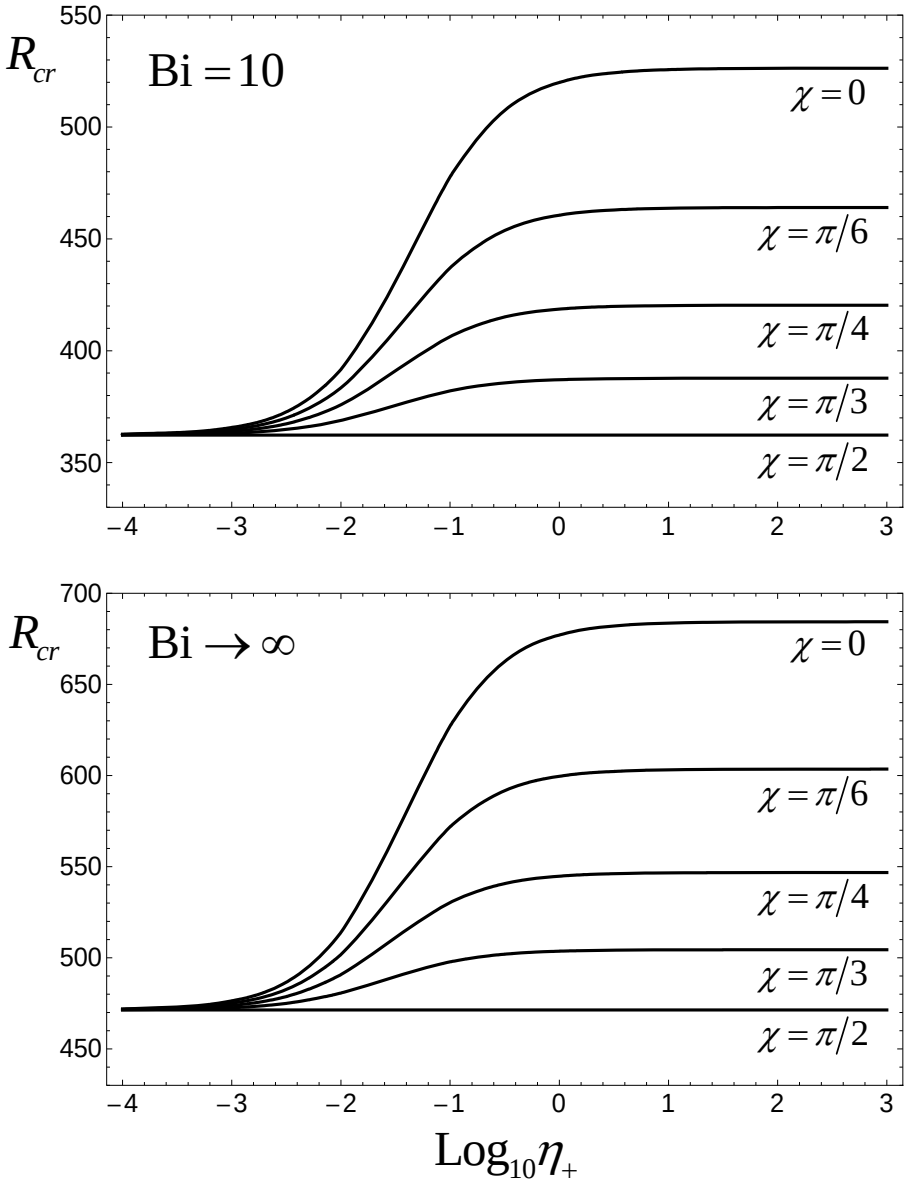

Figure 4.3: R_{cr} as a function of η_+ for different values of χ for $Bi = 10, \infty$.

	$\eta_+ \to 0$		$\eta_+ \to \infty; \quad \chi = 0$	
Bi	a_{cr}	R_{cr}	a_{cr}	R_{cr}
0	2.4483	61.867	3.0342	97.184
0.1	2.5078	69.411	3.1069	108.23
0.5	2.7258	99.728	3.3683	151.92
1	2.9697	135.71	3.6482	202.88
2	3.3637	195.12	4.0789	286.62
4	3.8150	270.68	4.5706	394.22
8	4.1709	342.66	4.9727	497.87
10	4.2573	362.32	5.0722	526.30
16	4.3989	396.65	5.2369	576.00
100	4.6270	457.59	5.5047	664.34
∞	4.6752	471.38	5.5616	684.36

Table 4.1: Asymptotic values of a_{cr} and R_{cr} for different Biot numbers.

significantly smaller than the other terms. Thus, one can easily infer that neglecting this term allows one to set $\gamma = 0$, so that the problem becomes self-adjoint and only admits real solutions for $(\mathcal{P}, \Theta)$. The Biot number Bi affects the bottom boundary condition. On account of Eq. (25), in the limit of an adiabatic boundary, one has

$$Bi \to 0 \quad \Rightarrow \quad B(y) = y, \tag{4.47}$$

while, in the limit of a perfectly isothermal boundary, one has

$$Bi \to \infty \quad \Rightarrow \quad B(y) = y - \frac{1}{2}. \tag{4.48}$$

From Figures 4.2-4.3 one can see that, for any chosen parameter set, the values of R_{cr} are higher in the case of an isothermal bottom boundary than in the case of an adiabatic bottom boundary. This feature could have been expected. In fact, when examining the basic flow in the case of isothermal bottom boundary ($Bi \to \infty$), one can see from Eq. (4.48) that the midplane $y = 1/2$ is adiabatic, i.e. $B(1/2) = 0$. In other words, in the analysis of the basic flow, the layer with adiabatic bottom boundary

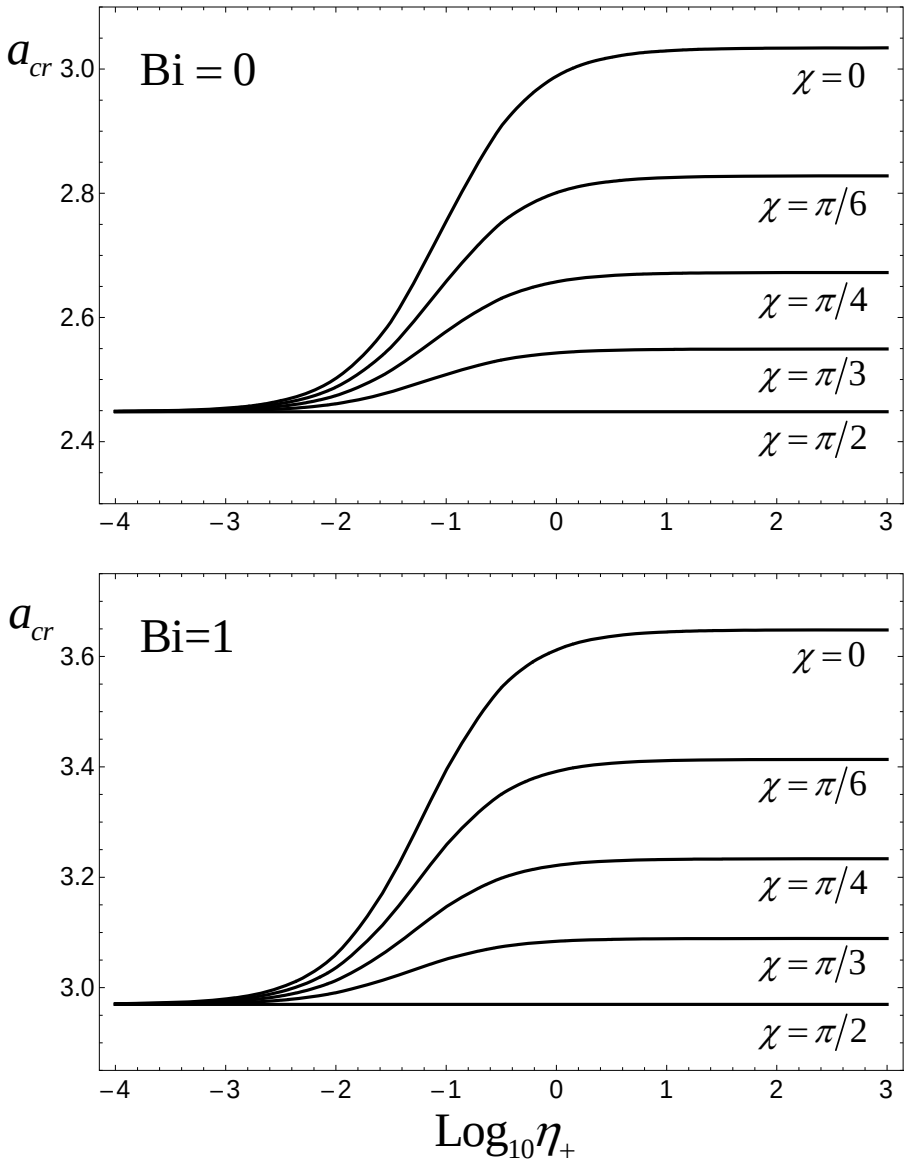

Figure 4.4: a_{cr} as a function of η_+ for different values of χ for $Bi = 0, 1$.

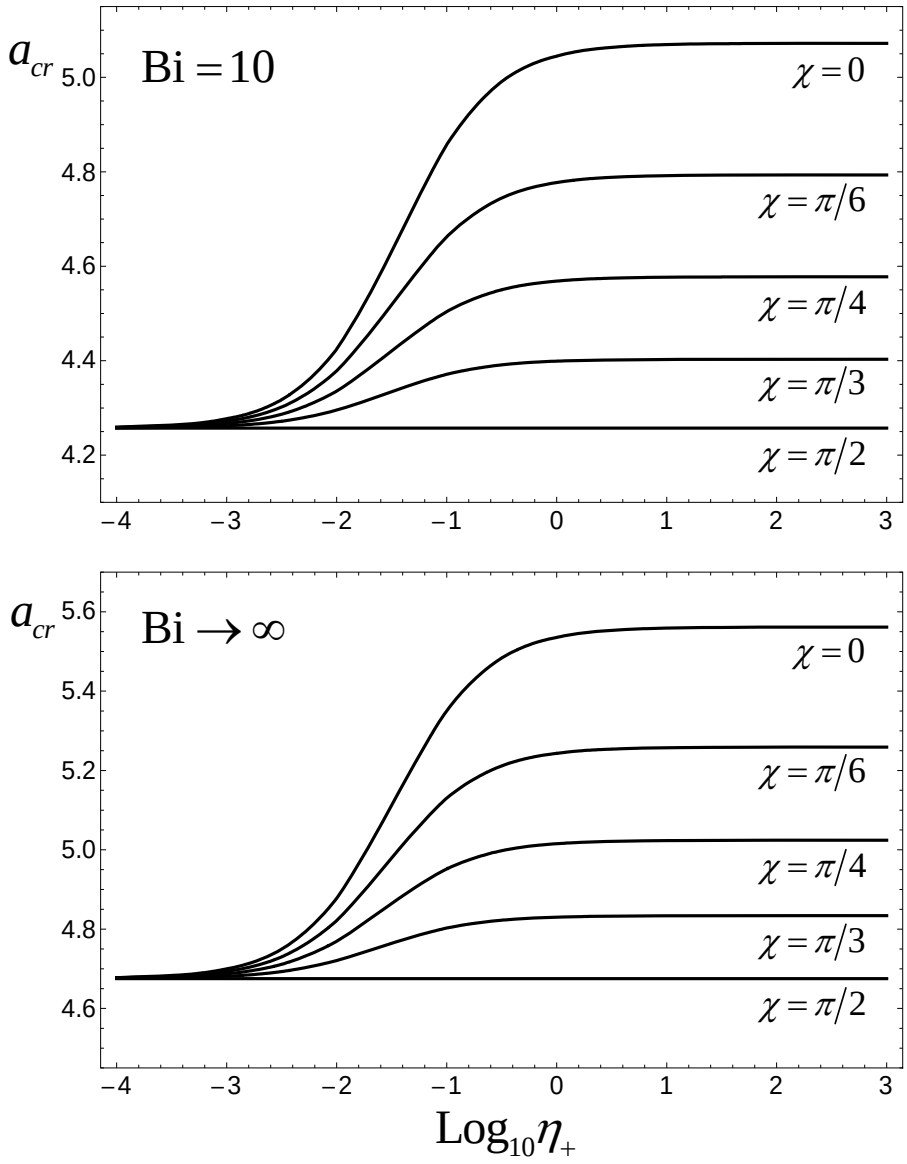

Figure 4.5: a_{cr} as a function of η_+ for different values of χ for $Bi = 10, \infty$.

is coincident with the upper half of the layer with isothermal bottom boundary, except for the thickness. One sees that R is proportional to L^3. Therefore, one would expect that the critical value of R in the case of a layer with isothermal bottom boundary is 8 times that in the case of a layer with adiabatic bottom boundary. The factor 8 would be exact if, in the perturbed flow of the layer with isothermal bottom boundary, the midplane $y = 1/2$ is both adiabatic and impermeable. In fact, these conditions are perfectly fulfilled by the basic flow, but not by the disturbances. It should be mentioned, however, that the lower half of the layer with isothermal bottom boundary is expected to be affected only marginally by roll disturbances as the midplane $y = 1/2$ is, in the basic state, hotter than the bottom boundary $y = 0$.

In Figures 4.2-4.3 one may also notice that R_{cr}, for every Biot number Bi, is not affected by the orientation angle χ in the limit of validity of Darcy law, $\eta_+ \to 0$. On the contrary, in the limit of important form-drag effects with $Ge \ll 1$ ($\eta_+ \to \infty$), one finds an important dependence of R_{cr} on the orientation of the oblique rolls. In particular, longitudinal rolls ($\chi = \pi/2$) appear to be the most unstable. For longitudinal rolls, R_{cr} is independent of η_+. This feature is evident from Eqs. (4.44)-(4.46) as the parameter η_+ disappears from the equations when $\chi = \pi/2$. For $\eta_+ \to 0$ there appears an asymptotic behaviour described in Table 1. For $\eta_+ \to \infty$, a different asymptotic value of either R_{cr} or a_{cr} is reached for every χ. The highest asymptotic values of R_{cr} or a_{cr} refer to transverse rolls ($\chi = 0$). These values are reported in Table 1.

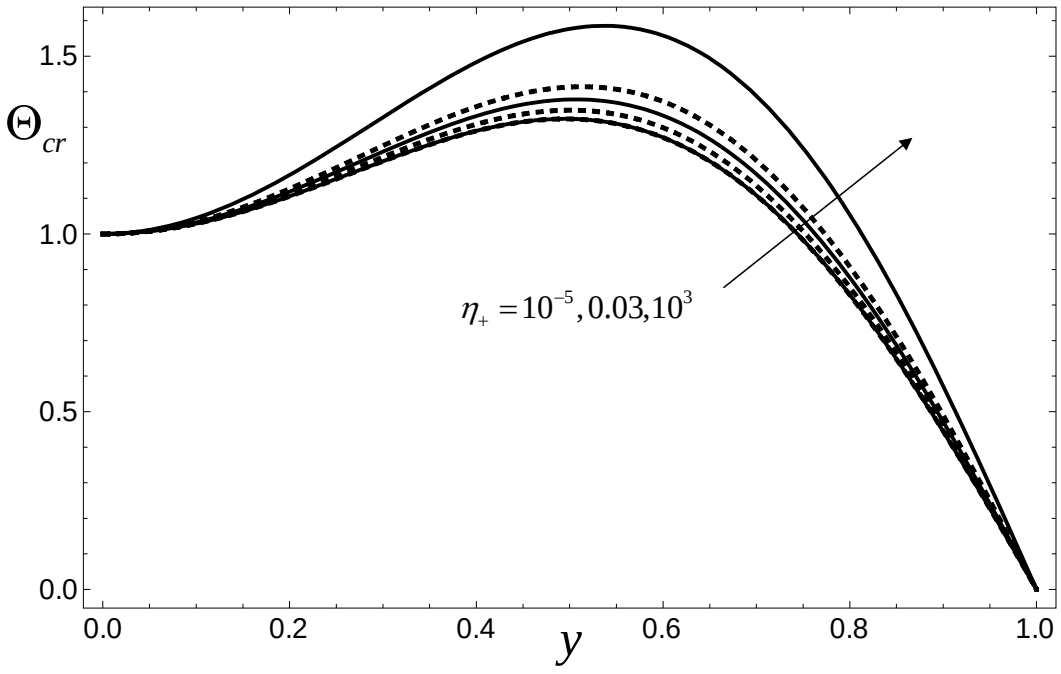

Figure 4.6: Plots of Θ_{cr} as a function of y for $Bi = 0$ and $\eta_+ = 10^{-5}, 0.03, 10^3$. Solid lines refer to $\chi = 0$, while dashed lines refer to $\chi = \pi/4$.

Figures 4.4-4.5 show the plots of the critical wavenumber a_{cr} versus η_+ for different orientation angles χ and Biot numbers Bi. The qualitative behaviour of a_{cr} is similar to that of R_{cr}. The curves display the asymptotic behaviour for $\eta_+ \to 0$ and for $\eta_+ \to \infty$. Both the lower and the upper asymptotic values are specified in Table 1.

The plots reported in Figs. 4.6-4.9 suggest a weak dependence of $\Theta_{cr}(y)$ on both η_+ and χ. In particular, for $\eta_+ = 10^{-5}$, the solid and the dashed lines corresponding respectively to $\chi = 0$ and $\chi = \pi/4$ are perfectly coincident. Indeed, the eigenvalue problem (4.44)-(4.46) becomes independent of χ in the limit $\eta_+ \to 0$ (i.e. in the limit of validity of Darcy's law). The temperature profiles $\Theta_{cr}(y)$ represented in Figure 4.6 refer to an adiabatic bottom boundary, while those reported in Figs. 4.7-4.9 refer to an imperfectly isothermal boundary ($Bi = 1, 10$) and to a perfectly isothermal boundary ($Bi \to \infty$). Due to Eq. (4.46), all the profiles reported in Figs. 4.6-4.9 display at $y = 0$ a fixed temperature, $\Theta(0) = (Bi + 1)/(Bi^2 + 1)$, and a fixed heat flux, $\Theta'(0) = Bi\,(Bi + 1)/(Bi^2 + 1)$.

Figs. 4.10-4.11 refer to critical conditions and show the isotherms, $\theta = constant$, and

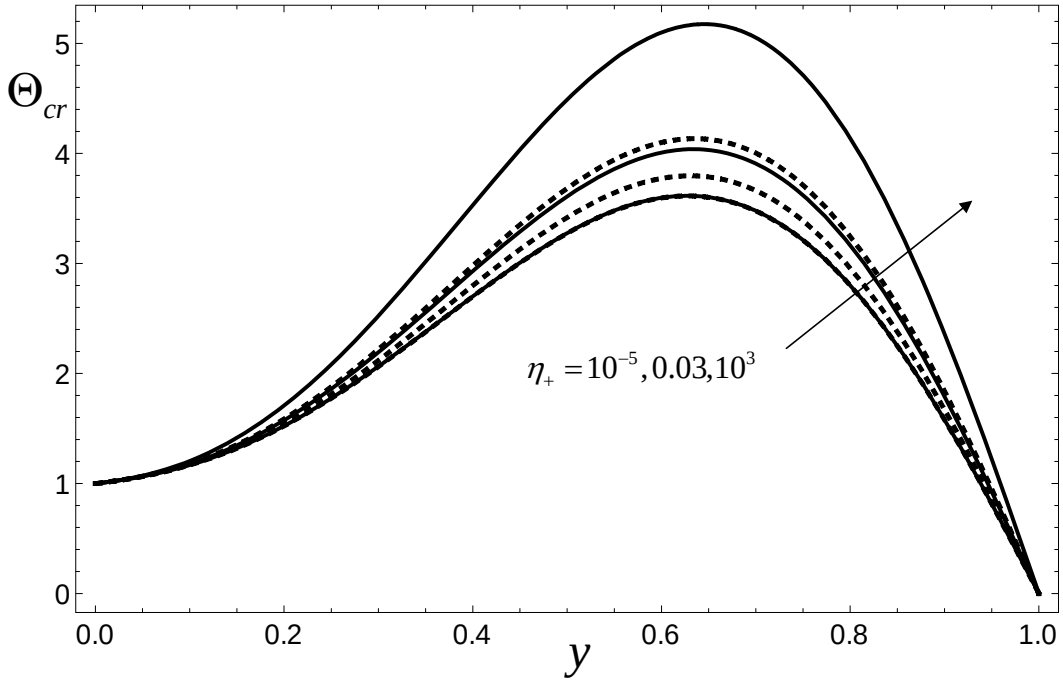

Figure 4.7: Plots of Θ_{cr} as a function of y for $Bi = 1$ and $\eta_+ = 10^{-5}, 0.03, 10^3$. Solid lines refer to $\chi = 0$, while dashed lines refer to $\chi = \pi/4$.

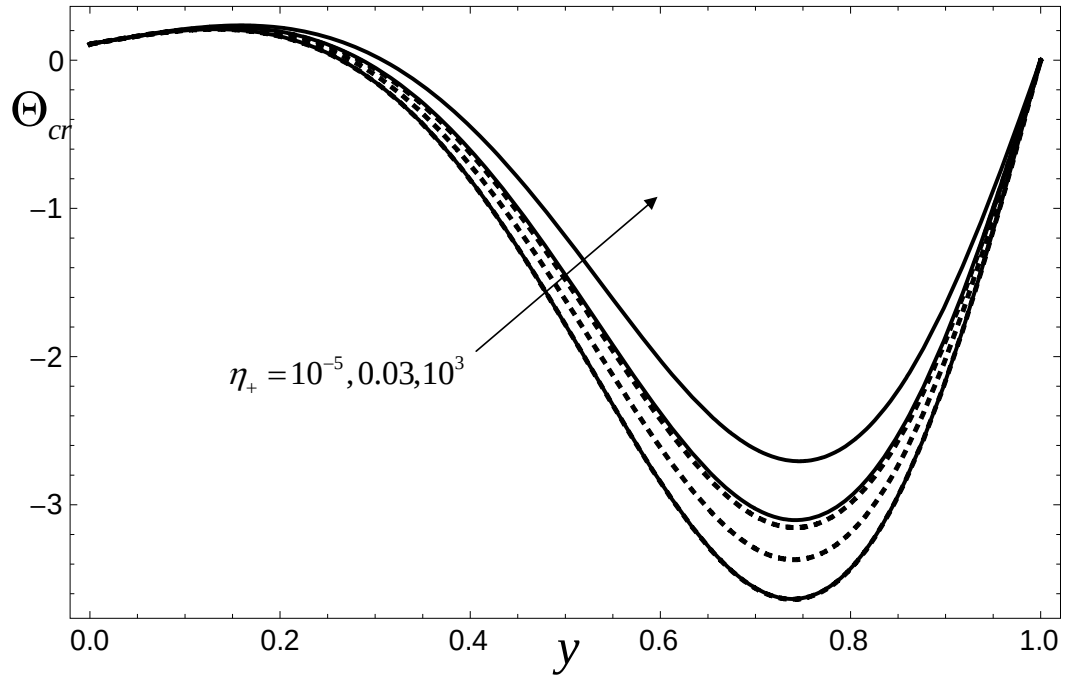

Figure 4.8: Plots of Θ_{cr} as a function of y for $Bi = 10$ and $\eta_+ = 10^{-5}, 0.03, 10^3$. Solid lines refer to $\chi = 0$, while dashed lines refer to $\chi = \pi/4$.

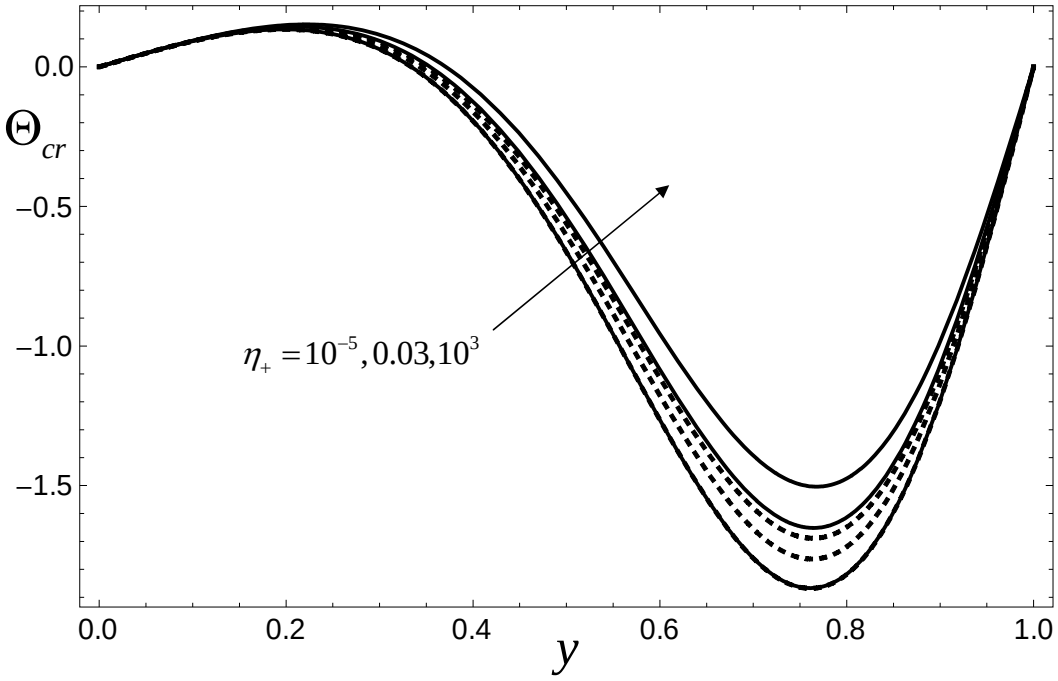

Figure 4.9: Plots of Θ_{cr} as a function of y for $Bi \to \infty$ and $\eta_+ = 10^{-5}, 0.03, 10^3$. Solid lines refer to $\chi = 0$, while dashed lines refer to $\chi = \pi/4$.

the streamlines of the two-dimensional velocity disturbance field (U, V), respectively, for the orientation angle $\chi = 0$ and $\eta_+ = 10^3$. In fact, from Eq. (4.23), one has $W = 0$ as Eq. (4.28) predicts for $\chi = 0$ that P is independent of z. For the adiabatic case, $Bi = 0$ (Fig. 4.10), one may see that the velocity rolls are spread over the whole channel width and are almost symmetric with respect to the horizontal midplane. When the bottom boundary is isothermal, $Bi \to \infty$ (Fig. 4.11), the velocity rolls are placed predominantly within the upper part of the channel. This upward displacement is justified since the fluid is unstably stratified only in the upper part of the porous layer. In fact, in the basic flow solution Eq. (4.18) for $Bi \to \infty$, the horizontal midplane is hotter than the boundary planes.

4.5 Conclusions

A stability analysis of the basic parallel uniform flow in a horizontal porous layer with impermeable boundaries has been performed. The Forchheimer model, together with the Oberbeck-Boussinesq approximation, has been adopted. The basic temperature profile is nonlinear due to the effect of viscous dissipation. The top boundary plane has been taken to be isothermal. The bottom boundary has been assumed to be subject to a third kind boundary condition described in the nondimensional equations through the Biot number, Bi. The conditions of vanishing heat flux and of uniform temperature at the bottom boundary are mathematically expressed as two limiting cases $Bi \to 0$ (adiabatic boundary) $Bi \to \infty$ (isothermal boundary). Arbitrarily oriented roll disturbances have been studied by adopting a pressure-temperature formulation. The resulting eigenvalue ODE problem has been solved numerically by means of a fourth order Runge-Kutta method coupled with the shooting method.
The main results obtained are the following:

- the governing parameter describing the onset of convective instability is $R = Ge\, Pe^2$, where Ge is the Gebhart number and Pe is the Péclet number;
- under the physically reasonable assumption $Ge \ll 1$, the eigenvalue ODE problem becomes self-adjoint, thus admitting real solutions;
- the most unstable rolls are the longitudinal;

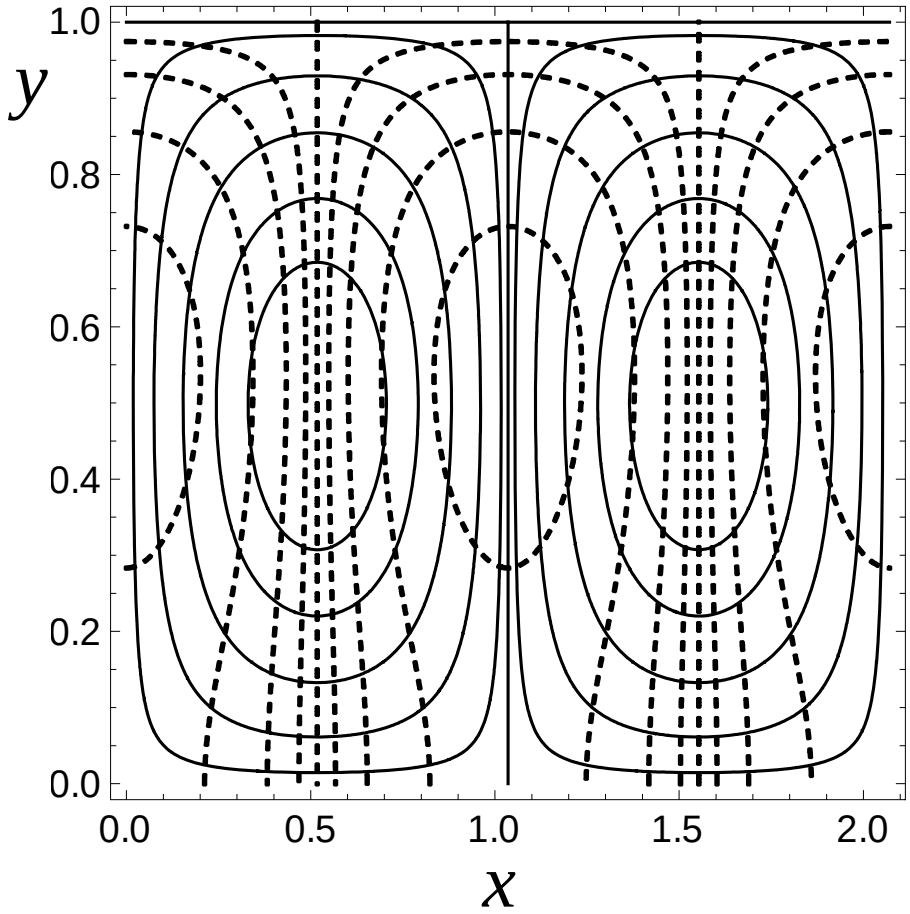

Figure 4.10: Plots of the streamlines (solid lines) of the velocity disturbances, **U**, and the isotherms (dashed lines) of the temperature disturbances, Θ, under critical conditions, $a = a_{cr}$ and $R = R_{cr}$, for $\chi = 0$, $\eta_+ = 10^3$ and for $Bi = 0$.

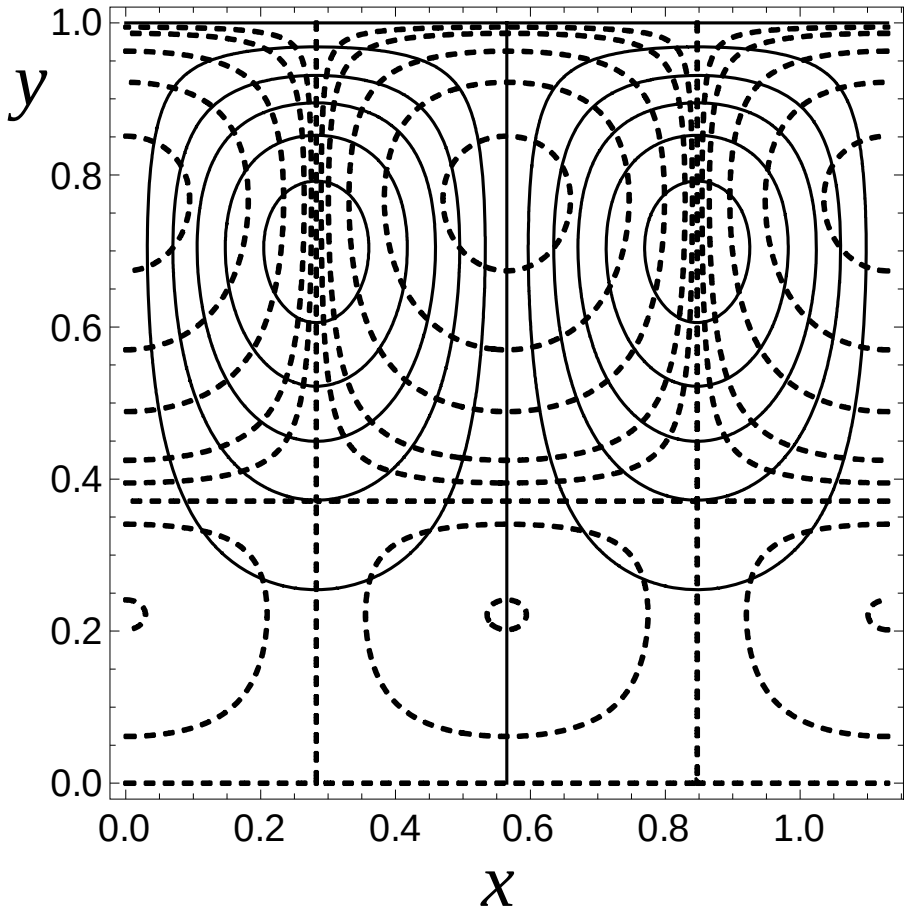

Figure 4.11: Plots of the streamlines (solid lines) of the velocity disturbances, **U**, and the isotherms (dashed lines) of the temperature disturbances, Θ, under critical conditions, $a = a_{cr}$ and $R = R_{cr}$, for $\chi = 0$, $\eta_+ = 10^3$ and for $Bi = \infty$.

- in the limit of validity of Darcy's law $\eta_+ \to 0$ the inclination of oblique rolls does not influence the critical conditions for the onset of the instability;
- the critical wavenumber and the critical value of R for the onset of longitudinal rolls are independent of the form-drag coefficient;
- the critical wavenumber and the critical value of R for the onset of transverse or oblique rolls other than longitudinal depend on the form-drag coefficient;
- the layer with an isothermal bottom boundary is more stable than the layer with an adiabatic bottom boundary.

5

Darcy free convection with a basic linear velocity profile

5.1 Introduction

In this chapter we study a free convection flow in a horizontal porous layer with an adiabatic bottom boundary and a top boundary with a stationary and non-uniform temperature distribution. The problem treated is, in several respects, analogous to the HRL problem. The top boundary temperature distribution is assumed to have a constant gradient and the effect of viscous dissipation is taken into account. A basic parallel buoyant flow develops in the horizontal direction where the top boundary temperature changes. The governing parameters are the Gebhart number and the horizontal Rayleigh number associated with the gradient of the prescribed boundary temperature distribution. In fact, the system experiences a more and more intense effect of the frictional heating as the Gebhart number increases. A linear stability analysis of the basic buoyant flow is carried out. Oblique roll disturbances in any arbitrary horizontal direction are studied and the critical values of the horizontal Rayleigh number are evaluated numerically. It is shown that, for realistic values of the Gebhart number, the longitudinal rolls are the most unstable. Moreover, it is proved that the viscous dissipation yields a destabilising effect.

The contents of this chapter are based on the paper (8) by Barletta, Celli and Nield.

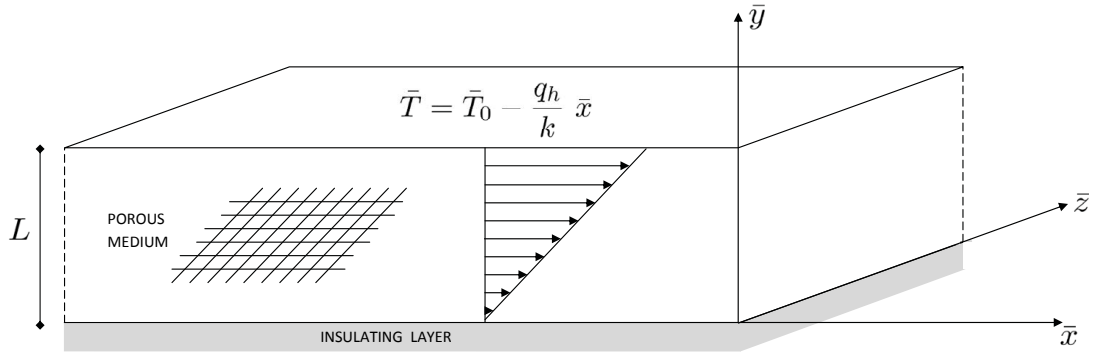

Figure 5.1: Drawing of the porous layer, of the boundary conditions and of the basic flow profile.

5.2 Mathematical model

We consider a plane porous slab with thickness L bounded by two horizontal impermeable planes $\bar{y} = 0$ and $\bar{y} = L$, so that $\mathbf{g} = -g\,\mathbf{e}_y$. The bottom boundary plane is adiabatic, while the top boundary $\bar{y} = L$ is subject to a linear change in the horizontal $\bar{x}$-direction. A sketch of the channel is shown in Figure 5.1.

Here both the Darcy model and the Oberbeck-Boussinesq approximation are invoked. It is assumed that local thermal equilibrium holds. Heat generation due to the viscous dissipation contribution is taken into account. Then, the governing equations can be expressed as in Chapter 3, namely

$$\bar{\nabla} \cdot \bar{\mathbf{u}} = 0, \tag{5.1}$$

$$\frac{\mu}{K}\,\bar{\mathbf{u}} = -\bar{\nabla}\bar{p} + \rho_0\, g\, \beta\, \left(\bar{T} - \bar{T}_0\right) \mathbf{e}_y, \tag{5.2}$$

$$\sigma\,\frac{\partial \bar{T}}{\partial \bar{t}} + \bar{\mathbf{u}} \cdot \bar{\nabla}\bar{T} = \tilde{\alpha}\,\bar{\nabla}^2\bar{T} + \frac{\nu}{K\,c}\,\bar{\mathbf{u}} \cdot \bar{\mathbf{u}}, \tag{5.3}$$

where σ is defined by Eq.(2.10). The boundary conditions applied on the system are

$$\bar{y} = 0: \qquad \bar{v} = 0, \qquad \frac{\partial \bar{T}}{\partial \bar{y}} = 0, \tag{5.4}$$

$$\bar{y} = L: \qquad \bar{v} = 0, \qquad \bar{T} = \bar{T}_0 - \frac{q_h}{\tilde{k}}\,\bar{x}. \tag{5.5}$$

5.2.1 Nondimensional formulation

The characteristic unit measures of the variable used here are the same introduced in the last two Chapters and they are defined as

$$(\bar{x}, \bar{y}, \bar{z}) = (x, y, z)\, L, \qquad \bar{t} = t\, \frac{\sigma\, L^2}{\tilde{\alpha}}, \qquad (\bar{u}, \bar{v}, \bar{w}) = (u, v, w)\, \frac{\tilde{\alpha}}{L}, \tag{5.6}$$

$$\bar{T} = \bar{T}_0 + T\, \frac{\nu\, \tilde{\alpha}}{g\, \beta\, L\, K}, \qquad \bar{p} = p\, \frac{\mu\, \tilde{\alpha}}{K}. \tag{5.7}$$

Moreover it is necessary to introduce the new nondimensional number

$$Ra_h = \frac{g\, \beta\, q_h\, K\, L^2}{\nu\, \tilde{\alpha}\, k}, \tag{5.8}$$

where Ra_h is the horizontal Rayleigh number associated with the streamwise temperature change forced by the condition at the top boundary $\bar{y} = L$. Then, Eqs. (5.1)-(5.3) can be rewritten as

$$\nabla \cdot \mathbf{u} = 0, \tag{5.9}$$

$$\mathbf{u} = -\nabla p + T\, \mathbf{e}_y, \tag{5.10}$$

$$\frac{\partial T}{\partial t} + \mathbf{u} \cdot \nabla T = \nabla^2 T + Ge\ \mathbf{u} \cdot \mathbf{u}. \tag{5.11}$$

On the other hand, the boundary conditions expressed by Eqs. (5.4)-(5.5) can be rewritten in a nondimensional form as

$$y = 0: \qquad v = 0, \qquad \frac{\partial T}{\partial y} = 0, \tag{5.12}$$

$$y = 1: \qquad v = 0, \qquad T = -\,Ra_h\ x, \tag{5.13}$$

where Ge is the Gebhart number, defined by Eq. (3.16).

5.2.2 Fully developed basic flow

A solution of Eqs. (5.9)-(5.13) is sought under the assumptions of stationary regime and fully developed horizontal flow along the x-direction. These assumptions are taken

to let the viscous term contribute to the linear stability analysis. The fully developed horizontal flow can be expressed as

$$u_B = u_B(y), \qquad v_B = w_B = 0. \tag{5.14}$$

It is easily proved that

$$u_B(y) = Ra_h\, y, \tag{5.15}$$

$$T_B(x,y) = -\,Ra_h\; x + \frac{Ra_h^2}{12}\left[Ge\left(1-y^4\right) + 2\left(1-y^3\right)\right], \tag{5.16}$$

$$p_B(x,y) = -\,Ra_h\, x\, y + \frac{Ra_h^2\, y}{12}\left[Ge\left(1-\frac{y^4}{5}\right) + 2\left(1-\frac{y^3}{4}\right)\right], \tag{5.17}$$

where the arbitrary integration constant for the pressure distribution has been chosen such that $p_B(0,0) = 0$. Plots of the reduced temperature,

$$\hat{T}_B(y) = \frac{12}{Ra_h^2}\left[T_B(x,y) + Ra_h\; x\right] = Ge\left(1-y^4\right) + 2\left(1-y^3\right), \tag{5.18}$$

are given in Figure 5.2. From this figure, we see that the bottom boundary has a temperature higher than the top boundary for every cross-section $x = constant$, the distribution being monotonically decreasing. From Eq. (5.16), this nondimensional temperature difference is

$$\Delta T_B = T_B(x,0) - T_B(x,1) = \frac{Ra_h^2}{12}\left(Ge + 2\right). \tag{5.19}$$

5.2.3 Linear disturbances

The method used here to investigate the stability analysis is, again, the normal mode method. This method needs the main flow to be split in two contributions: a mean basic flow and an arbitrarily small disturbances. The main flow can thus be expresses as

$$p = p_B + \varepsilon\, P, \qquad u = u_B + \varepsilon\, U, \qquad v = \varepsilon\, V, \qquad w = \varepsilon\, W, \qquad T = T_B + \varepsilon\, \theta, \tag{5.20}$$

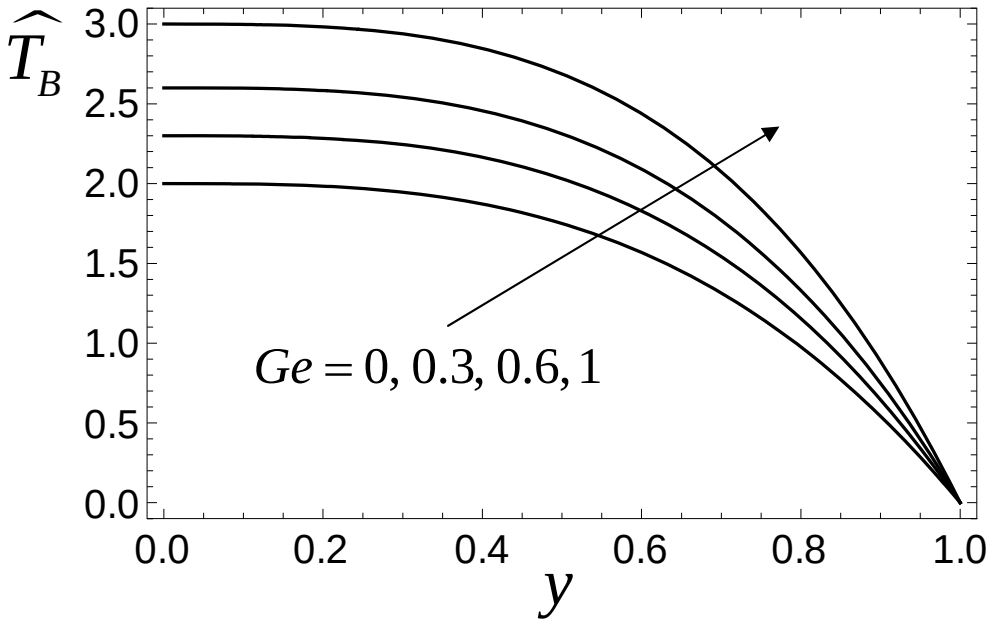

Figure 5.2: Basic flow: reduced temperature distribution for different values of Ge.

where ε is the perturbation parameter. The latter is supposed to be so small that terms of order higher than ε can be neglected. Then, by substituting Eq. (5.20) in Eqs. (5.9)-(5.13) one obtains

$$\nabla \cdot \mathbf{U} = 0, \tag{5.21}$$

$$\mathbf{U} = -\nabla P + \theta\, \mathbf{e}_y, \tag{5.22}$$

$$\frac{\partial \theta}{\partial t} + u_B \frac{\partial \theta}{\partial x} + U \frac{\partial T_B}{\partial x} + V \frac{\partial T_B}{\partial y} = \nabla^2 \theta + 2\ Ge\ u_B\ U, \tag{5.23}$$

$$y = 0: \qquad V = 0, \qquad \frac{\partial \theta}{\partial y} = 0, \tag{5.24}$$

$$y = 1: \qquad V = 0, \qquad \theta = 0. \tag{5.25}$$

By rearranging Eqs. (5.21)-(5.25), one obtains a pressure-temperature formulation,

$$\nabla^2 P = \frac{\partial \theta}{\partial y}, \tag{5.26}$$

$$\frac{\partial \theta}{\partial t} + u_B \frac{\partial \theta}{\partial x} - \frac{\partial P}{\partial x}\frac{\partial T_B}{\partial x} - \left(\frac{\partial P}{\partial y} - \theta\right)\frac{\partial T_B}{\partial y} = \nabla^2\theta - 2\, Ge\, u_B \frac{\partial P}{\partial x}, \tag{5.27}$$

$$y = 0: \qquad \frac{\partial P}{\partial y} = \theta, \qquad \frac{\partial \theta}{\partial y} = 0, \tag{5.28}$$

$$y = 1: \qquad \frac{\partial P}{\partial y} = 0, \qquad \theta = 0. \tag{5.29}$$

5.3 Instability with respect to oblique rolls

As in the last Chapter, to consider all the possible oblique rolls, the direction of the disturbances is assumed to be variable with an inclination angle χ with respect to x axis. Let us seek solutions of Eqs. (5.26)-(5.29) in the form of plane waves,

$$\begin{aligned} P(x,y,z,t) &= \Re\left\{\mathcal{P}(y)\, e^{\lambda t} e^{ia(x\,\cos\chi + z\sin\chi)}\right\}, \\ \theta(x,y,z,t) &= \Re\left\{\Theta(y)\, e^{\lambda t} e^{ia(x\,\cos\chi + z\sin\chi)}\right\}, \end{aligned} \tag{5.30}$$

where $\lambda = \lambda_1 + i\,\lambda_2$ is a complex coefficient and χ is the inclination angle between the basic flow direction and the propagation direction of the disturbance wave. By setting $\Re(\lambda) = \lambda_1 = 0$ in order to investigate neutral stability, Eqs. (5.26)-(5.29) can be rewritten as

$$\mathcal{P}'' - a^2\,\mathcal{P} - \Theta' = 0, \tag{5.31}$$

$$\begin{aligned} \Theta'' - \left[a^2 - \frac{Ra_h^2\, y^2}{6}\,(2\,Ge\, y + 3) + i\,(\lambda_2 + a\,\cos\chi\, Ra_h\, y)\right]\Theta + \\ - \frac{Ra_h^2\, y^2}{6}\,(2\,Ge\, y + 3)\,\mathcal{P}' - i\,a\,\cos\chi\, Ra_h\,(2\,Ge\, y + 1)\,\mathcal{P} = 0, \end{aligned} \tag{5.32}$$

$$\begin{aligned} y = 0: &\quad \mathcal{P}' = \Theta, \quad \Theta' = 0, \\ y = 1: &\quad \mathcal{P}' = 0, \quad \Theta = 0. \end{aligned} \tag{5.33}$$

5.3.1 Longitudinal rolls

The longitudinal rolls can be defined by substituting $\chi = \pi/2$ into Eqs. (5.31) - (5.32), namely

$$\mathcal{P}'' - a^2\,\mathcal{P} - \Theta' = 0, \tag{5.34}$$

$$\Theta'' - \left[a^2 - \frac{Ra_h^2\,y^2}{6}\,(2\,Ge\,y + 3) + i\lambda_2\right]\Theta \; - \; \frac{Ra_h^2\,y^2}{6}\,(2\,Ge\,y + 3)\,\mathcal{P}' = 0, \tag{5.35}$$

One can note that the eigenvalue problem Eqs. (5.34)-(5.35) becomes self-adjoint upon setting $\lambda_2 = 0$. This implies that, for $\chi = \pi/2$, the eigenfunctions $(\mathcal{P}, \Theta)$ are real-valued and the disturbance waves, defined by Eq. (5.30), have a vanishing phase velocity in the z-direction.

5.3.2 Transverse rolls

In the case of transverse rolls, by substituting $\chi = 0$ into Eqs. (5.31) - (5.32) one obtains a differential problem that, unlike the one for longitudinal rolls, is not self-adjoint,

$$\mathcal{P}'' - a^2\,\mathcal{P} - \Theta' = 0, \tag{5.36}$$

$$\begin{aligned}\Theta'' - \left[a^2 - \frac{Ra_h^2\,y^2}{6}\,(2\,Ge\,y + 3) + i\,(\lambda_2 + a\,Ra_h\,y)\right]\Theta + \\ - \; \frac{Ra_h^2\,y^2}{6}\,(2\,Ge\,y + 3)\,\mathcal{P}' - i\,a\,Ra_h\,(2\,Ge\,y + 1)\,\mathcal{P} = 0.\end{aligned} \tag{5.37}$$

5.3.3 Numerical solution

The eigenvalue problem given by Eqs. (5.31)-(5.33) can be solved numerically by a fourth order Runge-Kutta technique and by using the shooting method. In detail, the Runge-Kutta technique is used to solve Eqs. (5.31)-(5.33) as an initial value problem. The initial conditions at $y = 0$ specified in Eq. (5.33) are not sufficient to determine a unique solution. In fact, the values of $\mathcal{P}(0)$ and $\Theta(0)$ must be assigned. Since

Eqs. (5.31)-(5.33) are homogeneous, the additional condition $\Theta(0) = 1$ can be prescribed in order to normalise the scale of the disturbances. A parameter Ξ can be defined such that $\mathcal{P}(0) = \Xi$. Therefore, Eq. (5.33) becomes

$$\begin{aligned} y = 0: \quad & \mathcal{P} = \Xi, \quad \mathcal{P}' = 1, \quad \Theta = 1, \quad \Theta' = 0, \\ y = 1: \quad & \mathcal{P}' = 0, \quad \Theta = 0. \end{aligned} \tag{5.38}$$

For $0 \leq \chi < \pi/2$, the eigenfunctions $(\mathcal{P}, \Theta)$ are complex valued, so that also Ξ is a complex parameter. Then, for an assigned pair of input parameters (a, Ge), the constraints $\mathcal{P}'(1) = 0$ and $\Theta(1) = 0$ yield four real equations that allow one to obtain Ra_h, λ_2, as well as the real and the imaginary parts of Ξ. The latter task can be accomplished by coupling a shooting method to the Runge-Kutta numerical solution. A convenient environment for implementing this procedure is *Mathematica 7* (© Wolfram Research, Inc.). The function `NDSolve` is used for the numerical solution of the initial value problem, while the constraints at $y = 1$ are dealt with the function `FindRoot`. After obtaining the eigenvalue pairs (Ra_h, λ_2) that correspond to given pairs of input values (a, Ge), we can determine the critical values a_{cr} and $Ra_{h,cr}$ by seeking the minimum of function $Ra_h(a)$ for every assigned Ge.

A convergence test of the numerical solution has been carried out by changing the fixed step-size δy of the Runge-Kutta method. Function `NDSolve` allows one to use an adaptive step-size control. A comparison of the results obtained by the adaptive and the fixed step-size Runge-Kutta solutions is reported in Table 5.1. This table shows that by decreasing the fixed step-size δy one obtains for $\delta y = 0.001$, within 9 significant digits, a perfect agreement with the results found by the adaptive step-size control.

A crucial point in the development of the shooting method is the assignment of an initial guess for the eigenvalue pairs (Ra_h, λ_2) that correspond to given pairs of input values (a, Ge). The nearer is this initial guess to the exact eigenvalue pair the more rapidly converging and the more efficient is the shooting method. This task can be accomplished for the case of longitudinal rolls ($\chi = \pi/2$) by the approximate solution obtained through Galerkin's method of weighted residuals in the next section.

5.4 Weighted residuals solution for longitudinal rolls

In the case of longitudinal rolls, an approximate solution of Eqs. (5.21)-(5.25) can be found by using Galerkin's method of weighted residuals (29).

On account of Eq. (5.30), for longitudinal rolls both P and θ are independent of x. Then, Eq. (5.22) implies that U is zero, so that Eqs. (5.21)-(5.25) yield

$$\frac{\partial V}{\partial y} + \frac{\partial W}{\partial z} = 0, \tag{5.39}$$

$$V = -\frac{\partial P}{\partial y} + \theta, \qquad W = -\frac{\partial P}{\partial z}, \tag{5.40}$$

$$\frac{\partial \theta}{\partial t} + V\,\frac{\partial T_B}{\partial y} = \frac{\partial^2 \theta}{\partial y^2} + \frac{\partial^2 \theta}{\partial z^2}, \tag{5.41}$$

$$y = 0: \qquad V = 0, \qquad \frac{\partial \theta}{\partial y} = 0, \tag{5.42}$$

$$y = 1: \qquad V = 0, \qquad \theta = 0. \tag{5.43}$$

On introducing the streamfunction,

$$V = \frac{\partial \psi}{\partial z}, \qquad W = -\frac{\partial \psi}{\partial y}, \tag{5.44}$$

Eq. (5.39) is identically satisfied. Then, by rearranging Eqs. (5.40)-(5.43) we are led to the streamfunction-temperature formulation,

$$\frac{\partial^2 \psi}{\partial y^2} + \frac{\partial^2 \psi}{\partial z^2} - \frac{\partial \theta}{\partial z} = 0, \tag{5.45}$$

$$\frac{\partial \theta}{\partial t} + \frac{\partial \psi}{\partial z}\,\frac{\partial T_B}{\partial y} = \frac{\partial^2 \theta}{\partial y^2} + \frac{\partial^2 \theta}{\partial z^2}, \tag{5.46}$$

$$y = 0: \qquad \psi = 0, \qquad \frac{\partial \theta}{\partial y} = 0, \tag{5.47}$$

$$y = 1: \qquad \psi = 0, \qquad \theta = 0. \tag{5.48}$$

In the streamfunction-temperature formulation, the plane wave solutions given by Eq. (5.30) with $\lambda_2 = 0$ can be expressed as

$$\psi(y, z, t) = \Psi(y)\; e^{\lambda_1 t} \sin(a\, z), \qquad \theta(y, z, t) = \Theta(y)\; e^{\lambda_1 t} \cos(a\, z). \tag{5.49}$$

By substituting Eq. (5.49) in Eqs. (5.45)-(5.48), one obtains for neutral stability ($\lambda_1 = 0$)

$$\Psi'' - a^2\,\Psi + a\,\Theta = 0, \tag{5.50}$$

$$\Theta'' - a^2\,\Theta + a\,\frac{Ra_h^2\,y^2}{6}\,(2\,Ge\,y + 3)\,\Psi = 0, \tag{5.51}$$

$$y = 0: \qquad \Psi = 0, \qquad \Theta' = 0, \tag{5.52}$$

$$y = 1: \qquad \Psi = 0, \qquad \Theta = 0. \tag{5.53}$$

Approximate expressions of $\Psi(y)$ and $\Theta(y)$ can be written through linear combinations of trigonometric trial functions that satisfy the boundary conditions, Eqs. (5.52) and (5.53),

$$\Psi(y) = \sum_{n=1}^{N} \Psi_n\,\sin(n\,\pi\,y), \qquad \Theta(y) = \sum_{n=1}^{N} \Theta_n\,\cos\left[\left(n - \frac{1}{2}\right)\pi\,y\right]. \tag{5.54}$$

Let us consider the lowest order, $N = 1$. Then, on account of Eq. (5.54), Eqs. (5.50) and (5.51) yield the residuals

$$E_\Psi(y) = -\left(\pi^2 + a^2\right)\Psi_1\,\sin(\pi\,y) + a\,\Theta_1\,\cos\left(\frac{\pi}{2}\,y\right), \tag{5.55}$$

$$E_\Theta(y) = a\,\frac{Ra_h^2\,y^2}{6}\,(2\,Ge\,y + 3)\,\Psi_1\,\sin(\pi\,y) - \left(\frac{\pi^2}{4} + a^2\right)\Theta_1\,\cos\left(\frac{\pi}{2}\,y\right). \tag{5.56}$$

We prescribe the orthogonality of $E_\Psi(y)$ with respect to the trial function $\sin(\pi\,y)$, and the orthogonality of $E_\Theta(y)$ with respect to the trial function $\cos(\pi\,y/2)$, namely

$$\int_0^1 E_\Psi(y)\,\sin(\pi\,y)\,dy = 0, \qquad \int_0^1 E_\Theta(y)\,\cos\left(\frac{\pi}{2}\,y\right)dy = 0. \tag{5.57}$$

Eq. (5.57) can be written as a linear system of algebraic equations,

$$\begin{pmatrix} M_{\Psi\Psi} & M_{\Psi\Theta} \\ M_{\Theta\Psi} & M_{\Theta\Theta} \end{pmatrix} \begin{pmatrix} \Psi_1 \\ \Theta_1 \end{pmatrix} = 0, \tag{5.58}$$

where

$$\begin{aligned} &M_{\Psi\Psi} = -\frac{1}{2}\left(\pi^2 + a^2\right), \qquad M_{\Psi\Theta} = \frac{4a}{3\pi}, \\ &M_{\Theta\Psi} = \frac{16a\left[9\pi^2(\,Ge + 1) - 80\,Ge - 21\pi\right]Ra_h{}^2}{81\pi^4}, \qquad M_{\Theta\Theta} = -\frac{1}{2}\left(\frac{\pi^2}{4} + a^2\right). \end{aligned} \tag{5.59}$$

Ge	$\delta y = 0.2$	$\delta y = 0.1$	$\delta y = 0.01$	$\delta y = 0.001$	*Adaptive*	
0	15.0492448	15.0328344	15.0310861	15.0310859	15.0310859	$Ra_{h,cr}$
	2.61980685	2.62211542	2.62246839	2.62246843	2.62246843	a_{cr}
0.2	14.4671485	14.4512942	14.4495614	14.4495612	14.4495612	$Ra_{h,cr}$
	2.63232262	2.63473566	2.63511981	2.63511986	2.63511986	a_{cr}
0.4	13.9470592	13.9317089	13.9299926	13.9299924	13.9299924	$Ra_{h,cr}$
	2.64344304	2.64594237	2.64635503	2.64635507	2.64635507	a_{cr}
0.6	13.4787926	13.4639021	13.4622030	13.4622028	13.4622028	$Ra_{h,cr}$
	2.65338114	2.65595226	2.65639100	2.65639105	2.65639105	a_{cr}
0.8	13.0543446	13.0398759	13.0381943	13.0381941	13.0381941	$Ra_{h,cr}$
	2.66231055	2.66494179	2.66540444	2.66540449	2.66540449	a_{cr}
1.0	12.6673294	12.6532495	12.6515858	12.6515856	12.6515856	$Ra_{h,cr}$
	2.67037366	2.67305557	2.67354018	2.67354024	2.67354024	a_{cr}

Table 5.1: Values of $Ra_{h,cr}$ and a_{cr} versus Ge for the longitudinal rolls, $\chi = \pi/2$; comparison between the adaptive step-size Runge-Kutta method and the Runge-Kutta method with fixed step-size δy.

Eq. (5.58) admits nontrivial solutions only if the matrix M has a vanishing determinant. This condition can be expressed as

$$Ra_h{}^2 = \left[\left(\frac{64\,a^2}{27\,\pi^3} - \frac{5120\,a^2}{243\,\pi^5}\right) Ge + \frac{64\,a^2}{27\,\pi^3} - \frac{448\,a^2}{81\,\pi^4}\right]^{-1} \left(\frac{a^4}{4} + \frac{5\,\pi^2\,a^2}{16} + \frac{\pi^4}{16}\right). \quad (5.60)$$

On seeking the minimum of the right hand side of Eq. (5.60), one determines the critical values

$$a_{cr} = \frac{\pi}{\sqrt{2}}, \qquad Ra_{h,cr}^2 = \frac{2187\pi^7}{1024\,[9\,\pi^2(Ge+1) - 80\,Ge - 21\,\pi]}. \quad (5.61)$$

Then,

$$a_{cr} \cong 2.22144147, \qquad Ra_{h,cr} \cong \frac{16.8007015}{\sqrt{1 + 0.386226840\,Ge}}. \quad (5.62)$$

Let us refer to the range $0 < Ge < 1$. With respect to a_{cr}, Eq. (5.62) is an underestimate of the accurate value obtained through the fourth order Runge-Kutta method with a relative error between 15% ($Ge = 0$) and 17% ($Ge = 1$). On the other hand, with respect to $Ra_{h,cr}$, Eq. (5.62) is an overestimate of the accurate value obtained through

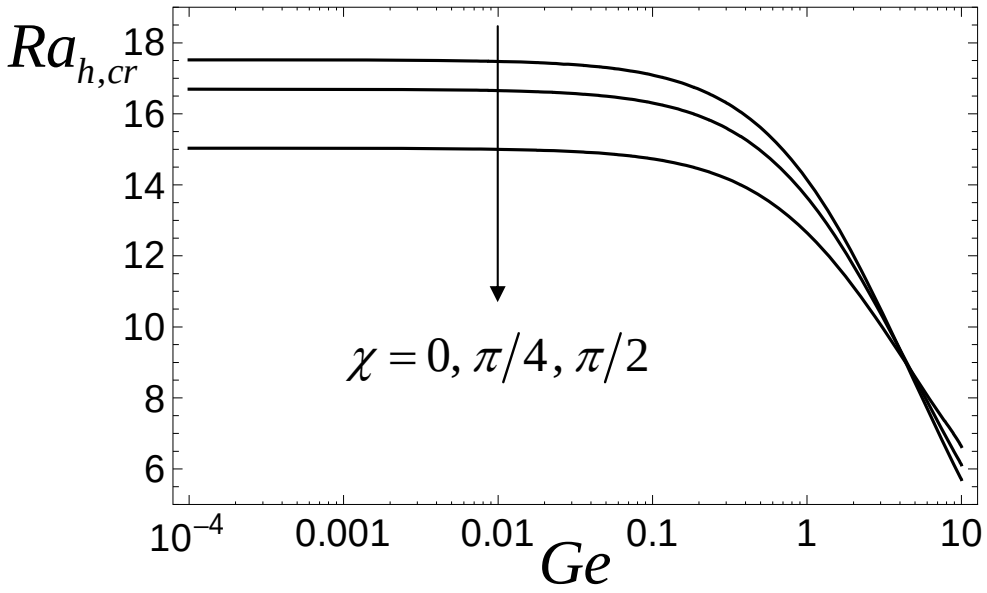

Figure 5.3: Plots of $Ra_{h,cr}$ versus Ge for different values of χ.

the fourth order Runge-Kutta method with a relative error between 12% ($Ge = 0$) and 13% ($Ge = 1$).

5.5 Discussion of the results

A fairly accurate correlation of $Ra_{h,cr}$ versus Ge for longitudinal rolls, determined by interpolating the data obtained through the fourth order Runge-Kutta method in the range $0 < Ge < 2$, is

$$Ra_{h,cr} \cong \frac{15.0310859}{\sqrt{1 + 0.411825090\, Ge}}, \tag{5.63}$$

the relative error being smaller than 0.025%. The functional form $Ra_{h,cr}(Ge)$ given by Eq. (5.63) is formally the same as that predicted by Galerkin's method and expressed by Eq. (5.62). On account of Eq. (5.63), we note that $Ra_{h,cr}$ is a decreasing function of Ge. This behaviour implies that the effect of viscous dissipation, one which vanishes in the limit $Ge \to 0$, is destabilising. The same conclusion can be drawn on examining the data reported in Table 5.1. This table shows that a_{cr} is a weakly increasing function of Ge.

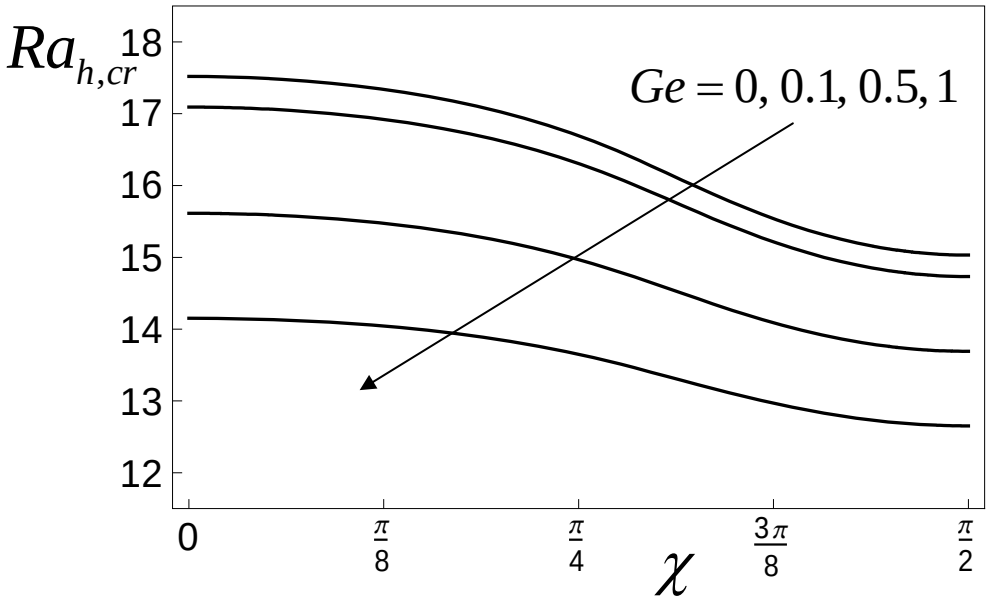

Figure 5.4: Plots of $Ra_{h,cr}$ versus χ for different values of Ge.

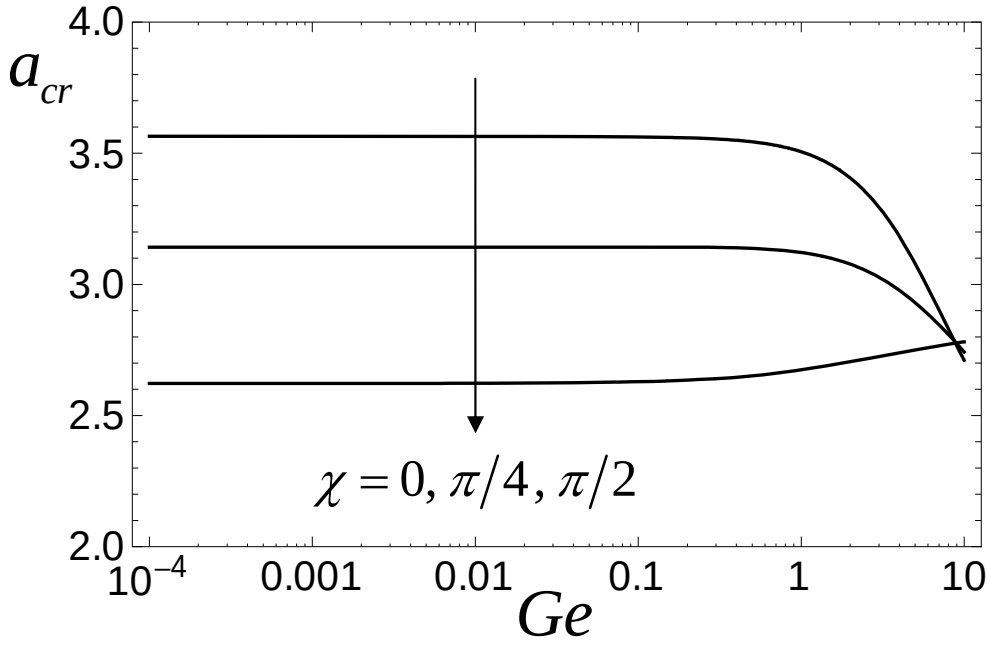

Figure 5.5: Plots of a_{cr} versus Ge for different values of χ.

Figure 5.3 displays the behaviour of $Ra_{h,cr}$ versus Ge for three different inclinations of the oblique rolls: $\chi = 0$ (transverse rolls), $\chi = \pi/4$ and $\chi = \pi/2$ (longitudinal rolls). This figure allows one to conclude that the longitudinal rolls are the most unstable at least in a physically meaningful range of Ge. In fact, Ge is usually lower than 1 and often much lower than 1. Then, the range $Ge \gtrsim 4$ where transverse rolls are the most unstable mode is definitely of minor interest. Whatever is the inclination angle of the disturbance rolls, Figure 5.3 shows that $Ra_{h,cr}$ is a monotonic decreasing function of Ge. The conclusion that the most unstable mode is the longitudinal rolls disturbance reinforces Eq. (5.63) as a significant correlation for obtaining the onset condition of linear instability.

Figure 5.4 illustrates the dependence of $Ra_{h,cr}$ on the inclination angle, χ, between the disturbance wave vector and the x-axis, for different values of Ge. In the range $0 \leq \chi \leq \pi/2$, the critical Rayleigh number is a weakly decreasing function of χ. This confirms the conclusion drawn from Figure 5.3 that longitudinal rolls ($\chi = \pi/2$) are the most unstable adding the information that $Ra_{h,cr}$ decreases monotonically with the inclination angle χ.

Figure 5.5 shows that the critical wavenumber a_{cr} depends weakly on the Gebhart number, at least in the physically significant range $0 < Ge < 1$. As the Gebhart number increases above this range, the critical wavenumber tends to change with Ge so that the dependence on the inclination angle χ is progressively reduced. One may see in Figure 5.5 that a value $Ge \approx 9$ exists where the dependence on χ disappears.

The convective roll patterns corresponding to the critical conditions for $Ge = 0$ are represented in Figures 5.6- 5.9. The streamlines of the velocity disturbance $\mathbf{U}$ (solid lines) and the isotherms $\theta = constant$ (dashed lines) are drawn for different oblique rolls from $\chi = \pi/2$ (longitudinal rolls) to $\chi = 0$ (transverse rolls). Figures 5.6- 5.9 shows a more and more marked bending of the convection rolls as the inclination angle decreases from $\pi/2$. This effect is a consequence of the drift of the disturbance rolls in the streamwise x-direction. We mention that the qualitative shape of the convection rolls is not apparently affected by the Gebhart number, i.e. by the effect of viscous dissipation. Then, values of Ge in the range $0 < Ge \leq 1$ yield critical convection patterns hardly distinguishable from those in Figures 5.6- 5.9.

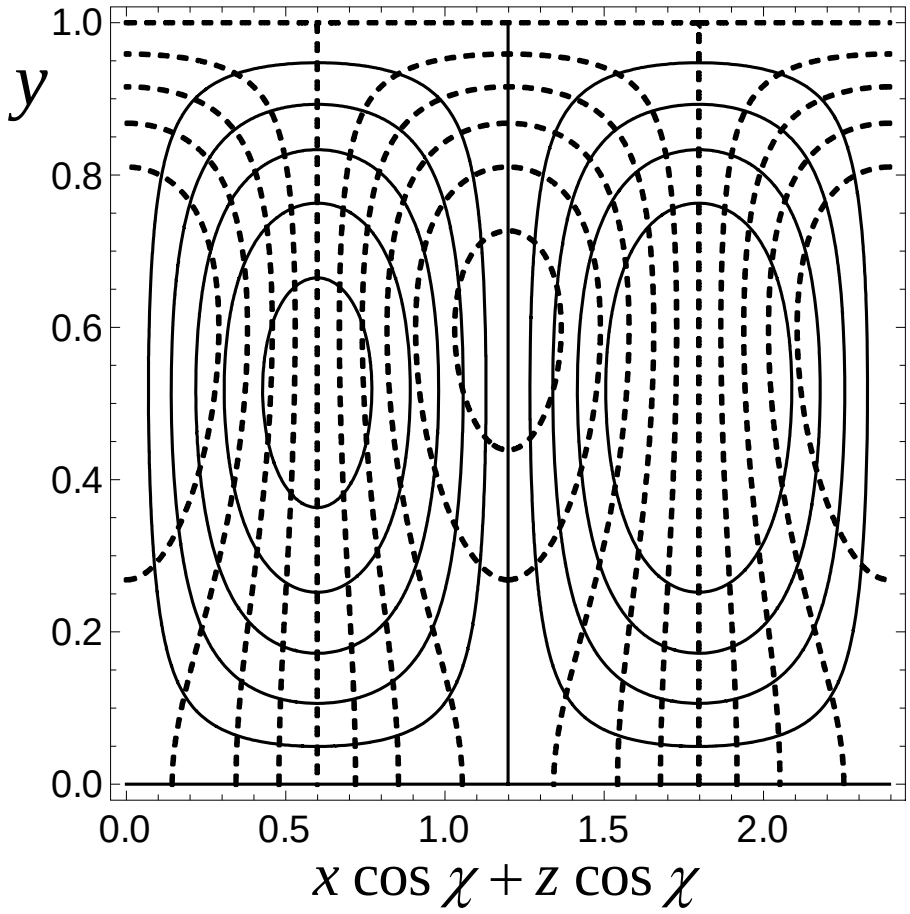

Figure 5.6: Plots of the streamlines (solid lines) of the velocity disturbance, **U**, and the isotherms (dashed lines) of the temperature disturbance, θ, under critical conditions, $a = a_{cr}$ and $Ra_h = Ra_{h,cr}$, for $Ge = 0$ and $\chi = \pi/2$.

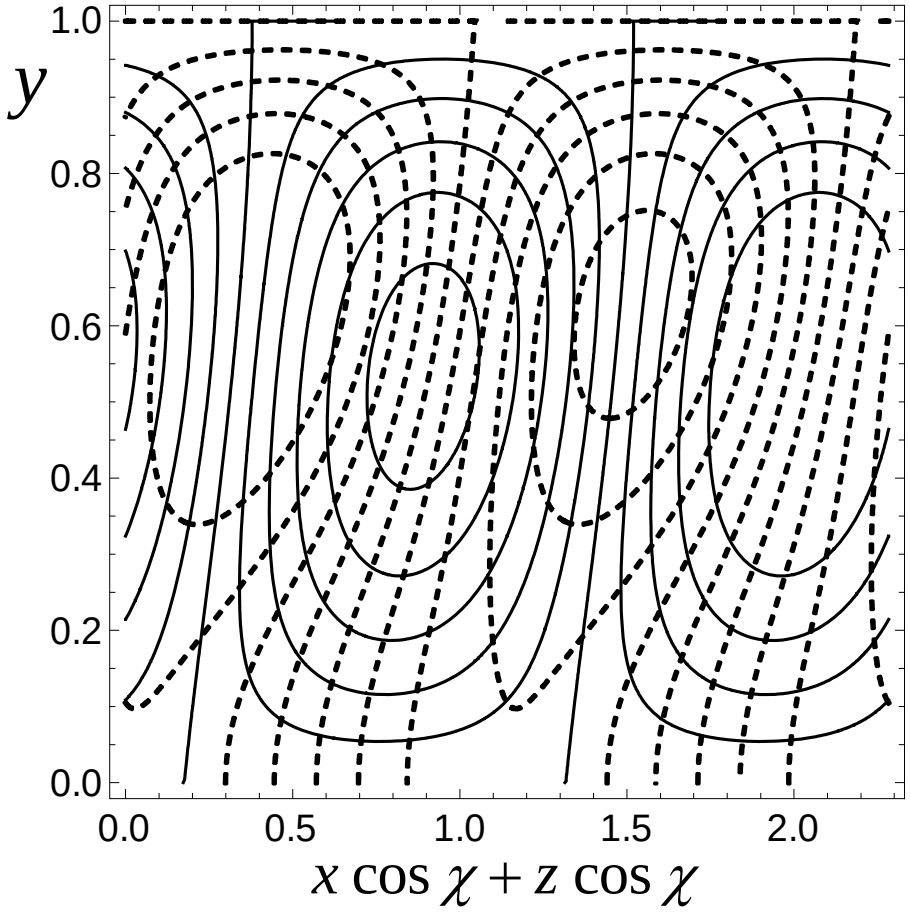

Figure 5.7: Plots of the streamlines (solid lines) of the velocity disturbance, **U**, and the isotherms (dashed lines) of the temperature disturbance, θ, under critical conditions, $a = a_{cr}$ and $Ra_h = Ra_{h,cr}$, for $Ge = 0$ and $\chi = \pi/3$.

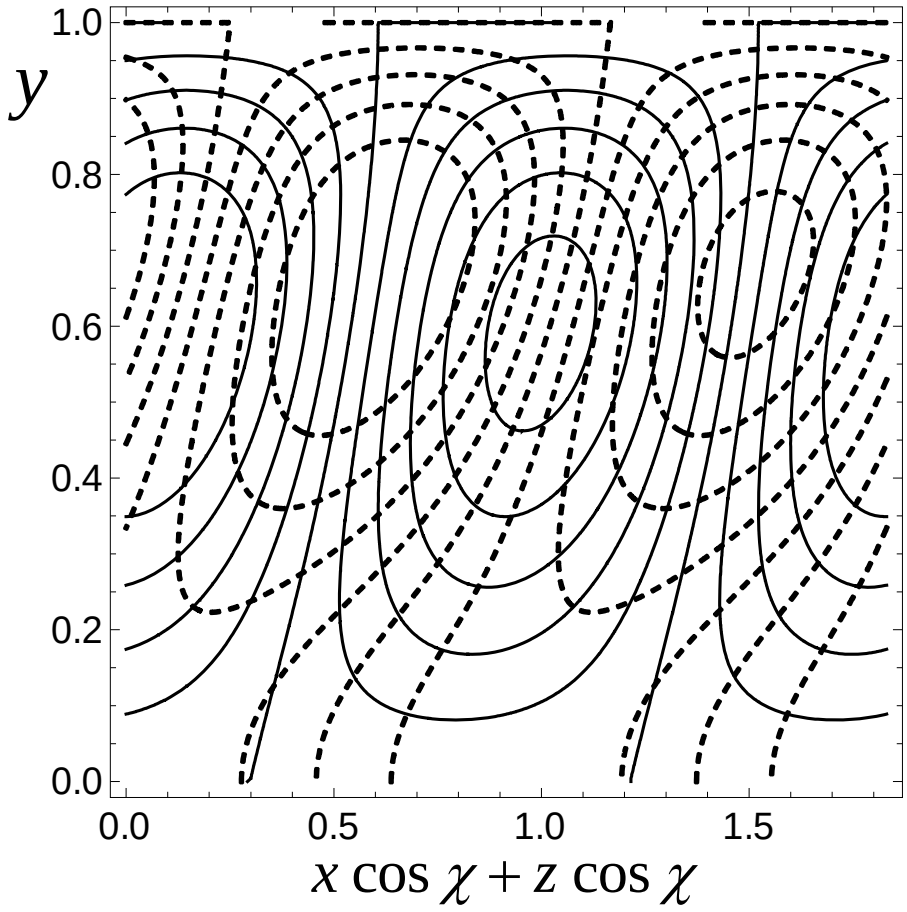

Figure 5.8: Plots of the streamlines (solid lines) of the velocity disturbance, **U**, and the isotherms (dashed lines) of the temperature disturbance, θ, under critical conditions, $a = a_{cr}$ and $Ra_h = Ra_{h,cr}$, for $Ge = 0$ and $\chi = \pi/6$.

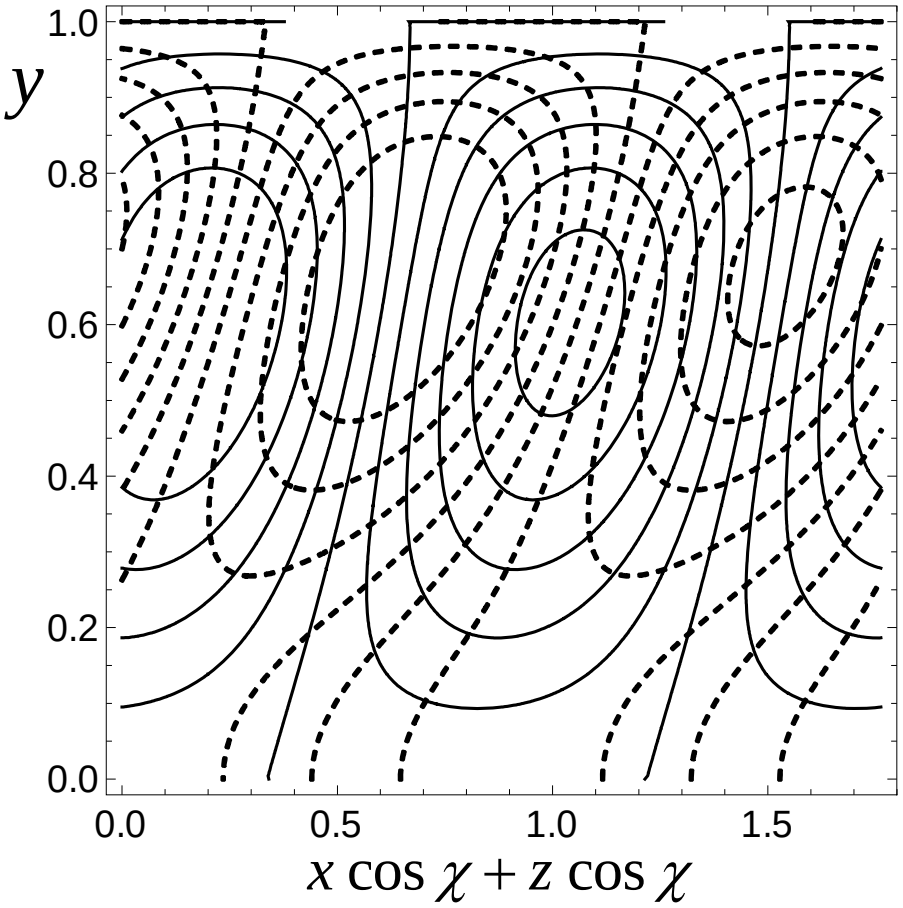

Figure 5.9: Plots of the streamlines (solid lines) of the velocity disturbance, **U**, and the isotherms (dashed lines) of the temperature disturbance, θ, under critical conditions, $a = a_{cr}$ and $Ra_h = Ra_{h,cr}$, for $Ge = 0$ and $\chi = 0$.

5.6 Conclusions

A non-uniform parallel buoyant flow in a horizontal plane porous layer with impermeable boundaries has been analysed. This basic flow is induced by the horizontal temperature gradient prescribed on the top boundary, as well as by the internal viscous heating. The basic temperature profile displays a maximum at the bottom boundary of the layer, where a condition of thermal insulation (vanishing heat flux) is assumed. Hence, a possibly unstable thermal stratification is present in the basic flow. The basic parallel velocity field has a linear profile, vanishing at the bottom boundary and being at its maximum at the top boundary. It has been shown that the governing parameter which drives the transition to instability is the horizontal Rayleigh number, Ra_h. Another governing parameter, the Gebhart number Ge, assesses the effect of the viscous dissipation. A linear stability analysis has been carried out in order to determine the critical conditions for the onset of oblique rolls with any inclination angle χ of the wave vector with respect to the basic flow direction.
The most important results obtained by the linear stability analysis of the basic flow are the following.

- In the physically significant range of values of Ge, the longitudinal rolls are the most unstable. Any other oblique roll disturbance yields higher values of the critical Rayleigh number, $Ra_{h,cr}$.

- In the absence of viscous dissipation, i.e. in the limit $Ge \to 0$, the minimum of the neutral stability curve $Ra_h(a)$ for longitudinal rolls is achieved for $a = a_{cr} = 2.6225$ and $Ra_h = Ra_{h,cr} = 15.031$.

- The effect of viscous dissipation is destabilizing. The critical value of Ra_h for the onset of convective rolls is in fact a decreasing function of Ge.

- The critical wavenumber, a_{cr}, is weakly dependent on the Gebhart number, unless $Ge \gtrsim 1$. The latter condition is hardly observed in physical systems.

6

LTNE in a forced convection boundary layer

6.1 Introduction

The chapter is focused on using the local thermal non-equilibrium model to analyse a thermal porous boundary layer. LTNE modelling assumes that the solid matrix may have a different temperature compared to the one of the saturating fluid, this being meant in terms of averages over representative elementary volumes. Thus, hot fluid may flow into a cold, relatively insulating, porous matrix and there will exist a difference in the average local temperature of the two phases. This difference will take some distance to reduce to values such that the phases share the practically the same local temperature (LTE), see (73), although there are configurations for which LTNE persists even in the steady state, e.g. (75) and (70).

In this chapter a steady forced convection thermal boundary layer flow in a porous medium is studied. This configuration bears a great deal of similarity to the classical Pohlhausen problem in that a thermal boundary layer is induced by a step change in the temperature of a semi-infinite flat plate (63). The only difference is that here we are dealing with saturated porous media and not with clear fluids.

Conditions are determined within which the boundary layer approximation may be made and we undertake an analytical and numerical study of the resulting temperature fields. After a suitable rescaling, the governing equations are found to depend on just

one parameter, γ, which, in turn, is defined in terms of the porosity of the medium and of the thermal conductivities of the two phases. The thermal boundary layer equations are then solved in three different ways: (i) analytically by means of a small-x asymptotic analysis, (ii) analytically using a large-x series solution, and (iii) numerically by means of a Keller box code. The small-x analysis requires the use of two asymptotic regions, one of which is narrow and is such that the temperature of the fluid phase drops to the ambient value at leading order, and a second much thicker region within which the temperature of the solid phase drops to the ambient. Asymptotic matching between these two regions is performed and described briefly. This analysis is guided by the earlier study of Rees and Pop (75) who considered the effect of LTNE on a vertical free convective boundary layer flow. The two-layer structure is then modeled numerically by using the results of the asymptotic analysis to devise a modified outer boundary condition for the solid temperature. The numerical solution is further facilitated by the use of properly rescaled variables.

Local thermal non-equilibrium between the phases is found to be at its strongest near the leading edge, but the maximum difference between the temperatures of the phases decreases with distance from the leading edge, and local thermal equilibrium is attained at large distances.

The contents of this chapter are based on the paper (22), yet to be submitted for publication, by Celli, Rees and Barletta.

6.2 Mathematical model

A two-dimensional forced convection flow over a horizontal flat plate is assumed. A sketch of the plate and of the coordinate system is shown in Figure 6.1.

The Darcy model for the porous medium is assumed to apply, and therefore the externally-generated fluid motion is both uniform in space and constant in time. The Oberbeck-Boussinesq approximation is invoked. The impermeable bounding surface, which is placed at $\bar{y} = 0$, is held at the temperature, T_w, in the range, $\bar{x} > 0$, but is held at the temperature of the free stream, T_∞, in the range, $\bar{x} < 0$. The point, $(\bar{x}, \bar{y}) = (0, 0)$, at which the boundary condition for the temperature changes, will be regarded as the leading edge of the surface.

Given that the solid and fluid phases are not in LTE, separate heat transport equations

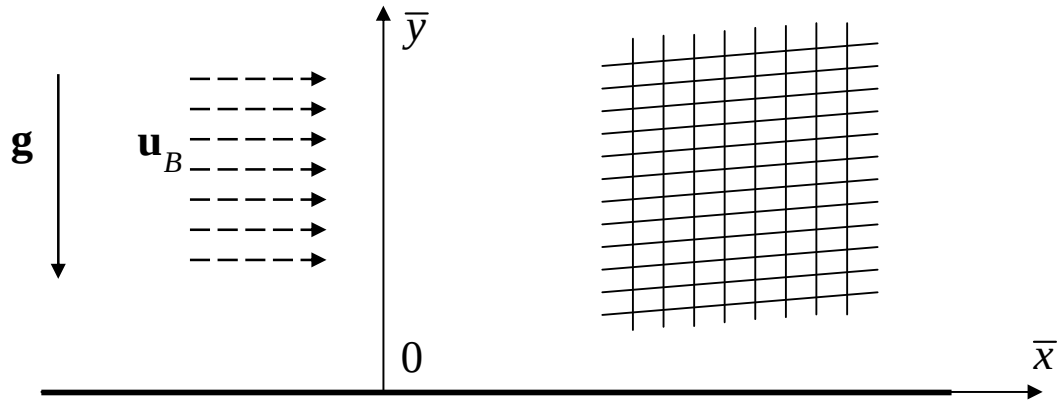

Figure 6.1: A geometrical sketch of the problem.

for the solid and fluid phases are employed. The formulation used to described these two heat transport equations is the one introduced by Eqs.(2.30) and (2.31), namely

$$\rho_0\, c\, \left(\varphi\, \frac{\partial \bar{T}_f}{\partial \bar{t}} + \bar{\mathbf{u}} \cdot \bar{\nabla} \bar{T}_f\right) = \varphi\, k\, \bar{\nabla}^2 \bar{T}_f + \mu\, \Phi + h\, (\bar{T}_s - \bar{T}_f), \tag{6.1}$$

$$(1-\varphi)\, (\rho_0\, c_v)_s\, \frac{\partial \bar{T}_s}{\partial \bar{t}} = (1-\varphi)\, k_s\, \bar{\nabla}^2 \bar{T}_s + h\, (\bar{T}_f - \bar{T}_s), \tag{6.2}$$

Thus, given the Darcy model and the continuity equation used in the previous chapters and considering negligible the contribution of viscous dissipation, the local balance equations in the steady state may be expressed in the form,

$$\frac{\partial \bar{u}}{\partial \bar{x}} + \frac{\partial \bar{v}}{\partial \bar{y}} = 0, \tag{6.3}$$

$$\bar{u} = -\frac{K}{\mu}\frac{\partial \bar{p}}{\partial \bar{x}}, \qquad \bar{v} = -\frac{K}{\mu}\frac{\partial \bar{p}}{\partial \bar{y}}, \tag{6.4}$$

$$\varphi\alpha \left(\frac{\partial^2 \bar{T}_f}{\partial \bar{x}^2} + \frac{\partial^2 \bar{T}_f}{\partial \bar{y}^2}\right) + \frac{h_{sf}}{\rho_0\, c}\, (\bar{T}_s - \bar{T}_f) = \bar{u}\frac{\partial \bar{T}_f}{\partial \bar{x}} + \bar{v}\frac{\partial \bar{T}_f}{\partial \bar{y}} \tag{6.5}$$

$$(1-\varphi)\alpha_s \left(\frac{\partial^2 \bar{T}_s}{\partial \bar{x}^2} + \frac{\partial^2 \bar{T}_s}{\partial \bar{y}^2}\right) + \frac{h_{sf}}{(\rho_0\, c_v)_s}\, (\bar{T}_f - \bar{T}_s) = 0, \tag{6.6}$$

where h_{sf} is the interphases heat transfer coefficient. The thermal boundary conditions are given by

$$\begin{aligned} \bar{y} = 0 \ (\bar{x} < 0): &\qquad \bar{T}_s = \bar{T}_f = \bar{T}_\infty \\ \bar{y} = 0 \ (\bar{x} > 0): &\qquad \bar{T}_s = \bar{T}_f = \bar{T}_w, \\ \bar{y} \to \infty: &\qquad \bar{T}_s, \bar{T}_f \to \bar{T}_\infty. \end{aligned} \tag{6.7}$$

The quantity, h_{sf}, which appears in Eqs. (6.5) and (6.6), is a function of the microscopic geometry of the medium, the conductivities of the phases and the strength of the flow. Some values of h_{sf} for stagnant two- and three-dimensional media of various types are given in Rees (71; 72).

6.2.1 Nondimensional formulation

Given that this is a forced convection problem, the velocity field is given by,

$$(\bar{u}, \bar{v}) = (\bar{u}_\infty, 0), \tag{6.8}$$

and this may be used immediately in Eq. (6.5). The fact that the domain is semi-infinite means that there is no natural physical lengthscale on which to basic a Péclet number and to use for nondimensionalization. However, the quantity $\alpha\,/\bar{u}_\infty$, i.e. the ratio between the thermal diffusivity of the fluid phase and the velocity of the forcing flow, has the dimensions of a length, and may be used for this purpose. It turns out to be a little more convenient to use $\varphi\,\alpha/\bar{u}_\infty$ as the lengthscale, and therefore let us introduce nondimensional variables using the following scalings,

$$(\bar{x}, \bar{y}) = \frac{\varphi\,\alpha}{\bar{u}_\infty}\,(\tilde{x}, \tilde{y}), \qquad (\bar{T}_f, \bar{T}_s) = (\bar{T}_w - \bar{T}_\infty)(T_f, T_s) + \bar{T}_\infty. \tag{6.9}$$

On using Eqs. (6.8) and (6.9) in Eqs. (6.5) and (6.6) the set of equations become,

$$\frac{\partial^2 T_f}{\partial \tilde{x}^2} + \frac{\partial^2 T_f}{\partial \tilde{y}^2} + H(T_s - T_f) = \frac{\partial T_f}{\partial \tilde{x}}, \tag{6.10}$$

$$\frac{\partial^2 T_s}{\partial \tilde{x}^2} + \frac{\partial^2 T_s}{\partial \tilde{y}^2} + H\gamma(T_f - T_s) = 0, \tag{6.11}$$

where

$$H = \frac{\varphi\,h_{sf}\,\alpha}{\bar{u}_\infty^2\,\rho_0\,c}, \qquad \gamma = \frac{\varphi\,k}{(1-\varphi)\,k_s} = \frac{\varphi\,\alpha\,(\rho_0 c_v)_s}{(1-\varphi)\,\alpha_s\,\rho_0\,c}. \tag{6.12}$$

The boundary condition described by Eq. (6.7) in nondimensional coordinates can be written as

$$\begin{aligned} \tilde{y} = 0 \ (x < 0): &\qquad T_s = T_f = 0 \\ \tilde{y} = 0 \ (x > 0): &\qquad T_s = T_f = 1, \\ \tilde{y} \to \infty: &\qquad T_s,\, T_f \to 0. \end{aligned} \tag{6.13}$$

6.2.2 Boundary layer approximation

The system formed by Eqs. (6.10) and (6.11) is elliptic, and therefore, for $O(1)$ values of H, a fully elliptic numerical simulation should be undertaken to obtain the resulting temperature fields of the two phases. The forced convection regime assumed implies that a high velocity basic flow is taken into account so that the limit $\bar{u}_\infty \gg 1$ is considered. From the definition of H in Eq. (6.12), $\bar{u}_\infty \gg 1$ implies that $H \ll 1$. Assuming now that $H \ll 1$, it is necessary to balance the magnitudes of the last three terms in Eq. (6.10), and it may be shown easily that the appropriate orders of magnitude are $\tilde{x} = O(H^{-1})$ and $\tilde{y} = O(H^{-1/2})$. Therefore the scalings,

$$\tilde{x} = H^{-1}x, \qquad \tilde{y} = H^{-1/2}y, \tag{6.14}$$

are introduced into Eqs. (6.10) and (6.11) to obtain,

$$H\frac{\partial^2 T_f}{\partial x^2} + \frac{\partial^2 T_f}{\partial y^2} + (T_s - T_f) = \frac{\partial T_f}{\partial x}, \tag{6.15}$$

$$H\frac{\partial^2 T_s}{\partial x^2} + \frac{\partial^2 T_s}{\partial y^2} + \gamma(T_f - T_s) = 0. \tag{6.16}$$

Formally allowing $H \to 0$ yields the boundary layer approximation naturally, and the governing equations are now,

$$\frac{\partial T_f}{\partial x} = \frac{\partial^2 T_f}{\partial y^2} + (T_s - T_f), \tag{6.17}$$

$$\frac{\partial^2 T_s}{\partial y^2} + \gamma\,(T_f - T_s) = 0. \tag{6.18}$$

This rescaling allows one to compress the region close to edge of the plate. In fact, in the limit $H \ll 1$, if the coordinates x and y are $O(1)$ then $\tilde{x} \gg 1$ and $\tilde{y} \gg 1$, that

identifies a region far from the leading edge.
The assumption of forced convection regime implies that for $x = 0$ and $y \neq 0$ the fluid phase temperature will be $T_f = 0$. From Eqs. (6.18) one can thus deduce that, for $x = 0$ and $y \neq 0$, the solid phase temperature will be $T_s = e^{-\sqrt{\gamma}\, y}$.

6.2.3 Boundary layer transformation

It is well-known that the equation formed by the first two terms of Eq. (6.17) admits the self-similar solution

$$T_f = \texttt{Erfc}\,[y/2\sqrt{x}]. \tag{6.19}$$

The solution shown in Eq.(6.19) can be found, for instance, in Ozisik (60), and it motivates the following coordinate transformations,

$$\eta = \frac{y}{2\,\sqrt{x}}, \quad \xi = \sqrt{x}, \qquad T_f = \Theta(\xi,\eta), \quad T_s = \Phi(\xi,\eta), \tag{6.20}$$

where Θ and Φ will henceforth denote the respective temperatures of the fluid and solid phases in this new coordinate system while T_f and T_s correspond to the solution written in Cartesian coordinates. Eqs. (6.17) and (6.18) become

$$\frac{\partial^2\Theta}{\partial\eta^2} - 2\,\xi\,\frac{\partial\Theta}{\partial\xi} + 2\,\eta\,\frac{\partial\Theta}{\partial\eta} + 4\,\xi^2\,(\Phi - \Theta) = 0, \tag{6.21}$$

$$\frac{\partial^2\Phi}{\partial\eta^2} + 4\,\xi^2\,\gamma\,(\Theta - \Phi) = 0, \tag{6.22}$$

which are to be solved subject to the boundary conditions,

$$\begin{aligned} \eta = 0: &\qquad \Theta = \Phi = 1, \\ \eta \to \infty \ \text{ and } \ \xi > 0: &\qquad \Theta,\, \Phi \to 0. \end{aligned} \tag{6.23}$$

It is important to note that the coefficient, ξ^2, of the source/sink terms in Eqs. (6.21) and (6.22) plays the same role as H does in Eqs. (6.10) and (6.11). Therefore it is possible to observe immediately that large values of ξ will correspond to local thermal equilibrium, while local thermal non-equilibrium effects will be at their strongest near the leading edge, $\xi = 0$. These equations have only one nondimensional parameter, namely γ.

6.3 Asymptotic analyses

The numerical solution of Eqs. (6.21) and (6.22) will be preceded by asymptotic analyses close to and far from the leading edge at $\xi = 0$. The near-leading-edge analysis must be performed before the numerical solution because the former provides boundary conditions that are essential for performing the latter.

6.3.1 Close to the leading edge

The system formed by Eqs. (6.21) and (6.22) may be solved in the region relatively close to the leading edge by searching for a solution in the form of a power series in the variable ξ,

$$\begin{aligned} \Theta(\xi,\eta) &= \Theta_0(\eta) + \xi\Theta_1(\eta) + \xi^2\Theta_2(\eta) + \cdots , \\ \Phi(\xi,\eta)) &= \Phi_0(\eta) + \xi\Phi_1(\eta) + \xi^2\Phi_2(\eta) + \cdots . \end{aligned} \tag{6.24}$$

At leading order in the expansion, the equations for Θ_0 and Φ_0 are,

$$\Theta_0'' + 2\,\eta\,\Theta_0' = 0, \quad \Phi_0'' = 0 \tag{6.25}$$

and their solutions are

$$\Theta_0 = \texttt{Erfc}\,[\eta], \quad \Phi_0 = 1. \tag{6.26}$$

In writing down the above expression for Φ_0, it is important to note that it is impossible to solve $\Phi_0'' = 0$ subject to both $\Phi_0(0) = 1$ and $\Phi_0 \to 0$ as $\eta \to \infty$, and $\xi > 0$. The boundary condition at the heated surface was employed, the implication being that the temperature of the solid phase near the leading edge must then vary over a lengthscale which is much greater than that represented by $O(1)$ values of η. This is consistent with a previous analysis in (75). It is also clear that Eq. (6.18) provides a means of satisfying the far field boundary condition; in this regime where $y = O(1)$ the leading order temperature of the fluid phase, Θ_0, has already decayed to zero, leaving a system which admits an exponentially decaying solution. Therefore it is natural to attempt a corresponding solution in this 'outer' region where $y = O(1)$ (noting that the 'inner' region where $\eta = O(1)$ corresponds to $y = O(x^{1/2}) = O(\xi)$). Thus an outer solution of the form,

$$\begin{aligned} T_f(x,y) &\sim T_{f,0}(y) + \sqrt{x}T_{f,1}(y) + xT_{f,2}(y) + \cdots , \\ T_s(x,y) &\sim T_{s,0}(y) + \sqrt{x}T_{s,1}(y) + xT_{s,2}(y) + \cdots , \end{aligned} \tag{6.27}$$

is sought. On taking $T_{f,0} = 0$ because of the superexponential decay of Θ_0 in the inner region, the leading order equations in the outer region are,

$$T_{f,2} = T_{s,0}, \qquad T''_{s,0} - \gamma\, T_{s,0} = 0. \tag{6.28}$$

Given that $\Phi_0 = 1$, the appropriate matching condition for $T_{s,0}$ is that $T_{s,0}(0) = 1$. Hence $T_{s,0}$ and $T_{f,2}$ are given by,

$$T_{f,2} = T_{s,0} = e^{-\sqrt{\gamma}\, y}, \tag{6.29}$$

which shows that the leading order terms of both temperature fields decay exponentially; this has important implications later for the numerical solutions.
These solutions now provide us with the appropriate matching conditions for the inner solutions at the next order in ξ. On expanding the solutions given in Eq. (6.29) about $y = 0$ one obtains,

$$T_f \sim (1 - \sqrt{\gamma}\, y + \frac{\gamma\, y^2}{2} + \cdots)\, x, \tag{6.30}$$

$$T_s \sim 1 - \sqrt{\gamma}\, y + \frac{\gamma\, y^2}{2} + \cdots, \tag{6.31}$$

and if y is replaced by $2\eta\,\xi$ then the large-η matching conditions for small values of ξ are found to be,

$$\Theta \sim \xi^2 - 2\,\sqrt{\gamma}\,\eta\,\xi^3 + \cdots, \qquad \Phi \sim 1 - 2\,\sqrt{\gamma}\,\eta\,\xi + 2\,\gamma\,\eta^2\,\xi^2 + \cdots. \tag{6.32}$$

Therefore the following conditions as $\eta \to \infty$ may be written,

$$\Phi_1 \sim -2\,\sqrt{\gamma}\,\eta, \qquad \Phi_2 \sim 2\,\gamma\,\eta^2, \qquad \Theta_2 \sim 1. \tag{6.33}$$

The next terms in the inner region arise at $O(\xi)$. From the expansion at this order one obtains the system

$$\Theta''_1 + 2\,\eta\,\Theta'_1 - 2\,\Theta_1 = 0, \quad \Phi''_1 = 0. \tag{6.34}$$

which is to be solved subject to the conditions,

$$\begin{aligned} \eta = 0: &\qquad \Theta_1 = 0, \quad \Phi_1 = 0, \\ \eta \to \infty \ \text{ and } \ \xi > 0: &\qquad \Theta_1 \to 0, \quad \Phi_1 \sim -2\,\sqrt{\gamma}\,\eta. \end{aligned} \tag{6.35}$$

The solutions are

$$\Theta_1 = 0, \qquad \Phi_1 = -2\,\sqrt{\gamma}\,\eta. \tag{6.36}$$

The solution for $T_{s,1}$ is clearly passive, and it is caused by the leading order exponential properties of $T_{s,0}$.
At $O(\sqrt{x})$ in the outer region, the governing equations are

$$T''_{f,1} + T_{s,1} - T_{f,1} - 2\,T_{f,3} = 0, \qquad T''_{s,1} + \gamma(T_{f,1} - T_{s,1}) = 0, \tag{6.37}$$

which are to be solved subject to

$$y = 0: \quad T_{f,1} = T_{s,1} = 0, \qquad y \to \infty: \quad T_{f,1}, T_{s,1} \to 0. \tag{6.38}$$

Given that these equations are homogeneous, the solutions are

$$T_{f,1} = 0, \quad T_{f,3} = 0, \quad T_{s,1} = 0. \tag{6.39}$$

At $O(\xi^2)$ in the inner region, the governing equations are,

$$\Theta''_2 - 4\,\Theta_2 + 2\,\eta\,\Theta'_2 + 4\,\mathtt{Erf}\,[\eta] = 0, \quad \Phi''_2 - 4\,\gamma\,\mathtt{Erf}\,[\eta] = 0, \tag{6.40}$$

$$\begin{aligned} &\eta = 0: \quad \Theta_2 = 0, \quad \Phi_2 = 0, \\ &\eta \to \infty \ \text{ and } \ \xi > 0: \quad \Theta_2 \to 1, \quad \Phi_2 \sim 2\,\gamma\,\eta^2, \end{aligned} \tag{6.41}$$

and the solutions are

$$\Theta_2 = \mathtt{Erf}\,[\eta], \quad \Phi_2 = \eta\,\frac{2e^{-\eta^2}\gamma}{\sqrt{\pi}} + \gamma\left(1 + 2\eta^2\right)\mathtt{Erf}\,[\eta]. \tag{6.42}$$

This is a reasonable point at which to stop the expansion for the inner region because three terms have now been obtained for Φ. At $O(x)$ for the outer region one has

$$T''_{f,2} + T_{s,2} - T_{f,2} - 2\,T_{f,4} = 0, \quad T''_{s,2} + \gamma(T_{f,2} - T_{s,2}) = 0. \tag{6.43}$$

which are to be solved using Eq. (6.29) and subject to

$$y = 0: \quad T_{s,2} = 0, \qquad y \to \infty: \quad T_{s,2} \to 0, \tag{6.44}$$

the solution for Eq. (6.43) is

$$T_{f,4} = \frac{e^{-y\sqrt{\gamma}}}{4}\left(2\,\gamma - 2 + y\,\sqrt{\gamma}\right), \quad T_{s,2} = e^{-y\sqrt{\gamma}}\left(\frac{y\,\sqrt{\gamma}}{2}\right). \tag{6.45}$$

To summarise, the solutions found by the power series expansion for both the inner and the outer regions are:

$$\begin{aligned}
&\Theta \sim \texttt{Erfc}\,[\eta] + \xi^2\,\texttt{Erf}\,[\eta], \\
&\Phi \sim 1 - 2\sqrt{\gamma}\xi\,\eta + \left[\eta\,\frac{2\gamma e^{-\eta^2}}{\sqrt{\pi}} + \gamma\left(1+2\eta^2\right)\texttt{Erf}\,[\eta]\right]\xi^2,
\end{aligned} \tag{6.46}$$

$$\begin{aligned}
&T_f \sim x\,e^{-y\sqrt{\gamma}}, \\
&T_s \sim e^{-y\sqrt{\gamma}} + x\left(\frac{y\sqrt{\gamma}}{2}\right)e^{-y\sqrt{\gamma}}.
\end{aligned}$$

6.3.2 Far from the leading edge

The solutions of Eqs. (6.21)-(6.22) at large distances from the leading edge are considered now. When $\xi \gg 1$ there are two possible order-of-magnitude balances that may be obtained from Eq. (6.22). The first suggests that there is an inner layer of width $\eta = O(\xi^{-1})$ within the main boundary layer, for which we assume that $\eta = O(1)$. The second, and more reasonable one on physical grounds, is that $T_f - T_s = O(\xi^{-2})$, and that there is only one asymptotic region. This second balance corresponds to the approach to LTE. Therefore one may investigate the region far from the leading edge by searching for a solution expressed as a power series expansion of the form

$$\Theta(\xi,\eta) \sim \Theta_0(\eta) + \xi^{-1}\Theta_1(\eta) + \xi^{-2}\Theta_2(\eta) + \cdots, \tag{6.47}$$

$$\Phi(\xi,\eta) \sim \Theta_0(\eta) + \xi^{-1}\Theta_1(\eta) + \xi^{-2}\Theta_2(\eta) + \cdots. \tag{6.48}$$

The leading order, i.e. $O(1)$, equations are

$$\Theta_0'' + 2\,\eta\,\Theta_0' + 4\,(\Phi_2 - \Theta_2) = 0, \tag{6.49}$$

$$\Phi_0'' + 4\,\gamma\,(\Theta_2 - \Phi_2) = 0, \tag{6.50}$$

while the boundary conditions are

$$\begin{aligned}
\eta = 0: &\qquad \Theta = \Phi = 1, \\
\eta \to \infty: &\qquad \Theta, \Phi \to 0.
\end{aligned} \tag{6.51}$$

Given the above argument, one may reasonably assume that $\Phi_0 = \Theta_0$. On multiplying Eq. (6.49) by γ and adding it to Eq. (6.50), one obtains

$$(1+\gamma)\,\Theta_0'' + 2\,\eta\,\gamma\,\Theta_0' = 0, \tag{6.52}$$

the solution for which is,

$$\Phi_0 = \Theta_0 = \mathrm{Erfc}\left[\eta\sqrt{\frac{\gamma}{1+\gamma}}\right]. \tag{6.53}$$

At $O(\xi^{-1})$ of the expansion the governing equations are,

$$\Theta_1'' + 2\,\Theta_1 + 2\,\eta\,\Theta_1' + 4\,(\Phi_3 - \Theta_3) = 0, \tag{6.54}$$

$$\Phi_1'' + 4\,\gamma\,(\Theta_3 - \Phi_3) = 0. \tag{6.55}$$

The terms in Θ_3 and Φ_3 may be eliminated by means of the same process of combination of the equations, and this results in the following equation,

$$(1+\gamma)\,\Theta_1'' + 2\,\eta\,\gamma\,\Theta_1' + 2\,\gamma\,\Theta_1 = 0. \tag{6.56}$$

Given the above scaling argument that $\Theta - \Phi = O(\xi^{-2})$, it has been assumed that $\Theta_1 = \Phi_1$. Equation (6.56) has the general solution,

$$\Phi_1 = \Theta_1 = C_1\,e^{-\frac{\eta^2\gamma}{1+\gamma}}\,\texttt{Erfi}\left[\eta\sqrt{\frac{\gamma}{1+\gamma}}\right] + C_2 e^{-\frac{\eta^2\gamma}{1+\gamma}}, \tag{6.57}$$

where C_1 and C_2 are constants. This solution should satisfy zero boundary conditions for Θ_1 at both $\eta = 0$ and as $\eta \to \infty$. This implies that $C_2 = 0$, but C_1 remains indeterminate. Clearly, then, the function multiplying C_1 in Eq. (6.57) is an eigensolution of the equation. Although further terms in this expansion will only be expressed in terms of C_1 and any further eigensolutions which might arise, it is possible, nevertheless, to determine precisely the leading order departure from LNTE. If Eq. (6.53) is substituted into Eqs. (6.49) and (6.50), then it is straightforward to show that

$$\Theta_2 - \Phi_2 = \frac{\Phi_0''}{4\,\gamma} = \sqrt{\frac{\gamma}{\pi\,(1+\gamma)^3}}\;\eta\,e^{-\frac{\eta^2\gamma}{1+\gamma}}. \tag{6.58}$$

Eq. (6.58) corresponds to an $O(\xi^{-2})$ difference between the temperatures of the phases. It is also worthy of note that the magnitude of this difference decreases as γ increases; the mathematical reason lies in the fact that a large value of γ forces the difference between the temperatures to be small, as seen in Eq. (6.22).

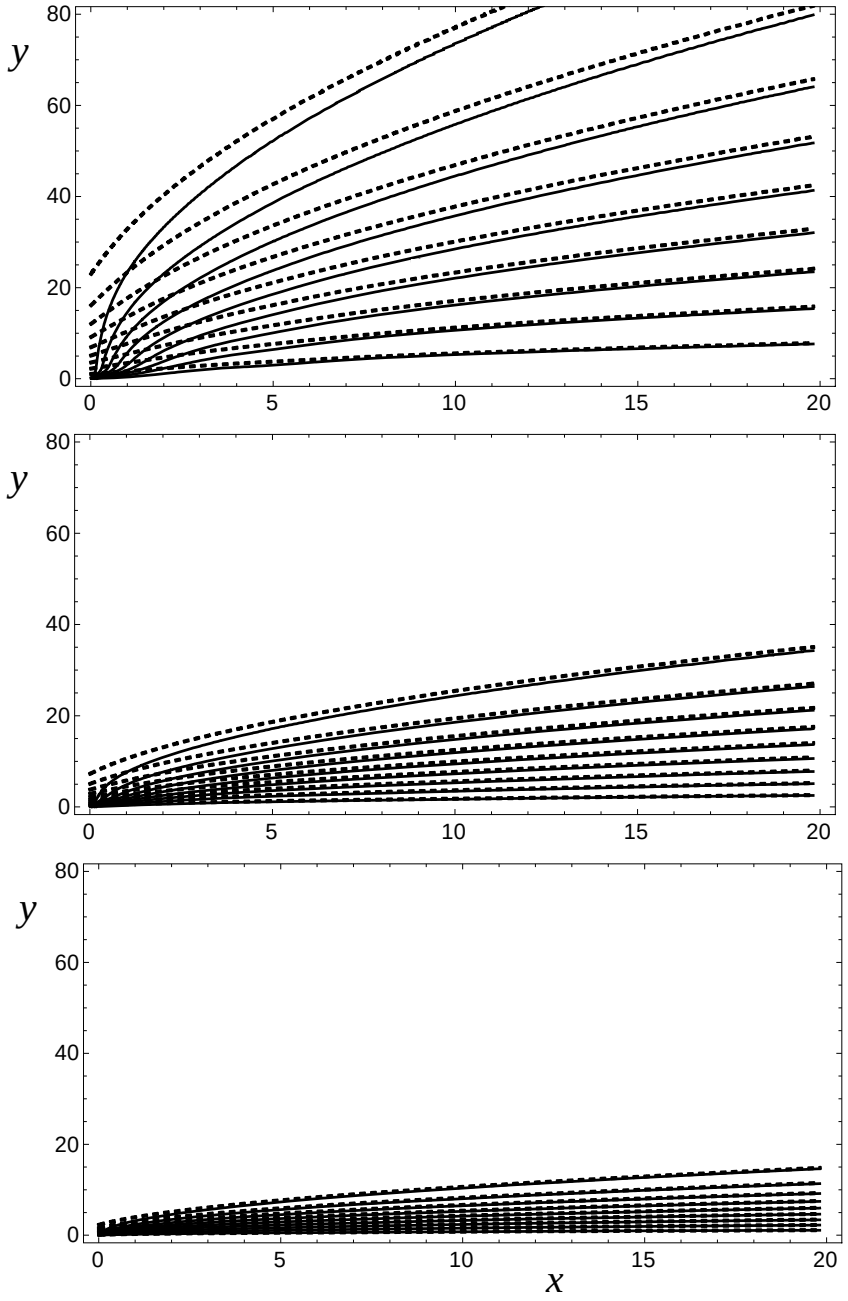

Figure 6.2: Isotherms for both the solid and fluid phases for $\gamma = 0.01$ (upper), $\gamma = 0.1$ (middle), $\gamma = 1$ (lower). Dashed lines refer to the solid phase and solid lines refer to fluid phase.

6.4 Numerical solutions

The numerical scheme which was used to solve numerically the system of Eqs. (6.21)-(6.22) is a standard Keller box method, which is a generic method for time or space marching problems. Most often, the system is reduced to first order form in η, the resulting equations discretised half way between the grid points in both the η and ξ directions, and it is therefore of second order accuracy. An initial profile is not required, because the system of parabolic partial differential equations reduces to an ordinary differential system at $\xi = 0$, and a suitably written code will be able to solve this system easily. Although the present system of equations is linear, the general methodology uses a multidimensional Newton-Raphson iteration scheme to solve the discretised equations. In our case the corresponding iteration matrix is computed numerically, and a standard block-Thomas algorithm is used to solve the iteration equations. The x variable is treated here as a time-like variable, and the solution is marched downstream.
In the present implementation we have adopted a backward difference method in x in order to maximise numerical stability, and good accuracy is ensured by employing the small steplength, $\delta\xi = 10^{-2}$. In the η-direction, the steplength, $\delta\eta = 10^{-2}$, is taken with $\eta_{\max} = 20$. However, in the above small-ξ analysis we determined that the leading order temperature fields in the outer region decay as $\exp(-y\sqrt{\gamma})$, i.e. as $\exp(2\eta\xi\sqrt{\gamma})$ from the point of view of the boundary layer. Therefore it is clear that this rate of decay cannot be contained within a finite computational domain when ξ is sufficiently small. However, it is possible to model this rate of decay by adopting a different set of boundary conditions from those given earlier in Eqs. (6.23). We used the following,

$$\Theta' + 2\xi\sqrt{\gamma}\Theta = 0, \qquad \Phi' + 2\xi\sqrt{\gamma}\Phi = 0, \qquad \text{at } \eta = \eta_{\max}. \tag{6.59}$$

These conditions were used from $\xi = 0$ until the first value of ξ at which both Θ and Φ are less than 10^{-6}, and thereafter the conditions given in Eqs. (6.23) were adopted. In this way the full presence of the outer layer is modelled by means of a modified boundary condition. Figures 6.2 - 6.4 show the temperature profiles obtained by the numerical simulations, and are plotted in the (x, y)-coordinates, as defined in Eq. (6.14). The three frames in Figure 6.2 are drawn using the same range of values of x and y, but for different values of γ: the upper frame refers to $\gamma = 0.01$, the central frame to $\gamma = 0.1$ and the lower refers to $\gamma = 1$. Dashed lines refer to the solid phase and solid lines refer

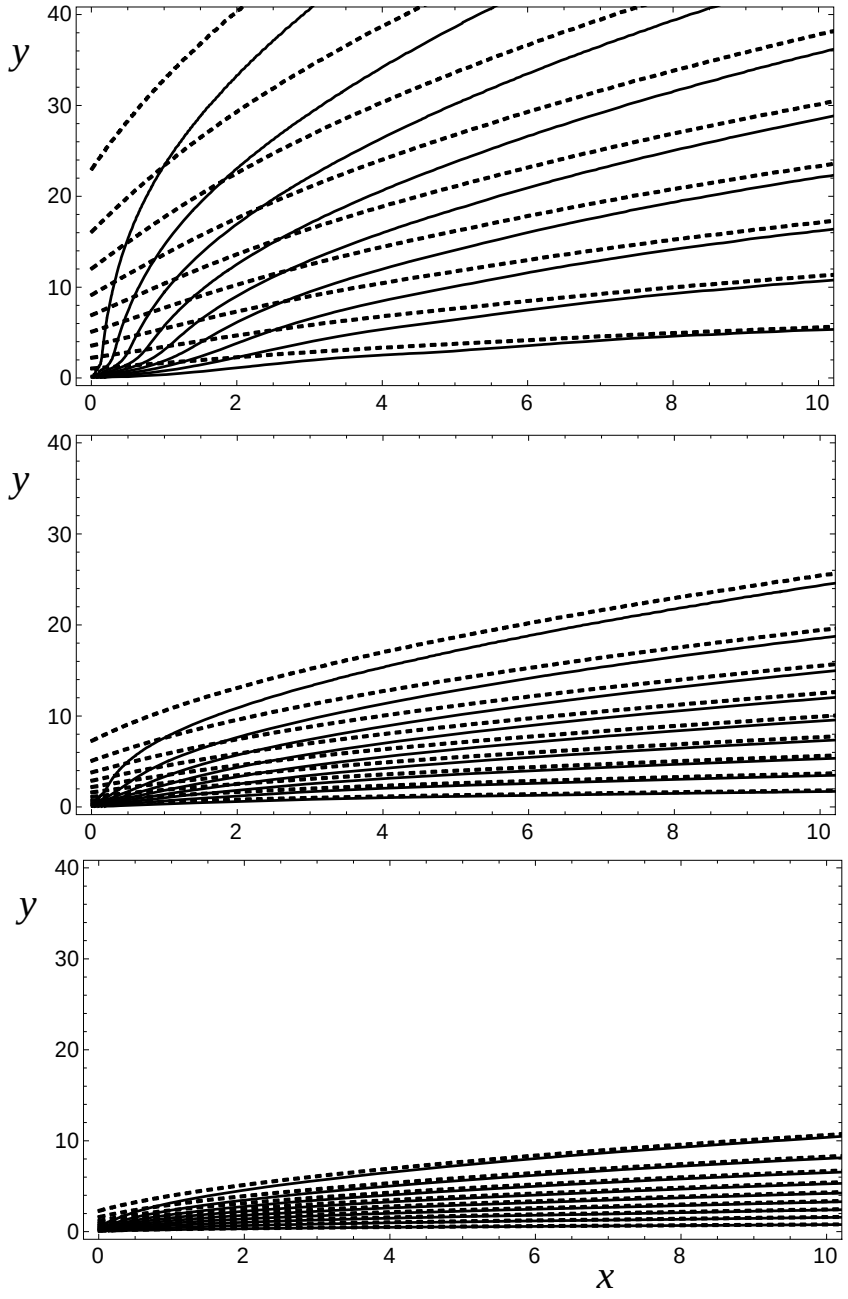

Figure 6.3: Isotherms for both the solid and fluid phases for $\gamma = 0.01$ (upper), $\gamma = 0.1$ (middle), $\gamma = 1$ (lower). Dashed lines refer to the solid phase and solid lines refer to fluid phase. This Figure has a different vertical resolution to that shown in Figure 6.2.

to fluid phase. In this figure it is clear that the thickness of the thermal boundary layer at all values of x is strongly dependent on the magnitude of γ. This is consistent with Eq. (6.53) which shows clearly that the large-x thickness of the boundary layer increases as γ decreases. Likewise, near the leading edge, the thickness of the thermal boundary layer corresponding to the solid phase increases as γ decreases; see Eq. (6.28). That this should be so is understood by referring to the physical implications of different values of γ. When γ is small, heat is conducted easily away from the heated surface, and only a small amount is imparted to the fluid. On the other hand, when γ is large, heat is transferred easily to the fluid and is therefore advected downstream, which decreases the thickness of the boundary layers. The ease of heat transfer between the phases may also be seen in Figure 6.7 local thermal equilibrium is attained at much smaller values of x when $\gamma = 1$ than when $\gamma = 0.01$.

Figures 6.4 and 6.3 shows the same information as Figure 6.2, but for a progressively smaller range of values of y and x. The variation with γ of the boundary layer thickness of the solid phase near the leading edge may be seen clearly, but it is also possible to see that the boundary layer thickness of the fluid phase is independent of γ there. This independence is consistent with Eq. (6.26). At slightly increased distances from the leading edge the boundary layer thickness of the fluid phase increases rapidly at a rate which is dependent on γ.

Although γ is the sole parameter of the system being studied, Figures 6.2 - 6.4 already indicate substantial variations of the resulting temperature fields as the parameter varies. The rate of heat transfer is an important quantity, and the manner in which its evolution with ξ varies with γ is shown in Figure 6.5. All of our previous observations are seen clearly in this Figure, particularly the magnitude of the rate of heat transfer far from the leading edge. Given that we have plotted the η-derivative of the temperatures, the solid phase now has a zero rate of heat transfer at the leading edge, but this varies rapidly as ξ increases, and does so at a γ-dependent rate. However, of most interest is the distance at which one might say that local thermal equilibrium has been attained. Such a criterion is necessarily arbitrary; we can define x_{LTE} to be the distance beyond which the relative difference of the surface rates of heat transfer, Λ, is less than 1%, namely, that

$$\Lambda = 2\Big(\frac{\partial T_f}{\partial \eta}\Big|_{\eta=0} - \frac{\partial T_s}{\partial \eta}\Big|_{\eta=0}\Big) \Big/ \Big(\frac{\partial T_f}{\partial \eta}\Big|_{\eta=0} + \frac{\partial T_s}{\partial \eta}\Big|_{\eta=0}\Big) \leq 0.01. \tag{6.60}$$

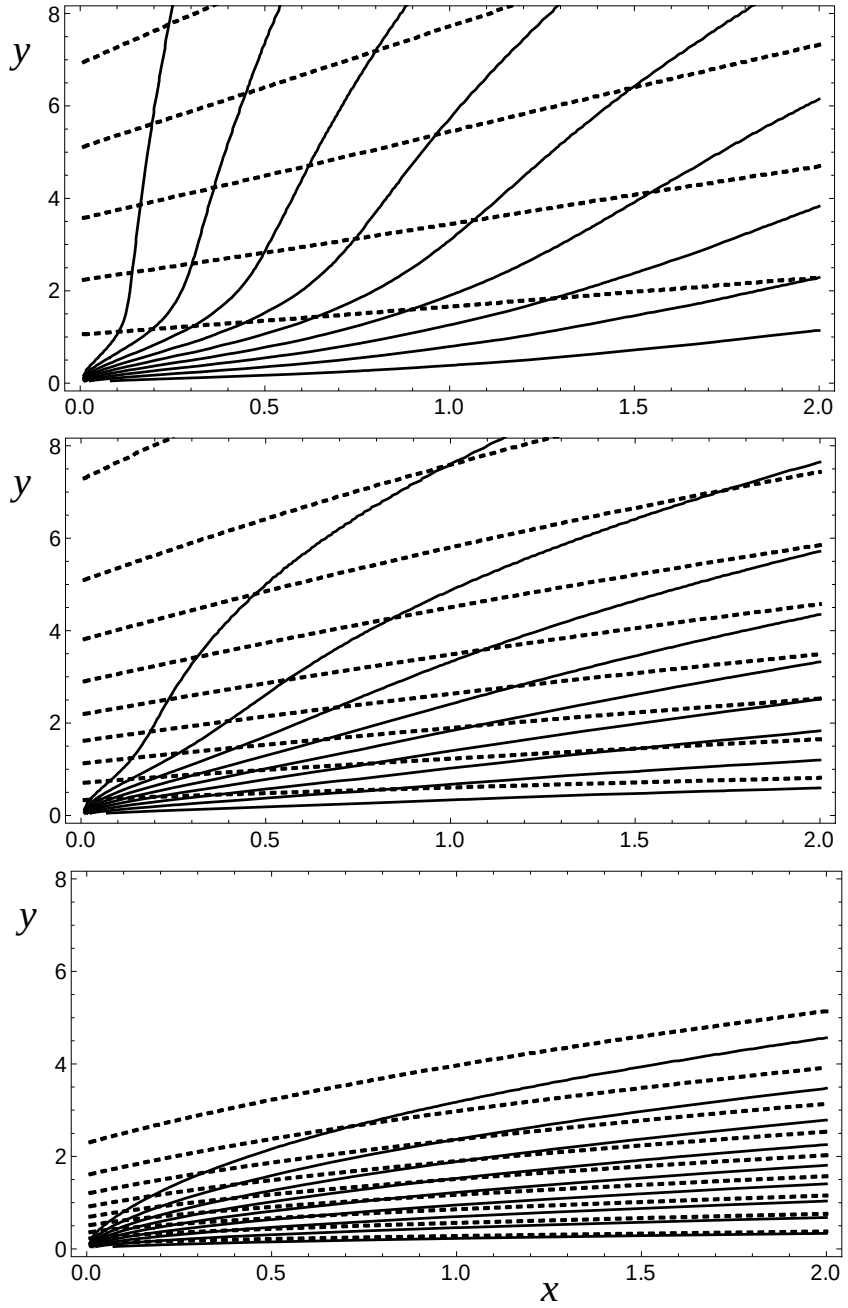

Figure 6.4: Isotherms for both the solid and fluid phases for $\gamma = 0.01$ (upper), $\gamma = 0.1$ (middle), $\gamma = 1$ (lower). Dashed lines refer to the solid phase and solid lines refer to fluid phase. This Figure has a different vertical resolution to that shown in Figure 6.2 and 6.3.

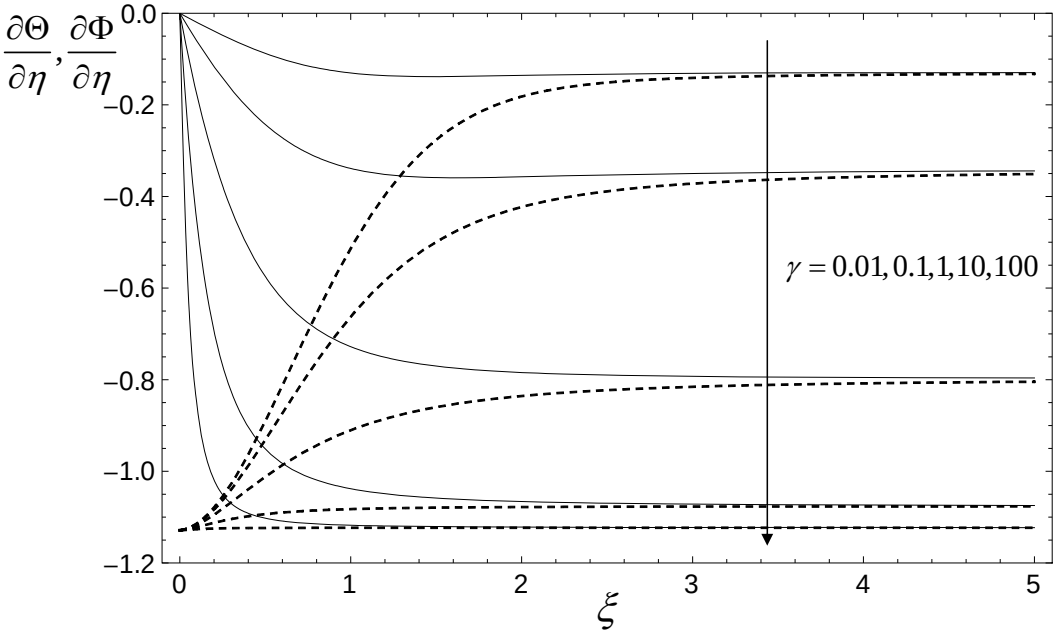

Figure 6.5: Variation with ξ of the rates of heat transfer, $\partial\Theta/\partial\eta$ and $\partial\Phi/\partial\eta$ versus the distance from the edge ξ, for different values of γ and for fixed $\eta = 10$. Dashed lines refer to the solid phase and solid lines to the fluid phase.

The behaviour of the parameter Λ as a function of x is shown in Figure 6.6. This figure confirms the results previously obtained in Figure 6.5 for which as γ increases the heat transfer between the two phases decreases more quickly. Thus also the distance from the leading edge x_{LTE} defined by Eq.(6.60) decreases as γ increases. This behaviour is displayed in Figure 6.7 and the relative Table 6.1. The value of x_{LTE}, in fact, decreases monotonically as γ increases.

6.5 Conclusions

A steady two−dimensional forced convection thermal boundary layer in a porous medium has been studied both analytically and numerically. The main focus has been on the effect of local thermal non−equilibrium between the solid and fluid phases. Separate asymptotic analyses which are valid at small distances and at large distances from the leading edge have been obtained. In particular, we have determined that the boundary layer in the near-leading-edge region splits into two well-defined asymptotic regions,

γ	x_{LTE}
0.01	51.4806
0.02	51.1225
0.05	49.7025
0.1	46.9225
0.2	42.9025
0.5	33.9306
1	25.0000
2	16.6056
5	8.2297
10	4.4627
50	2.3256
100	0.9604
500	0.4830
1000	0.0490

Table 6.1: Variation with γ of the distance, x_{LTE}, at which local thermal equilibrium is attained. Threshold for the achieving of LTE is chosen to be when the parameter $\Lambda \leq 0.01$.

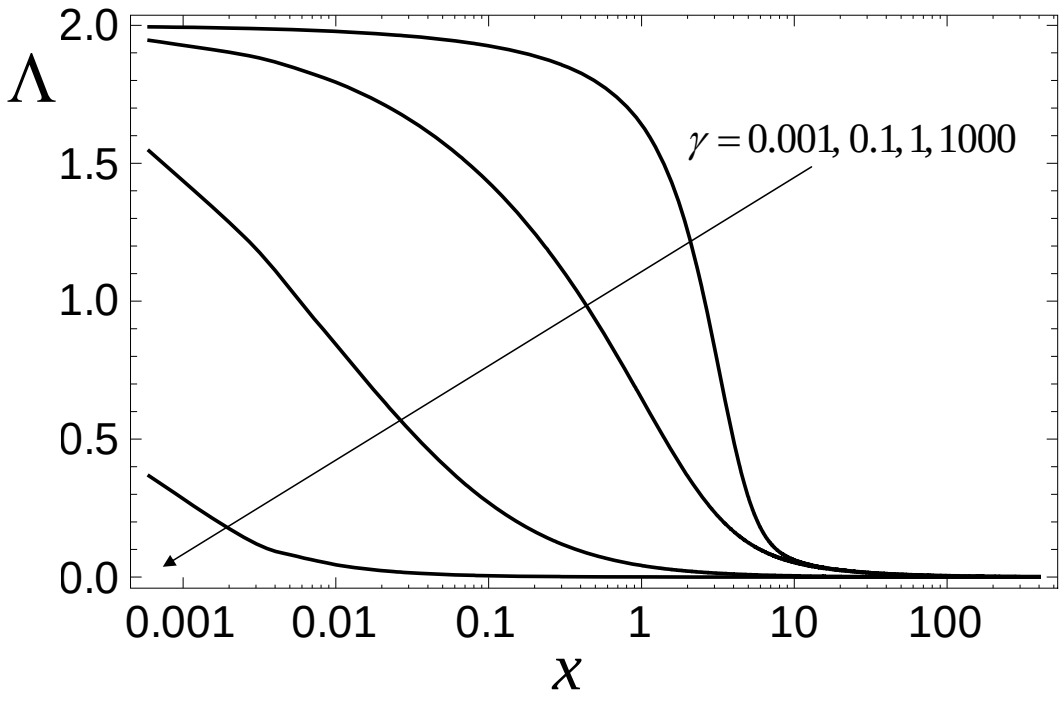

Figure 6.6: Behaviour of the parameter Λ as a function of x for different values of γ.

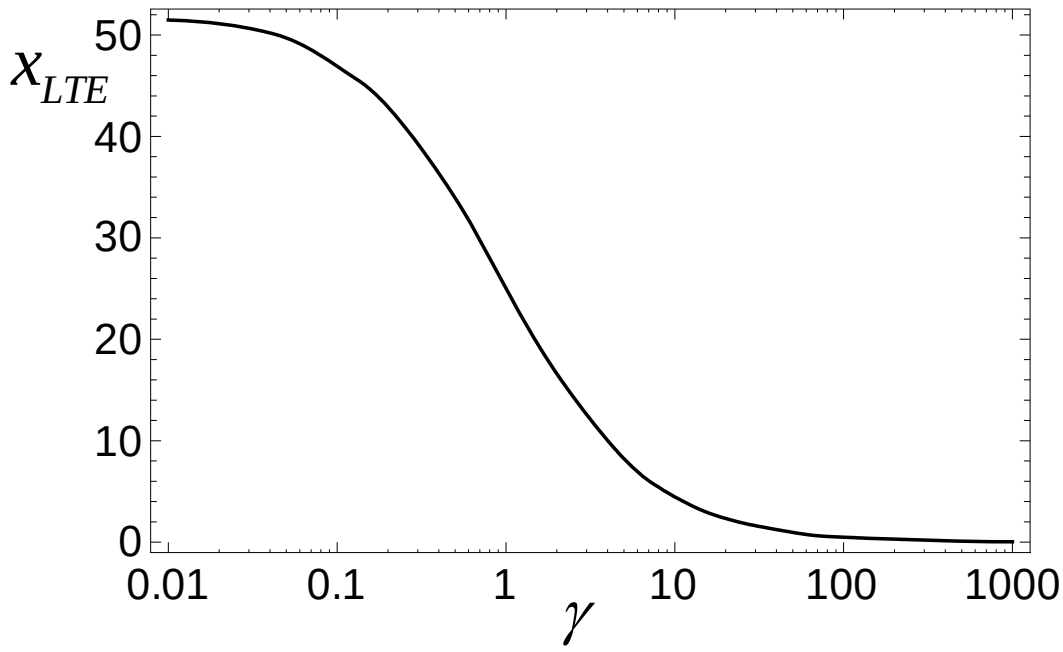

Figure 6.7: Variation with γ of the distance, x_{LTE}, at which local thermal equilibrium is attained.

one in which y is the natural variable, and the other in which η is the natural variable. This analysis was used to obtain an effective outer boundary condition for the numerical study which would take into account accurately the presence of the outer region. The large-ξ asymptotic analysis shows that local thermal equilibrium is attained in this limit, with local thermal non-equilibrium effects being of $O(x^{-1})$ in magnitude. A full numerical solution was also obtained and solutions presented.
We found that:

- the thickness of the boundary layers of each phase depends strongly on the value of γ;
- the thickness of fluid boundary layer near the leading edge is independent of γ;
- the boundary layer corresponding to the solid phase is always thicker than that of the fluid phase;
- local thermal equilibrium was attained at decreasing distances from the leading edge as γ increases; this was related to the increasing ease of heat transfer between the phases.

7

Appendix

7.1 Some examples of Mathematica notebooks

In this thesis, on approaching the linear stability analysis of fluid saturated porous media, we found a number of eigenvalue problems to solve. On achieving this aim, we used original codes and also we made use of a commercial code, *Mathematica* 7 (© Wolfram Research, Inc.). In the following, few examples of notebook used to solve our eigenvalue problems are shown.

For instance, the series solution described in Section 3.4, has been implemented in Mathematica in order to be solved. In the case of a self-adjoint problem, i.e. for longitudinal rolls, the recursion law on which one can deduce the power series coefficients has been defined as in Notebook 1 that follows. In the latter, the resulting coefficients of the power series, the power series expansion described in Eq.(3.45), the code used to draw the neutral stability curves and the code used to find the minima of the neutral stability curves are also shown.

On the other hand, an implicit method to solve an eigenvalue problem is now described. In particular, the analysis of the longitudinal rolls described by Eqs.(5.36)-(5.37) is shown. The study is performed again with the aid of the commercial code Mathematica. In this case a solver based on the explicit Runge-Kutta method has been employed. The notebook used is shown in the Notebook 2 that follows. The system of Eqs.(5.36)-(5.37) and its derivative with respect to the wavenumber are taken into account in order to ensure the closure of the problem. Two different Runge-Kutta methods are used: the

first with an adaptive stepsize and the second with the fixed stepsize.

8

Discussion

In this thesis, the role of heat generation due to the viscous dissipation contribution in fluid saturated porous media has been analysed. On studying this topic, different approaches to the momentum balance equation and the thermal energy balance equation have been used. Also different thermal boundary conditions have been used to analyse the topic: imperfect isothermal boundaries and also a linear change of temperature in the streamwise direction for the top boundary are used. A linear stability analysis of parallel steady basic flows has been performed. The basic steady flows have been thus perturbed with disturbances of the form of plane waves. The stability analysis is focused on the study of the onset of convective rolls. These rolls are chosen to be inclined of an arbitrary angle with respect to the basic flow. In particular, this allowed us to investigate the onset of both longitudinal and transverse rolls.

The viscous dissipation contribution introduced in the thermal energy balance equation produced different effects. On considering a Prats problem with an imperfect isothermal top boundary, one can note that, by adding the viscous dissipation term, the resulting basic flow describes a parabolic thermal profile and not a linear one. This feature yields a higher average temperature of the basic flow and thus, for the same kind of problem, the effect of the buoyancy is more intense when the viscous dissipation is taken into account. As a consequence, a lower Rayleigh number value is sufficient for the onset of instability, with respect to the Prats case. Moreover, the transverse rolls requires a lower basic flow velocity to became unstable than any other kind of oblique rolls. One can also note that the nonlinearity characteristic of the viscous dissipation

term, in the local energy balance, introduces a source of instability in addiction to the convective term. In this case, in fact, the terms that couple the thermal energy balance equation and the momentum balance equation are two and not only one as when just the convective term is present.

On considering a Prats-like problem taking into account the Forchheimer model, the relative viscous dissipation contribution and an imperfect isothermal bottom boundary one finds that the basic temperature profile is still parabolic. It is found that, in Darcy's limit when the Forchheimer coefficient tends to zero, the critical value of the stability parameter does not depend on the inclination of the wave disturbance with respect to the basic flow. Analysing the onset of the longitudinal rolls one can note that, unlike the case of the Darcy problem with an imperfect isothermal top boundary, this orientation of the rolls is more unstable. Moreover, the longitudinal rolls are independent of the Forchheimer parameter. On the other hand, the critical value of the stability parameter for the case of the transverse rolls shows a maximum of variability with respect to the Forchheimer parameter.

We also applied, to a parallel horizontal buoyant flow, a linear change of temperature in the streamwise direction for the top boundary. The resulting basic flow displays a linear velocity profile and a nonlinear temperature profile, namely a fourth degree polynomial. The analysis of this particular system shows clearly that the viscous dissipation plays a destabilising role. Given that the Gebhart number is the nondimensional parameter scaling the viscous dissipation term, the critical parameter value being a decreasing function of the Gebhart number implies that the viscous dissipation contribution is destabilising. Again the most unstable stable rolls are the longitudinal ones.

In the cases discussed above an imperfect isothermal boundary produces a change in the critical value of the stability parameter at which the system starts to be unstable. More precisely, the threshold values of the stability parameter for the onset of instability increases monotonically with the Biot number: one can find a minimum for the adiabatic condition, $Bi = 0$, and a maximum value for the isothermal condition, $Bi \to \infty$.

The last analysis performed focused on using a local thermal non-equilibrium model to analyse a thermal boundary layer in forced convection regime. The forced convection hypothesis allowed us to assume a local thermal non equilibrium between the two phases, fluid and solid. The temperature difference between the solid porous matrix

and the fluid phase has thus a maximum close to the leading edge of the plate. This temperature difference reduces his value as the thermal boundary layer develops until a local thermal equilibrium between the solid and the fluid temperature is attained at large distances from the leading edge. The boundary layer corresponding to the solid phase is always thicker than that of the fluid phase. Moreover, the boundary layer depends just on one parameter defined by a ratio of the thermal conductivities of the two phases. This parameter drives the heat transfer between the phases: as it increases the heat transfer is more efficient, the thickness of the thermal boundary layer decreases and the local thermal equilibrium is achieved closer to the leading edge.

8.1 Opportunities for future work

The analysis of the convective instability activated by the effect of viscous dissipation is a relatively novel subject. This thesis has provided a first account to this subject with reference to the field of fluid saturated porous media. The engineering aspects of these researches are manifold and, among the others, I quote the diffusion of chemical or nuclear contaminants in the soil. The latter, modelled as a groundwater saturated porous medium, is a typical example of a system where the control of the possible convective instability may have a practical importance. The effect of the viscous dissipation is, strictly speaking, an important phenomenon if highly viscous and lowly conductive fluids are involved. A magnification of this effect is expected when the external conditions imply the presence of very low heat fluxes at the system boundaries. The viscous dissipation may be coupled or not to effects of local thermal non-equilibrium. The latter being a relatively novel aspect in the thermal modelling of fluid flow and heat transfer in porous media. The non-equilibrium effects can be important when fast transient processes or high-speed flows take place. Future developments of the researches developed in this thesis may be oriented to the investigation of more realistic models of the fluid saturated porous media encountered in the industrial or geothermal design. For instance, highly viscous fluids with potentially important effects of viscous heating have generally a strongly temperature-dependent viscosity. An effect that has been disregarded in this thesis, but certainly interesting as an opportunity for future work. Models of the temperature change may be based on exponential models,

such as the Nahme model or the Arrhenius model. In the framework of the Oberbeck-Boussinesq approximation, one involving relatively small temperature differences, also a linear model for the temperature change of the fluid viscosity is appropriate. The latter case is an approach certainly simpler that may offer a possibility of analytical or semi-analytical solutions for the basic flow. The thesis has its focus on the Darcy model and on the Forchheimer model. A quite interesting subject for future work can be the application of the Brinkman model, appropriate for porous media with a large permeability. The Brinkman model is, theoretically speaking, an important arena for testing the present models of the viscous dissipation source term in the local energy balance equation. This thesis contains a note on this point in Section 2.2. The results of the fluid stability analyses based on different models may provide useful information to develop further the scientific debate on this theoretical aspect of the fluid dynamics in porous media. The study, based on the LTNE theory, of the analogous of the Pohlhausen problem, for the thermal boundary layer external to a semi-infinite plate, can be expanded to systems with a finite vertical width, namely plane channels. In other words, LTNE can be used for revisiting classical thermal entrance problems in channels and ducts, such as the Graetz problem.

9

Publications

9.1 Journal papers

1. A. Barletta, M. Celli, E. Magyari, E. Zanchini: Buoyant MHD flows in a vertical channel: the levitation regime. Heat and Mass Transfer, 44, 1005-1013 (2008).

2. A. Barletta, M. Celli: Mixed convection MHD flow in a vertical channel: effects of Joule heating and viscous dissipation, International Journal of Heat and Mass Transfer. 51, 6110-6117 (2008).

3. A. Barletta, M. Celli, D.A.S. Rees: The onset of convection in a porous layer induced by viscous dissipation: a linear stability analysis. Int. J. of Heat and Mass Transfer, 52, 337–344 (2009).

4. A. Barletta, M. Celli, D.A.S Rees: Darcy-Forchheimer flow with viscous dissipation in a horizontal porous layer: onset of convective instabilities. J. of Heat Transfer. 131, 072602 (2009).

5. A. Barletta, M. Celli, D. Nield: Unstably stratified Darcy flow with impressed horizontal temperature gradient, viscous dissipation and asymmetric thermal boundary conditions. Int. J. of Heat and Mass Transfer. 53, 16211627 (2010).

9.2 Conference papers

1. A. Barletta, E. Zanchini, M. Celli, MHD con galleggiamento in un canale verticale con temperatura di parete uniforme. XXV congresso U.I.T. sulla trasmissione del calore (2007).

2. A. Barletta, M. Celli, D.A.S.Rees, Onset of convective instabilities for Darcy-Forchheimer flow in a horizontal porous layer: the effect of viscous dissipation. XXVI congresso U.I.T. sulla trasmissione del calore (2008).

3. M. Celli, D.A.S.Rees, A. Barletta, Darcy boundary layer in forced convection regime using Local Thermal Non Equilibrium model: analytical and numerical solution. XXVII congresso U.I.T. sulla trasmissione del calore (2009).

References

[1] A.K. Al-Hadhramy, L. Elliott, and D.B. Ingham. A new model for viscous dissipation in porous media across a range of permeability values. *Transp. Porous Media*, 53:117–122, 2003. 22

[2] A. Amiri and K. Vafai. Analysis of dispersion effects and non-thermal equilibrium, non-Darcian, variable porosity incompressible flow through porous media. *Int. J. of Heat and Mass Trans.*, 37:939–954, 1994. 24

[3] A. Amiri and K. Vafai. Transient analysis of incompressible flow through a packed bed. *Int. J. of Heat and Mass Trans.*, 41:4259–4279, 1998. 24

[4] A. Anzelius. Medien. zeit. ang. math. mech. *Über Erwärmung vermittels durchströmender*, 6:291–294, 1926. 23

[5] J.L. Auriault. On the domain of validity of Brinkman's equation. *Trans. in Porous Media*, 79:215–223, 2009. 7

[6] N. Banu and D.A.S. Rees. Onset of Darcy-Bénard convection using a thermal non-equilibrium model. *Int. J. of Heat and Mass Transfer*, 45:2221–2228, 2002. 33

[7] A. Barletta. Local energy balance, specific heats and the OberbeckBoussinesq approximation. *Int. J. of Heat and Mass Transfer*, 52:5266–5270, 2009. 15, 16, 23

[8] A. Barletta, M. Celli, and D. Nield. Unstably stratified darcy flow with impressed horizontal temperature gradient, viscous dissipation and asymmetric thermal boundary conditions. *Int. J. of Heat and Mass Transfer*, 53:1621–1627, 2010. 85

[9] A. Barletta, M. Celli, and D.A.S. Rees. Darcy-forchheimer flow with viscous dissipation in a horizontal porous layer: onset of convective instabilities. *J. of Heat Transfer*, 131:072602, 2009. 61

[10] A. Barletta, M. Celli, and D.A.S. Rees. The onset of convection in a porous layer induced by viscous dissipation: a linear stability analysis. *Int. J. of Heat and Mass Transfer*, 52:337–344, 2009. 34

[11] A. Barletta, M. Celli, and D.A.S. Rees. The onset of convection in a porous layer induced by viscous dissipation: a linear stability analysis. *Int. J. of Heat and Mass Transfer*, 52:337–344, 2009. 61

[12] A. Barletta and E. Zanchini. On the choice of the reference temperature for fully developed mixed convection in a vertical channel. *Int. J. of Heat and Mass Transfer*, 42:3169–3181, 1999. 14

[13] G.S. Beavers and D.D. Joseph. Boundary conditions at a naturally permeable wall. *J. Fluid Mech.*, 30:197–207, 1967. 10

[14] A. Bejan. *Heat transfer*. MWiley, New York, 1993. 15

[15] H. Bénard. Les tourbillons cellulaires dans une nappe liquide. *Rev. Gen. Sci. Pures Appl.*, 11:1261–1271 and 1309–1328, 1900. 12

[16] H. Bénard. Les tourbillons cellulaires dans une nappe liquide transportant de la chalaur par convection en regime permanent. *Ann. Chim. Phys.*, 23:62–114, 1901. 12, 13

[17] M.J. Block. Surface tension as the cause of Bénard cells and surface deformation in a liquid film. *Nature*, 178:115–121, 1956. 13

[18] J. Boussinesq. *Thorie Analytique de la Chaleur*, volume II. Gauthier-Villars, Paris, 1903. 13

[19] H.C. Brinkman. A calculation of the viscous force exerted by a flowing fluid on a dense swarm of particles. *Appl. Sci. Res. A*, 1:27–34, 1947. 6

[20] H.C. Brinkman. On the permeability of media consisting of closely packed porous particles. *Appl. Sci. Res. A*, 1:81–86, 1947. 6

[21] P.C. Carman. Fluid flow through granular beds. *Transactions, Institution of Chemical Engineers, London*, 15:150–166, 1937. 5

[22] M. Celli, D.A.S. Rees, and A. Barletta. The effect of local thermal non-equilibrium on forced convection boundary flow from a heated surface in porous media. *to be submitted.* 106

[23] S. Chandrasekhar. *Hydrodynamic and Hydromagnetic Stability.* Oxford University Press, Oxford, 1961. 14

[24] H. Darcy. *Les fontaines publiques de la ville de Dijon.* Victor Dalmont, Paris, 1856. 4

[25] S.H. Davis. On principle of exchange of stabilities. *Proc. Roy. Soc. A.*, 310:341–358, 1969. 28

[26] A. Delache, M.N. Ouarzazi, and M.C. Néel. Pattern formation of mixed convection in a porous medium confined laterally and heated from below: effect of inertia. *Comptes Rendues Mecanique*, 330:885–891, 2002. 33

[27] A.J.E.J. Dupuit. études theóriques et pratiques sur le mouvement des aux dans les canaux découverts et a travers les terrains perméables. *Victor Dalmont, Paris*, 1863. 6

[28] M. Faraday. Experimental researches in electricity. *Philos. Trans. R. Soc. London*, 122:163–177, 1832. 12

[29] L.E. Finlayson and B.A. Scriven. The method of weighted residuals – a review. *Appl. Mech. Rev.*, 19:735–748, 1966. 92

[30] P. Forchheimer. Wasserbewegung durch boden. *Zeitschrift des Vereines Deutscher Ingenieure*, 45:1736–1741 and 1781–1788, 1901. 6

[31] B. Gebhart. Effects of viscous dissipation in natural convection. *J. Fluid Mech.*, 14:225–232, 1962. 20

[32] C.W. Horton and F.T. Rogers. Convection currents in a porous medium. *J. Appl. Phy.*, 16:367–370, 1945. 18

[33] C. T. Hsu and P. Cheng. Thermal dispersion in a porous medium. *Int. J. Heat Mass Transfer*, 33:1587–1597, 1990. 8

[34] H. Jeffreys. Some cases of instability in fluid motion. *Proc. R. Soc. Lond. A*, 118:195–208, 1928. 28

[35] D.D. Joseph. Stability of frictionally-heated flow. *Phys. of Fluids*, 8:2195–2200, 1965. 19

[36] D.D. Joseph, D.A. Nield, and G. Papanicolaou. Nonlinear equation governing flow in a saturated porous medium. *Water Resources Res.*, 19:1049–1052, 1982. 6

[37] J.P. Joule. On the mechanical equivalent of heat. *Philos. Trans. R. Soc. London*, 140:61–82, 1850. 20

[38] J. Kozeny. Ueber kapillare leitung des wassers im boden. *Sitzungsberg Akad. Wiss.*, 136:271–306, 1927. 5

[39] P.K. Kundu and I.M. Cohen. *Fluid mechanics, second ed.* Elsevier, New York, 2002. 15

[40] J.L. Lage. Natural convection within a porous medium cavity: predicting tools for flow regime and heat transfer. *Int. Comm. Heat Mass Transfer*, 20:501–513, 1993. 7

[41] L.D. Landau and E.M. Lifshitz. *Fluid mechanics, second ed.* Pergamon Press, Oxford, 1987. 15

[42] E.R. Lapwood. Convection of a fluid in a porous medium. *Proc. Camb. Phil. Soc.*, 44:508–521, 1948. 18

[43] D.Y. Lee and K. Vafai. Analytical characterization and conceptual assessment of solid and fluid temperature differentials in porous media. *Int. J. of Heat and Mass Trans.*, 42:423–435, 1999. 24

[44] O. Lehmann. *Molecular Physik*, volume I. Engelmann Leipzig, Germany, 1888. 12

[45] T.S. Lundgren. Slow flow through stationary random beds and suspensions of spheres. *J. Fluid Mech.*, 51:273–299, 1972. 7

[46] O.G. Martynencko and P.P. Khramtsov Lundgren. *Free convective heat transfer*. Springer, Berlin, 2005. 15

[47] W.J. Minkowycz, A. Haji-Sheikh, and K. Vafai. On departure from local thermal equilibrium in porous media due to rapidly changing heat source: the Sparrow number. *Int. J. of Heat and Mass Transfer*, 42:3373–3385, 1999. 24

[48] A.D. Nield and A. Bejan. *Convection in Porous Media (3rd edition)*. Springer, New York, 2006. 3, 19, 23, 54

[49] D.A. Nield. Onset of thermohaline convection in a porous medium. *Water Resources Res.*, 11:553–560, 1968. 19

[50] D.A. Nield. Effects of local thermal non-equilibrium in steady convective processes in a saturated porous medium: forced convection in a channel. *J. of Porous Media*, 1:181–186, 1998. 23

[51] D.A. Nield. Resolution of a paradox involving viscous dissipation and nonlinear drag in a porous medium. *Trans. in Porous Media*, 41:349–357, 2000. 21

[52] D.A. Nield. Modelling fluid flow in saturated porous media and at interfaces. *D.B. Ingham, I. Pop eds. Transport Phenomena in Porous Media II, Pergamon*, pages 1–19, 2002. 20

[53] D.A. Nield. The modeling of viscous dissipation in a saturated porous medium. *ASMA J. of Heat Transfer*, 129:1459–1463, 2007. 19

[54] D.A. Nield. The modelling of viscous dissipation in a saturated porous medium. *ASME J. of Heat Transfer*, 129:1459–1463, 2007. 22

[55] D.A. Nield. Closure to "discussion of the modeling of viscous dissipation in a saturated porous medium (2009, asme j. heat transfer, 131, p.025501)". *ASME J. of Heat Transfer*, 131:# 025502, 2009. 19

[56] D.A. Nield and A. Barletta. Extended Oberbeck-Boussinesq approximation study of convective instabilities in a porous layer with horizontal flow and bottom heating. *submitted to Int. J. of Heat and Mass Transfer*. 19

[57] D.A. Nield and A. Barletta. The Horton-Rogers-Lapwood problem revisited: the effect of pressure work. *Transp. Porous Media*, 77:143–158, 2009. 19

[58] T. Nilsen and L. Storesletten. An analytical study on natural convection in isotropic and anisotropic porous channels. *Trans. ASME J. Heat Transfer*, 112:396–401, 1990. 19

[59] A. Oberbeck. ber die wrmeleitung der flssigkeiten bei bercksichtigung der strmungen infolge von temperaturdifferenzen. *Ann. Phys Chem.*, 7:271–292, 1879. 13

[60] M.N. Ozisik. *Heat conduction*, volume II edition. Wiley, John & Sons, 1993. 110

[61] E. Palm, J.E. Weber, and O. Kvernvold. On steady convection in a porous medium. *J. Fluid Mech.*, 54:153–161, 1972. 18

[62] J.R.A. Pearson. On convection cells induced by surface tension. *J. of Fluid Mechanics*, 4:489–500, 1958. 13

[63] J.R.A. Pohlhausen. Der wermeaustausch zwichen festen korpen und flussingkeiten mit kleiner reibung und kleiner warmeleitung. *Z. Angew. Math. Mech.*, 1:115–121, 1921. 105

[64] A. Postelnicu. Effect of inertia on the onset of mixed convection in a porous layer using a thermal nonequilibrium model. *J. of Porous Media*, 10:515–524, 2007. 33

[65] M. Prats. The effect of horizontal fluid flow on thermally induced convection currents in porous mediums. *J. of Geoph. Research*, 71:4835–4838, 1966. 19, 33, 42

[66] W. Prout. in bridgewater treatise. *Pickering, London*, 8:65, 1834. 11

[67] Lord Rayleigh. On the stability, or instability, of certain fluid motions. *Proc. Lond. Math. Soc.*, 11:57–70, 1880. 16

[68] Lord Rayleigh. On convection currentes in a horizontal layer of fluid, when the higher temperature is on the under side. *Philos. Mag.*, 32:529–546, 1916. 16

[69] D.A.S. Rees. The effect of inertia on the onset of mixed convection in a porous layer heated from below. *Int. Communications in Heat and Mass Transfer*, 24:277–283, 1997. 33

[70] D.A.S. Rees. Vertical free convective boundary-layer flow in a porous medium using a thermal nonequilibrium model: elliptical effects. *J. Appl. Math. Phys. (ZAMP)*, 54:437–448, 2003. 105

[71] D.A.S. Rees. Microscopic modelling of the two-temperature model for conduction in heterogeneous media. *J. of Porous Media*, to appear, 2009. 108

[72] D.A.S. Rees. Microscopic modelling of the two-temperature model for conduction in heterogeneous media: three-dimensional media. *Proceedings of the 4$^{\text{th}}$ International Conference on Applications of Porous Media, Istanbul, Turkey*, to appear, August 2009. 108

[73] D.A.S. Rees, A.P. Bassom, and P.G. Siddheshwar. Local thermal non-equilibrium effects arising from the injection of a hot fluid into a cold porous medium. *J. of Fluid Mech.*, 594:379–398, 2007. 105

[74] D.A.S. Rees, E. Magyari, and B. Keller. Vortex instability of the asymptotic dissipation profile in a porous medium. *Transport in Porous Media*, 61:1–14, 2005. 61

[75] D.A.S. Rees and I. Pop. Vertical free convective boundary-layer flow in a porous medium using a thermal nonequilibrium model. *J. of Porous Media*, 3:31–44, 2000. 105, 106, 111

[76] D.A.S. Rees and I. Pop. Local thermal nonequilibrium in porous medium convection. *D.B. Ingham and I. Pop, Editors, Transport in Porous Media vol. III, Pergamon*, pages 147–173, 2005. 23

[77] C. Rumford. Of the propagation of heat in fluids. *Am. Acad. Arts Sci., Complete Works Boston*, 1:239, 1797. 11

[78] M. Sahraoui and M. Kaviany. Slip and no-slip velocity boundary conditions at the interface of porous, plain media. *Int. J. Heat Mass Transfer*, 35:927–943, 1992. 10

[79] T.E.W. Schumann. Heat transfer: liquid flowing through a porous prism. *J. of the Franklin Institute*, 208:405–416, 1929. 23

[80] L. Storesletten and A. Barletta. Linear instability of mixed convection of cold water in a porous layer induced by viscous dissipation. *Int. J. of Thermal Sciences*, 48:655–664, 2009. 61

[81] J.M. Straus. Large amplitude convection in porous media. *J. Fluid Mech.*, 64:51–63, 1974. 18

[82] P.C. Sukanek, C.A. Goldstein, and R.L. Laurence. The stability of plane Couette flow with viscous heating. *J. Fluid Mech.*, 57:651–670, 73. 19

[83] G.I. Taylor. Stability of a viscous liquid contained between two rotating cylinders. *Phil. Trans. R. Soc. Lond.*, 223:289, 1923. 25

[84] J. Thomson. On a certain curious motion observable at the surface of wine and other alcoholic liquors. *Philos. Mag.*, 4:330–333, 1855. 12

[85] J. Thomson. On a changing tesselated structure in certain liquids. *Proc. R. Philos. Soc, Glasgow*, 13:464–468, 1882. 12

[86] D.L. Turcotte, A.T. Hsui, K.E. Torrace, and G. Shubert. Influence if viscous dissipation on Bénard convection. *J. Fluid Mech.*, 64:369–374, 1974. 15

[87] K. Vafai and M. Sozen. Analysis of energy and momentum transport for fluid flow through a porous bed. *ASME J. of Heat Trans.*, 112:690–699, 1990. 24

[88] K. Vafai and M. Sozen. An investigation of a latent heat storage packed bed and condensing flow through it. *ASME J. of Heat Trans.*, 112:1014–1022, 1990. 24

[89] K. Vafai and C.L. Tien. Boundary and inertia effects on flow and heat transfer in porous media. *Int. J. Heat Transfer*, 24:195–203, 1981. 8

[90] K. Vafai and C.L. Tien. Boundary and inertial effects on convective mass transfer in porous media. *Int. J. Heat Mass Transfer*, 25:1183–1190, 1982. 8

[91] J.C. Ward. Turbulent flow in porous media. *ASCE J. Hydraul. Div.*, 90:1–12, 1964. 6

[92] E.H. Weber. Mikroskopische beobachtungen sehr gesetzmssiger bewegungen, welche die bildung von niederschlgen harziger krper aus weingeist begleiten. *Ann. Phys. (Pogg. Ann., Leipzing)*, 84:447–459, 1855. 12

[93] A.L. Wegener. Die entstenhung edr kontinente. *Geologische Rundschau*, 3:276–292, 1912. 12

[94] S. Whitaker. Flow in porous media: a theoretical derivation of Darcys law. *Trans. in Porous Media*, 1:3–25, 1986. 5

[95] F.M. White. *Fluid mechanics, fourth ed.* McGraw-Hill, New York, 2002. 14